POLITECNICO DI TORINO

SCUOLA DI DOTTORATO
Dottorato in Scienza e Tecnologia dei Materiali
XXVII Ciclo

Ph.D. Thesis

Ceramic multilayer based on ZrB_2/SiC system for aerospace applications.

Advisor:
Prof. Claudio Francesco Badini

Candidate:
Elisa Padovano

Coordinator:
Prof. Claudio Francesco Badini

February 2015

Table of Contents

List of Figures

List of tables

Chapter 1
Aim of the work

The work of this PhD thesis is focused on the processing and characterisation of ZrB_2/SiC based multilayer materials, produced by tape casting and sintered without pressure assistance, for aerospace applications.

Great part of this research work was carried out in the context of an European project SMARTEES- Multifunctional component for aggressive environment in space applications- funded within the 7th Framework Programme and it targets on the creation of new multifunctional materials.

In fact the aim of this proposal was the development of composite structure to be used for applications in aggressive environments such as hot parts of reusable space vehicles for orbital re-entry. The TPS should protect a vehicle with selected APOLLO-type shape: it consisted of blunt body with two main area of interest, the front shield and the back one, submitted to different temperature range and thermal loads.

This multifunctional component is organized at three levels as shown in Figure 1.1:

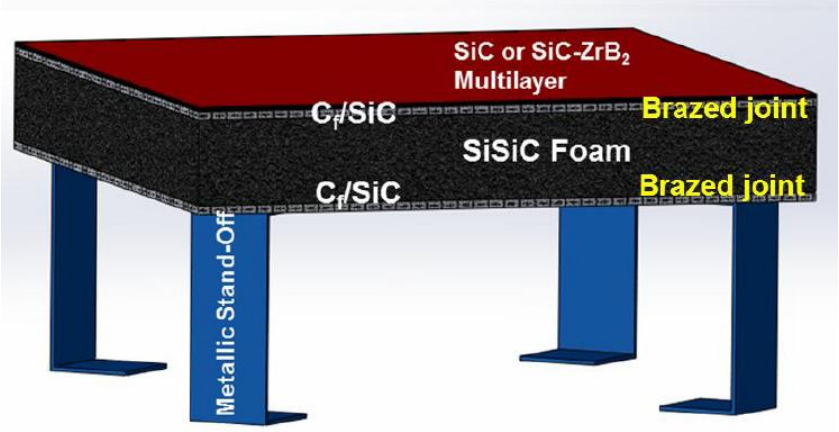

Figure 1.1 Scheme of multifunctional thermal protection system developed in the context of SMARTEES (Courtesy of "Airbus Defence and Space GmbH")

• 1st Level: The external part of the thermal protection system was constituted by ceramic multilayer based on ZrB_2/SiC system.

• 2nd Level: it is composed of a CMC-SiC foam-CMC sandwich structure where conventional ceramic matrix composites with structural or insulating properties were combined to novel porous structure such as SiC foam able to grant additional thermal insulation.

• 3thLevel: A metallic stand-off which consisted in a nonload-bearing support which is mechanically attached to the space vehicle.

These component involved the development of joints which have to be suitable for the different above mentioned materials and able to withstand oxidative and high temperature conditions.
Because of the design of this TPS incorporating components with very different properties, a material modelling and FEM simulation have been used in order to predict the interaction among elements: a computed tomography technique was used in order to obtain a real model of each part of the system. Both thermal and mechanical characterisation of the different component part was carried-out over different temperature ranges: this can help to obtain an accurate and realistic simulation of the insulation capability of the system. After the assembly of all components, the technology sample was tested in a relevant ground facility simulating the re-entry conditions with the aim to define the fundamental performance and the degradation mechanisms.

This thesis was inserted in the workpackage relative to the development of ceramic laminates based on high temperature ceramics (HTCs) and ultrahigh temperature ceramics (UHTCs) with tailored properties. The multilayer components were the external part of TPS directly facing the atmosphere so, in order to withstand high temperature, high heat fluxes and oxidizing environment, they have to show good oxidation and thermal shock resistance, high emissivity, thermal management capability, suitable strength, stiffness and hardness.
The development of materials was directed along three main concepts:

- SiC based multilayer system was developed for the back shield part of the re-entry vehicle which was moderately loaded. SiC is one of the most used material for this kind of applications thanks to the formation of a passive silica layer on its surface which prevented a further oxygen penetration up to 1600°C. At higher temperature the melting of the silica and the mechanism of active oxidation limited the use of this ceramic compound.
- ZrB_2/SiC composite multilayers showing different ZrB_2:SiC ratio were mainly designed for the front shield where the operating condition should be more severe (that means both higher temperature and thermal loads respect to those expected for the back shield). Among UHTCs, ZrB_2 shows an unique set of properties which makes it a good candidate for application at very high temperature; the addition of SiC helped to overcome some of ZrB_2 limitations such its poor sinterability, its oxidation resistance and moreover the mechanical properties of the composite material resulted enhanced.
- In the context of development of reusable TPS to be used for consecutive missions, hybrid multilayer with ZrB_2/SiC composite layers in between SiC ones have been

prepared: the aim was provide for the degradation of SiC/SiO_2 external part inserting an underlying material showing good mechanical and thermal properties at the higher temperature (over 1700°C).

In the present thesis will be detailed the work of processing and characterization performed on these three different classes of laminates.

Conclusively results of emissivity and re-entry tests conducted on the entire TPS assembly, so always involving the external multilayer part, were reported and discussed.

Chapter 2
Thermal Protection system for re-entry vehicles

From the beginning of the space program, engineers have invested many energies and efforts in studying the mechanisms involved during launch and re-entry; this last has been always considered the most problematic one.

A space vehicle which enters Earth atmosphere after an hypersonic flight requires a Thermal Protection System (TPS) able to protect and insulate the body from the severe heating conditions: this phase results hard both for the crew which undergoes more or less strong deceleration in function of the re-entry trajectories and for the vehicle itself that is submitted to intense heat fluxes resulting from friction between the structure and the air.

2.1 Physics of Re-entry

The main differences between a conventional and a re-entry flight is the very high velocity involved during the landing phase (for hypersonic mission it ranges between 8 and 11 km/sec) and consequently all the linked factors such as air friction, temperature and heat fluxes; in addition the atmosphere rarefaction (it can decrease from 1 bar at the sea level to 10^{-6} bar at 100 Km altitude) is to be considered.

The investigation on the body motion from space to Earth and then the problems linked to it involves the study of which forces affect the re-entry phase (Figure 2.1): the *force of gravity* is a well known natural force by which the Earth, such as others massively large object, attracts another object towards itself.

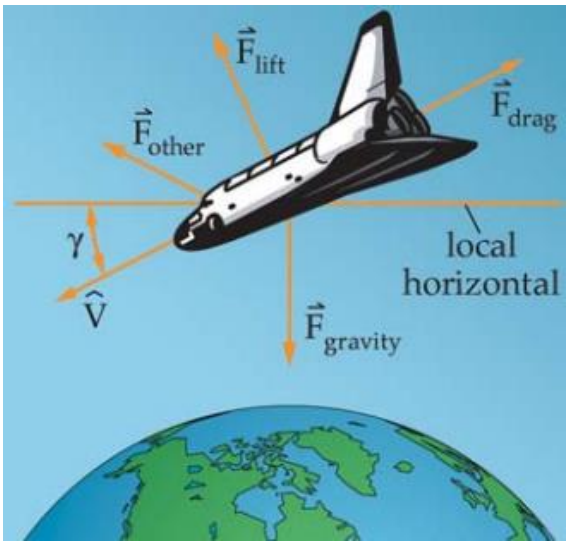

Figure 2.1 Significant forces on a re-entry vehicle.

Lift is a force produced at a right angle to the direction of motion as a result of air moving over the surface of an object. In this context the body shape it's very important; for example the

airplane's wing is able to generate enough lift force to overcome the gravity force and “lift” it into the air.

Drag is, among the reported force, the dominant one; it is a type of frictional force that resists motion through the atmosphere; it acts to oppose the motion of an object (1).

The drag force depends on the air density and in addition to the vehicle properties such as its size (cross-sectional area exposed to the wind), its drag coefficient and its rate.

$$F_{Drag} = \frac{1}{2} \cdot \rho \cdot V^2 \cdot C_D \cdot A \qquad \text{(Eq 2.1)}$$

where F_{drag} is drag force on a vehicle (N), ρ is the atmospheric density (kg/m^3), V is the vehicle’s velocity (m/s), C_D is the drag coefficient and A is vehicle’s cross-sectional area (m^2).

Knowing the mass of vehicle and the drag force acting on it, according to the Newton's Second Law, it is possible to determine its acceleration. In the case of re-entry the drag force pushes the object toward the rear respect to enters, so the acceleration can be called deceleration and can be expressed as following:

$$a = \frac{1}{2} \cdot \rho \cdot V^2 \cdot \frac{C_D \cdot A}{m} \qquad \text{(Eq. 2.2)}$$

Where m is the mass of the vehicle (Kg).

The quantity $C_D \cdot A/m$ defines an object moving through the atmosphere. By convention, inverse of this term is called the ballistic coefficient, β.

$$\beta = \frac{m}{C_D \cdot A} \qquad \text{(Eq. 2.3)}$$

For low β value the heating and deceleration are less intense and the object slows down much quicker than an object with higher β.

During the re-entry phase from a space mission three requirements have to be balanced: deceleration, heating and accuracy of landing (1).

The vehicle structure and payload limit the maximum deceleration that a space vehicle can undergo during re-entry: it must be low enough to prevent damage to the weakest part of the vehicle.

Others very important factors to consider in order to design the trajectories and the vehicle are the heat fluxes and the temperature developed during re-entry.

The Space Shuttle in orbit had , for example, a mass of 100000 kg, an orbital velocity of 7700 m/s and an altitude of 300 km, so it had both a kinetic energy due to its speed and a potential energy due to its altitude. Before landing this energy is converted in heat; you must limit as much as possible that this great heat flux is absorbed to the vehicle instead of being dispersed in the surrounding atmosphere. During the re-entry the Shuttle’s surfaces easily reaches temperatures up to 1500° C.

The heat flux on the vehicle bow can be defined as (2):

$$\dot{q} = k \cdot \frac{V^3}{\sqrt{R}}\sqrt{\rho} \qquad \text{(Eq. 2.4)}$$

where q is the heat flux (W/m^2), k is a constant equal to $1.15 \cdot 10^{-4}$, V is the vehicle velocity, R is the radius of curvature and ρ the atmosphere density.

The typical heat flux values have magnitude order of 10^6 W/m^2 which correspond a range of temperature to 2000-2500K.

There are only few class of materials which can withstand a so high heat flux and temperature; most of existing compounds melt or vaporize in these severe conditions.

In this context a blunt body has the proper shape able to dissipate the heat thank to its large radius of curvature (Figure 2.2).

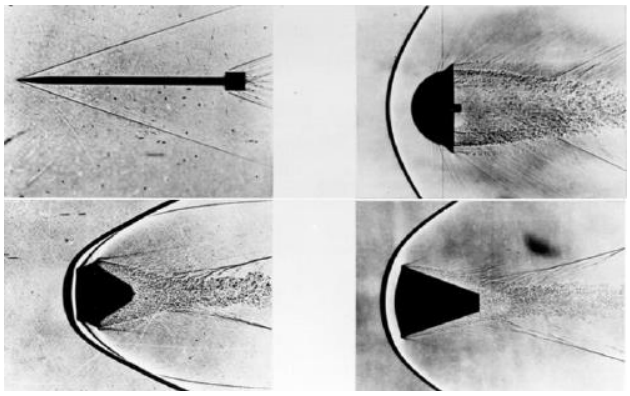

Figure 2.2 Effect of radius of curvature of the vehicle bow.

The third factor is the accuracy: for a safe landing the space vehicle must plan to hit the atmosphere at the precise angle and speed in the so called "re-entry corridor" through which the vehicle must pass to avoid skipping out or burning up. The size of this three-dimensional corridor also depend on the other two factor previously reported. Moreover the accuracy is function on the width of area for landing.

According to all these considerations, in order to establish the correct trajectory for the space vehicle and to keep it intact after landing, it is necessary to try a good equilibrium between deceleration, heating and accuracy.

With this aim the investigation on the main motion of re-entry structure is investigated.

2.2 Atmospheric Re-entry motion

There are two main re-entry modes on the base of which the choice of proper TPS is done (1; 3) :

Ballistic type entry: the vehicle crosses all the atmosphere layers with a very high velocity; this causes an high kinetic energy dissipation in form of heat and consequently high heat fluxes are produced. For mission which involves this kind of re-entry, an ablative material is used in order

to protect the vehicle to extreme conditions along a short time: the surface material can melt or vaporize transferring most of its heat to the surrounding atmosphere.

The first manned ballistic entry was in February 1962 with the flight of Colonel John Glenn's "Friendship 7" Mercury capsule; Figure 2.3 reported the "Friendship 7" Mercury Capsule Earth trajectories entry in term of velocity, entry time and acceleration.

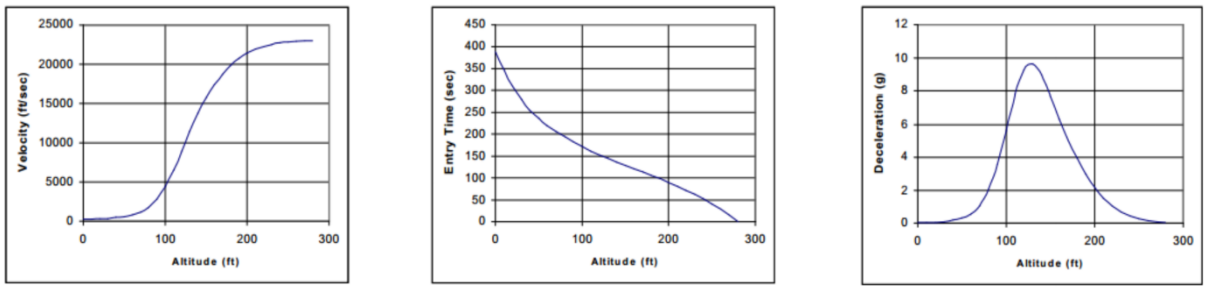

A) Velocity B) Entry time C) Deceleration

Figure 2.3 Ballistic entry: A) velocity, B) entry time and C) deceleration profiles

Colonel Glenn was subjected to a very high deceleration g load (higher than 8) for a not negligible time period of about 30 seconds. After experience like this there was born the necessity to develop a lifting entry for manned space flight with reduced sustained g loading over a long time period.

Lifting type entry: the established trajectory is long allowing a more conventional landing. The entry time is longer than the ballistic entry: this means that the kinetic energy conversion in to heat flux results lower.

The most representative design parameters for lifting entry is the lift-to-drag ratio:

L/D = Lift/Drag = C_L/C_D

Where C_L is the Lift coefficient and C_D id the Drag coefficient.

Low values of L/D produce moderate g loads, moderate levels of heating; on the other hand high values of L/D generate very low g loads, but entry is much more longer and have continuous heating.

For example the entry of Space Shuttle corresponded a L/D value around one with an entry time of 25 minutes: even if the maximum temperatures of a lifting entry are lower than the corresponding ones for ballistic entry, the total heat load that must be absorbed during the entry phase results higher.

Maneuverable Re-entry Vehicle (MaRV) flies a lifting entry trajectory in order to avoid interception by defensive systems.

Figure 2.4 shows the MaRV trajectories compared to the ballistic ones: the entry time is increased from about 85 seconds for pure ballistic entry to 352 seconds for lifting one; moreover a substantial reduction in deceleration g loads can be observed respect to the ballistic trajectory.

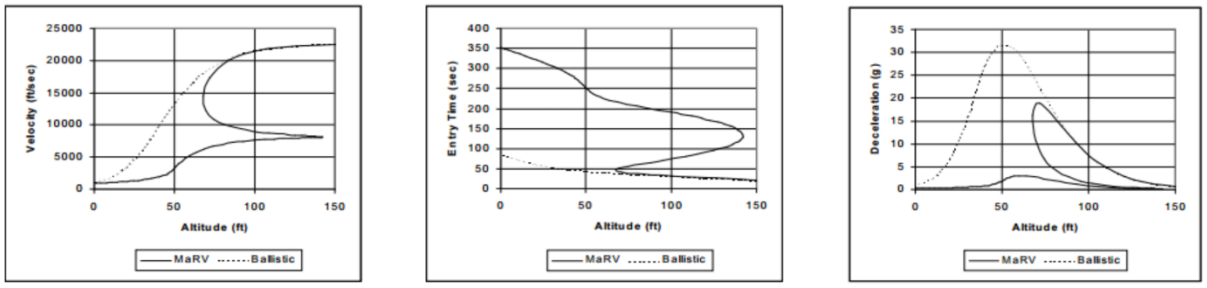

A) Velocity B) Entry time C) Deceleration

Figure 2.4 MaRV Lifting entry: A) velocity, B) entry time and C) deceleration profiles.

2.3 Thermal protection systems

On the base of the re-entry type previously described and the involved conditions in both of them, the thermal protection system can be divided in two main classes:

Ablative TPSs support high heat loads and heating rates through phase changes and mass losses (4): this kind of materials are able to protect the underlying structure by absorption or dissipation of heat produced after melting, decomposition, sublimation or erosion. The ablative TPS are consequently consumed and have to be replaced or restored after using.

Ablative materials have been the conventional approach to TPS used for over 40 years in a broad range of applications such as for all NASA planetary entry probes.

They represent an efficient solution to protect the vehicle and are generally cheaper than the reusable TPSs.

An ablator should have an high melting/sublimation point, high specific heat and latent heat of melting/vaporization, low thermal conductivity and good strength in order to withstand vibrating and aerodynamic solicitations.

Ablative thermal shield generally consists of an external part with more strictly ablative function so that it undergoes decomposition during re-entry and an inner part with insulating capability; it not suffers or only partially suffers thermal decomposition.

Their total thickness is estimated on the base of the supposed heat fluxes and temperature which the vehicle has to withstand.

Most ablative TPS materials are made of reinforced composites employing organic resins as binders. When heated, the resin pyrolysis producing gaseous products (mainly hydrocarbons) that percolate toward the heated surface and are then injected into the boundary layer (Figure 2.5). In addition a carbonaceous residual is produced which deposits on the reinforcement.

("Char" is used to define the resulting surface material). Because of this gas percolation, there is a transfer of energy from the solid to the gases which alters the boundary layer properties, typically resulting in a reduction of convective heating.

Furthermore, chemical reactions between the surface material and boundary layer species can result in consumption of the surface material leading to surface recession: those reactions can be both endothermic (vaporization, sublimation) or exothermic (oxidation) and will have an not negligible impact on net surface energy.

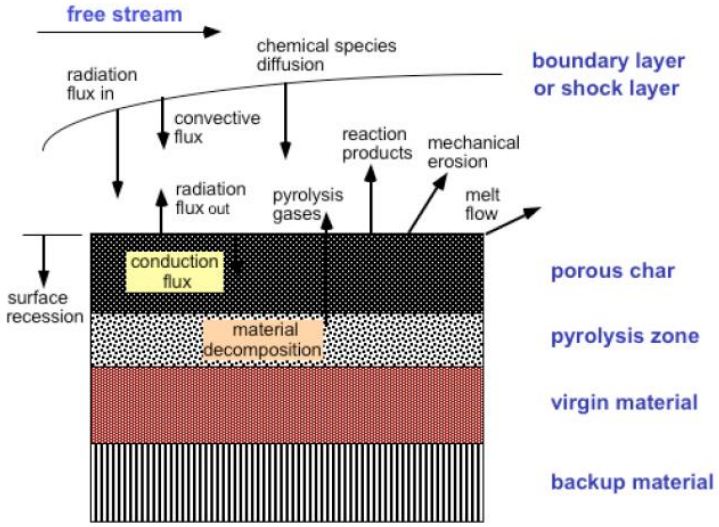

Figure 2.5 Heat exchanges involved in ablative material.

This is only one of the processes which involve the ablative TPS during re-entry; Figure 2.5 shows others examples:

- Quick increase of surface temperature
- Phase transformation due to melting, evaporation, sublimation and degradation
- Heat conduction to the material layers under the surface
- Production and emission of volatile substances
- Gas heating absorption after percolating toward the surface
- Formation and convection of a liquid phase
- Endo/exothermic chemical reactions
- Outwards radiation

The interaction of ablative TPS materials with the surrounding environmental gases is much more complex respect to the reusable TPS, because there are many more mechanisms to accommodate the entry heating.

Ablative thermal protection system can be classified in three group on the base of ablation mechanism: subliming/melting, charring and intumescent.

The subliming one collects heat up and the surface temperature reaches the melting/sublimation point. One of the most subliming material is PTEF (Teflon) which presents low density, god insulating capability and decomposition temperature around 500°C.

In the charring materials the thermal decomposition produces carbonaceous residual and volatile gases. They can withstand relative high heat fluxes and for this reason they are the most used ones, often in combination to the other two types.

Epoxy, Silicon and phenolic resin are the most diffused charring ablative.

The intumescent type is not usually used for re-entry application because of their high density and significant dimension changes during their decomposition; on the contrary respect to the charring, the decomposition mechanism results quite different starting to be mainly exothermic.

Reusable TPS are materials which don't undergo significant changes in mass or in mechanical properties after exposure to the entry environment.

The main characteristics of this kind of TPS are shown in Figure 2.6: radiative and convective heating results in a significant amount of energy being re-radiated from the heated surface with the remainder conducted into the TPS material.

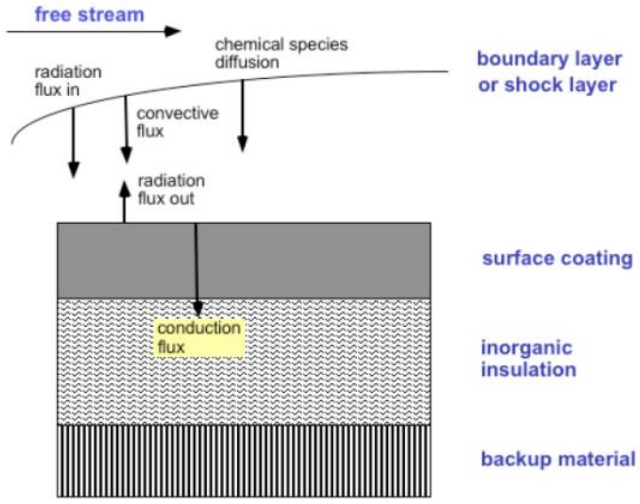

Figure 2.6 Heat exchanges involved in reusable material.

It is advantageous if, as often happens, surface coating has high emissivity (just in order to maximize the amount of re-radiated energy) and low surface catalysis (to minimize convective heating by suppressing recombination of dissociated boundary layer species at the heated surface).

The first manned space vehicles such as Mercury, Gemini and Apollo were not maneuverable and the entry was ballistic. These lenticular-shaped space capsules were protected by a thermal barrier consisting of phenolic epoxy resins in a nickel-alloy honeycomb matrix the capsule. For

the entry they slowed down their velocity by using a parachute and then landed in the ocean; meanwhile the astronaut jumped from ejector seat.

Researchers found that the heat shield was designed to ablate, so the external layer was sacrificial in order to protect the underlying structure layers (NASA Ames Research Center, 1994).

In spite of several advantages offered by this kind of TPS, the disadvantages were more important: first of all the degradation of TPS during landing changed the vehicle aerodynamic shape, then they had a higher density and could be used only for one mission.

In 1972 USA charged NASA and the Space Division of Rockwell International to design the first Space Shuttle orbiter, Columbia. Columbia was a revolutionary new space vehicle for mainly two reasons: it would fly back to Earth instead of plummeting into the ocean and moreover it was reusable, with an expected design life of 100 missions. So the Space Shuttle orbiter needed a new type of TPS which was lightweight and could survive many re-entry.

Many efforts and resources have been invested in the development of this new idea of TPS:

reusable launch vehicles show many advantages in comparison to the ablative system: they are able to protect the vehicle to higher heat fluxes withstanding extreme conditions without substantial degradation and moreover allow to reduce the payload transportation costs.

There are several approaches to acreage TPS on an hypersonic vehicles: the first one is an insulated structures such as those used on the Space Shuttle Orbiter. The second one is the standoff TPS approach as used on the X-33; for these structures an internal insulation below the outer surface is used (5).

2.4 Insulated structures

Because of they are placed on the external part of a vehicle and directly attached to the cold structure, they defines its aerodynamics and transfer the aeroloads to it. There are mainly two types of insulators: the blanket and the tiles. Both of them presented low density and low thermal conductivity.

The blankets show insulating capability and similar thermal expansion coefficient respect to the underlying structure, so they can be easily joint to the vehicle structure in short time e avoiding high installation costs. On the other hand the tiles stiffen the underlying structure, so it can withstand higher loads, but they need an insulator layer. There is usually a strain isolation pad (SIP) required between the tiles and aluminium structure due to the different thermal expansion of the two materials.

The classes of materials which satisfy the properties required for a TPS are reported in Figure 2.7.

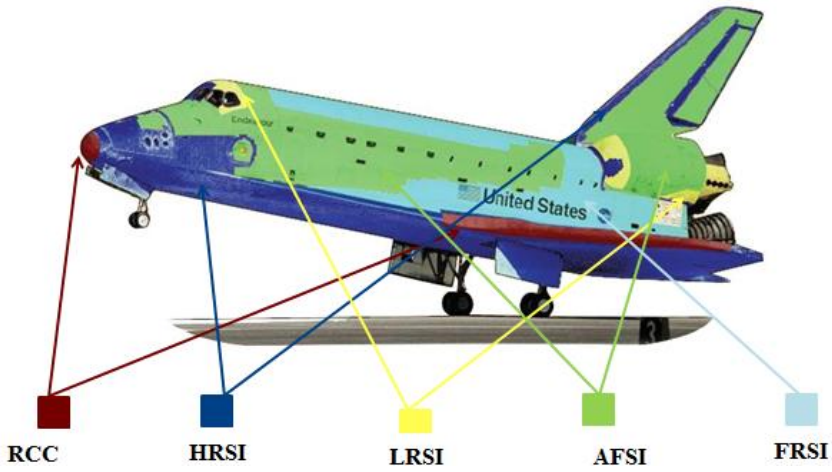

Figure 2.7 Avaible Thermal Protection System for different parts of vehicle.

2.4.1 RCC – Reinforced Carbon-Carbon

Reinforced Carbon-Carbon (RCC) is used for leading edges, nose cones, or any other areas where thermal (up to 1260°C) and mechanical loads are high.

The importance of RCC is due to some very interesting properties: high thermal shock and ablation resistance, chemical inertness in aggressive environments and good performance in not oxidising environment over 1500°C. The main disadvantages include the processing costs which are quite high due to the long time at high temperature required for its thermal treatment and to the Carbon fibres high cost too.

Moreover RCC has an high thermal conductivity, which requires the use of excessive surface insulation to protect the adjacent metallic attachments from exceeding temperature limits.

The RCC mechanical properties depend on different factors such as the preform design, the selected type of Carbon fibres, the matrix nature and the processing method. Thanks to the high fibres strength and stiffness and the low density of both fibres and matrix this material shows very good mechanical properties that resulted comparable to those of high performance metals or Titanium alloy.

It is possible to improve the mechanical properties of RCC by varying the fibres orientation: the poor shear stress on a plane or among them is mainly due to the tendency of the matrix to crack and produce pores during the graphitization process. Orienting the fibres along the thickness and with angles of +45° and -45° respect to the main composite direction, the shear stress results enhanced.

The main limit of RCC is the oxidation at temperature above 450°C; a possible way to overcome this problem is put a ceramic coating on its surface in order to protect RCC to the Oxygen penetration.

2.4.2 HRSI tiles – High-Temperature Reusable Surface Insulation titles

The HRSI tiles are treated with a special black-pigment coating to maximize emissivity (observed value higher than 0.85) and are used in areas such as the underside of the orbiter, where maximum heat dissipation is required during re-entry. They are made of low density and highly pure (99.8%) silica fibres which are produced into rigid billets by ceramic slurry, formed through a mould up to obtaining a soft and porous block which is subsequently machined to the desired specifications. Once these tiles have been machined, they are coated with Reaction Cured Glass (RCG) with the addition of a black pigments. The coated tile is then fired in a kiln at 1200°C where the coating forms a glossy and waterproof external layer.

Generally the thickness of HRSI is in the range 25.4-127 mm in function of the required maximum heat flux :usually they resulted thicker on the bow respect to anterior part.

To have an idea of their shock resistance you can image to heating the HRSI tile up to 1260°C and rapidly quench in water: any damage should be observed. In fact the surface can dissipate heat very quickly respect to the inner part.

The main limit of HRSI is its poor capability to sustain the standard strain at which the airframe is subjected due to in-service loading, thermal expansion or acoustic excitation. Therefore, HRSI are joint to the vehicle by a so called “Strain Isolation Pads” (SIPs): they are made from Nomex® (felt based on Aramid fibres) which isolate the tile from the orbiter’s structural deflections. The installation process is quite tedious: the tiles are firstly bonded to the SIP using a very thin and uniform layer of Room Temperature Vulcanizing (RTV) Silicon adhesive and then the tile/SIP assembly is bonded to the airframe by the same RTV process. Because of tiles contraction or expansion (even if very small) care must be taken during the installing/replacing operation in order to maintain a small gaps between the tiles and meanwhile prevent tile-tile contact.

2.4.3 LRSI titles - Low-Temperature Reusable Surface Insulation titles

LRSI have similar function respect to HRSI and are made from the same basic materials, but they are treated with a special white-pigment coating (instead of black one) in order to maximize thermal reflectivity. LRSI are in fact used in areas such as the anterior, central and posterior parts of fuselage and in the vertical part of the tile wing where heat reflection is desired. These tiles must sustain temperature up to 650°C.

2.4.4 FRCI titles – Fibrous Refractory Composite Insulation titles

FRCI tiles are a higher strength, lower density version of HRSI tiles.

This type of tiles are made using Nextel™ with AB312 fibres (alumina-borosilicate based fibres) added to the silica slurry during the billet forming process (the same described earlier for HRSI). During the sintering Nextel activates the melting of Boron welding pure silica fibres; the result is a composite material made of 20% of Nextel and 80% of pure silica.

Nextel™ has a coefficient of thermal expansion approximately ten times greater than silica; therefore, when the billet cools after its initial formation, the Nextel™ fibres add strength to the tile obtaining a tensile strength value three times greater than HRSI one and an operating temperature 50 degrees higher than HRSI.

2.4.5 AFRSI – Advanced Flexible Reusable Surface Insulation

AFRSI blankets replaced the LRSI tiles on the Discovery and Atlantis Space Shuttles; they are made up of a layer of low-density fibrous silica batting inserted between an external layer showing high temperature resistance and an inner layer made by glassy fibres with low temperature resistance. The three layers are then sewn to form a "quilted" blanket. These blankets are cut according to the desired shapes and joint to the vehicle structure by RTV process.

The major advantages of AFRSI over LRSI are that the former is more easily mould to the exterior contour of the vehicle, decreasing installation cost and time; moreover it provides a reduction in weight because the use of SIPs is no longer necessary and it is more easily manufactured and more durable.

2.4.6 FRSI – Felt Reusable Surface Insulation

FRSI blankets are made from Nomex®, the same material as the SIPs; their thickness is generally ranged between 4 and 10mm, in function of the expected thermal loads. They are used in areas with expected temperatures up to 650°C; approximately 50 percent of the orbiter's upper surface is covered with FRSI.

2.5 Stand-off TPS with internal insulation

The stand-off TPS approach is usually used on a cold or warm structures where the temperature reach 1000°C. An example is X-33 vehicle: the TPS panels were attached to stand-off brackets to create the desired aero shell. The critical challenge with this approach is to transfer the aero loads, but not the thermal loads, to the structure.

For hypersonic vehicles there is the need for higher temperature TPS such as CMC TPS showed in Figure 2.8.

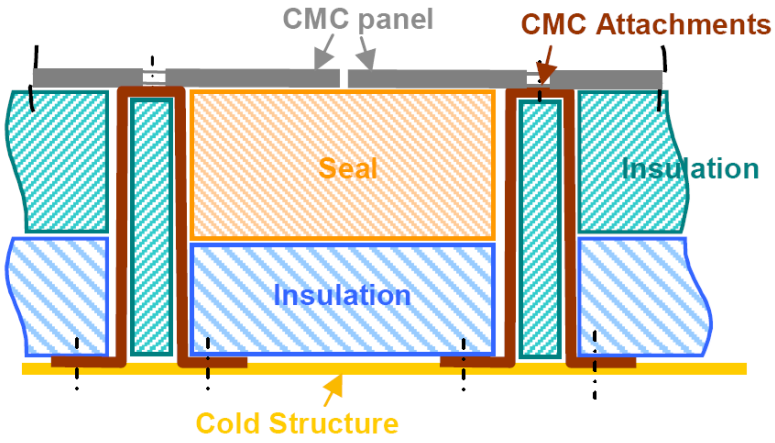

Figure 2.8 TPS based on C_f/SiC (Keraman®) CMC shield (6)

An external CMC panel with oxidation protection forms the aeroshell and the stand-off TPS includes an internal insulation. The insulation is placed in order to lower down the temperature to 100-200°C at the underlying cold metallic structure (fuselage of the space vehicle); materials which can be used as insulators are:

- Fibrous ceramics (Saffil silica and silica/alumina felt) encapsulated with a Nextel (alumina fibre fabric –3M) bag
- Flat composites plates of Nextel inserted in a matrix of alumina or mullite and processed by slurry infiltration , drying and sintering
- Carbon foams prepared starting from slurries of Carbon powder and spheres of low melting material (leaving cells of the foam)

High temperature seals and an attachment are used to attach this external CMC panel to the internal structure.

The primary challenge with any stand-off TPS is attaching the external panel to the substructure and transferring aero and pressure loads, but not thermal loads. Moreover, the entire system must withstand acoustic and vibration loads.

The TPS developed in SMARTEES project was design using the stand-off approach.

2.6 High and Ultra High Temperature Ceramics for space applications

Different TPS technologies have been previously described: ablative TPS used mainly on the Apollo capsules (7) and interplanetary entry probes (8), or reusable TPS integrating insulated (9) or stand-off (5) structures. Moreover thanks to the increasing interest in reusable launch vehicles (RLVs) (10; 11) also new metallic TPS concepts were developed (12; 13).

The long service life in harsh environmental conditions makes surface modifications an essential part of materials technology for aerospace applications. In fact, due to their specific designs, re-entry vehicles usually require control surfaces which include sharp leading edges. They are subjected to great aero-thermal heating and they can reach temperatures that may exceed 2000°C. Available thermal protection materials will not survive such extreme temperatures and new materials are required for advanced thermal protection systems.

Since the late 1960s the attention was focused especially on SiC and Si_3N_4 used for the production of ball bearings, armour, fibres and turbine blades (14) and on some oxides or RCC used on the space shuttle nose cone and wing leading edges. However the oxidation resistance of these high temperature materials was limited to 1600°C.

For hypersonic flights, TPS for re-entry vehicles and propulsion applications are required new materials that must have good performance in oxidizing atmospheres, at temperature higher than 2000°C and which can withstand these operative conditions for several missions.

The continuing researches and investigations with the pursuit to develop new materials for TPS and to improve the performance of re-entry vehicle lead to identify Ultra-High Temperature Ceramics as a promising class of material for aerospace applications.

In fact these materials offer a good combination of physical, mechanical and thermal properties that allow them to be used in extreme environmental like those associated with atmospheric re-entry, hypersonic flight and propulsion rockets.

There are more than 300 materials whose melting point exceed 2000°C (Figure 2.9) including the previously mentioned SiC, refractory metals such as Hf, Nb, Ir, Ta, Re and W, oxides including HfO_2, ZrO_2, UO_2 and ThO_2, and a variety of transition metals carbides, nitrides and borides.

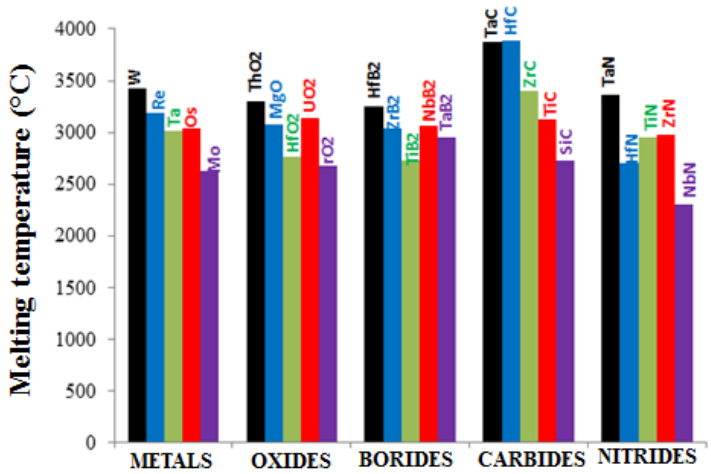

Figure 2.9 Comparison of melting temperature of different Ultra High Temperature Compounds

The high melting point was only one of the properties to be considered: the oxidation resistance is very important in this context in addition to the strength (both at room and application temperature), thermal conductivity, thermal expansion coefficient, density, process method and cost.

Oxides have to be considered thanks to their good oxidation resistance, but they presented a poor thermal shock resistance and low thermal conductivity. The Silicon based materials have very good oxidation resistance too thanks the formation of a silica passive layer which prevents further Oxygen penetration; however their use is limited to temperature up to 1700°C at which the active oxidation and other mechanism can occur destroying the passive layer.

Other materials such as Ti/Nb carbide and boride, at high temperature can form oxides with low melting points (T_m TiO_2 is 1840°C and T_m Nb_2O_5 is 1485°C) and the formation of a liquid phase have to be very limited for aerospace applications.

Carbide and Nitride have been studied since the 1930s and involved many applications, another class of material started to be studied in the 1960s and is now the most widely investigated for TPS that is the borides.

Following there will be an introduction on Silicon Carbide as one of the main compounds used for aerospace applications at high temperature; moreover the borides with particular interest in Zirconium Diboride will be presented as materials with promising applications at ultra high temperature.

2.6.1 Silicon Carbide

Sintered α-SiC has evolved as a major structural ceramics with applications in many fields which includes heat exchangers for high temperature, seal, bearing and water resistant component (15); moreover SiC is a good candidate for thermal protection concepts thank to some particular properties: thermal stability at very high temperature, low density, high stiffness and fairly good strength, high hardness and erosion resistance, self passivating behaviour in oxidising environment.

However SiC also presents some disadvantages that need to be overcome, especially for aerospace application: rather poor toughness, poor thermal insulation capability at room temperature (even if greatly increasing with temperature increase) and active oxidation at high temperature and under low partial pressure of Oxygen.

The oxidation mechanism for SiC will be detailed discussed in the next part (Chapter 6): fundamentally it is dependent on the partial pressure of Oxygen in the atmosphere in addition to the temperature. So under high partial pressure of Oxygen passive oxidation takes place which involves the formation of a passive silica layer; for temperature very high temperature and in

presence of a low Oxygen pressure SiC can undergo active oxidation. This justify the limitation in using SiC as single phase for very high temperature applications.

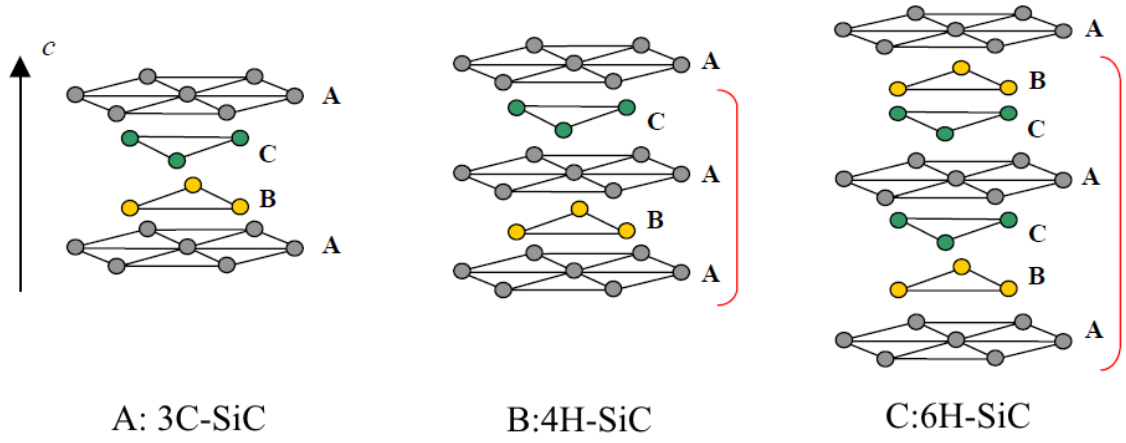

Figure 2.10 Stacking sequence of atomic planes for A) 3C, B) 4H and C) 6H SiC

Silicon Carbide exists in more than 200 crystalline forms: each polymorphism of SiC is characterized by a large family of similar crystalline structures called polytypes. They present the same chemical composition with identical structure in two dimensions and a difference in the third one; so they can be seen as layers stacked in a certain sequence.

A list of most common polytypes includes 3C, 2H, 4H, 6H, 8H, 9R, 10H, 14H, 15R, 19R, 20H, 21H and 24R where C, H and R indicates the three basic cubic, hexagonal and rhombohedral crystallographic types. In the cubic structure, labelled as 3C-SiC or β-SiC, the Si and C atoms show a similar configuration respect to diamond. It is not easily available in bulk form and has a relative few commercial use; only recently there is an increasing in using it as support for heterogeneous catalysis thank to its higher surface area respect to α form. The transformation from β to α is irreversible.

In the hexagonal type (nH-SiC, generally called α-SiC) and in the rhombohedral one (nR-SiC) bilayer of Si and C stack in a primitive unit cell, the main difference regards the stacking sequence. Alpha Silicon Carbide (α-SiC) is the most commonly encountered polymorph showing a stability up to 1700°C.

The nature of Si-C bonding is mainly covalent (88%) and only partially ionic (the remaining 12%).

Pure Silicon Carbide can be sintered very difficultly due to the low diffusion coefficients of Si and C. Thus, during the treatment, is easier to have grain growth than densification. To achieve high relative density, the use of sintering additives is necessary.

Silicon Carbide sintering can be effected in the *solid state*, with the use of Boron and Carbon (16; 17) at temperatures around 2100-2200 °C. Later other sintering aids were found to improve the densification of SiC; for example fine SiC powder could be sintered with the addition of B_4C (18).

Silicon Carbide can be also sintered in *liquid phase*; in this case it typically presents a very fine SiC microstructure. Y_2O_3 e Al_2O_3 are the most used sintering aids: during sintering an yttrium-aluminium granate (YAG, $Y_3Al_5O_{12}$) is formed. Choosing the proper treatment times the liquid phase assembles at the border of the grains, contributing to generate clean grain boundaries. It was moreover observed that if the sintering process is performed in presence yttria and alumina, under an argon atmosphere and at 1900 °C, a little quantity of C can help to reduce the presence of SiO_2.

In this work of thesis α-SiC powder was used; XRD measurement (Figure 2.11) on the starting powder has been done in order to verify the purity of it: any impurities are noticeable from this XRD spectrum; all peaks belong to the Silicon Carbide.

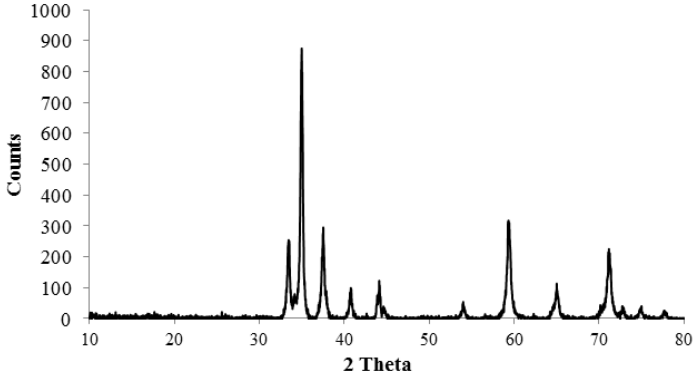

Figure 2.11 XRD measurement on α-SiC starting powder.

2.6.2 Borides

The diborides have extremely high melting temperatures (over 3000°C) and a relatively good resistance to oxidation in simulated re-entry environments; moreover they are widely used in other application fields such as refractory coating, electrodes, microelectronics and cutting machine.

Borides show a wide range of composition with a ratio Boron/Metals (B/M) varying from 1/4 to 12/1: this value defines both the properties and the electronic configuration of the compound (19). Changing B:M ratio the electronic structure of Boron changes, leading to the formation of

different structural systems containing one-, two-, or three-dimensional B networks. Increasing the number of B atoms , the strength of B–B bond increases as well as the stiffness of the crystal lattice, the melting temperature (T_m), hardness (HV), strength (s), and chemical stability.
The M–B bond strength in diborides depends on the degree of electron localization around the metal atoms: in the metal borides the external electron configuration of Boron is sp^2 and sp^3 promoting the formation of strong covalent bond. In the diborides the Boron atoms are electron acceptors, while the M atoms are electron donors. In this case the electronic configuration changes in function on the Metal donor character; the interactions between donors and acceptors makes ionic the M-B bond in addition to a partial covalent nature.

Borides are characterised by high thermal conductivity which decreases thermal gradients into the internal part of the material: a heat transfer from higher temperature areas (e.g. stagnation points) to lower ones lets the maximum temperature decreasing and the thermal shock resistance raising.
The strength of diborides which are reported in literature have very widely dispersed values: this is because this property has a strong dependence to the processing methods and to the microstructure of the sintered materials; it has been for example reported that the strength of diborides often increases with the decreasing of grain size according to Hall-Petch relationship (20).
The oxidation resistance of this class of materials can be improved by addition of a second phase: Silicon Carbide was firstly added both to HfB_2 and ZrB_2 in order to improve their strength (21); moreover the formation of silica in the diborides was reported improving the oxidation resistance of the resultant composites (22).

The most representative compounds belonging to this class of materials are TiB_2, ZrB_2 and HfB_2. TiB_2 is both covalent and ionic bonded compound so it requires very high sintering temperature. It is usually densified by hot pressing or hot isostatic pressing: the relative low crystalline boundary diffusion coefficient slow down the densification speed and increase the time necessary for sintering (23). The pressureless sintering is also possible in presence of liquid forming sintering aids such as Iron, Chromium and Nickel (24).
However the cost of densifying the material at high temperature, the uncontrollable variability in mechanical properties, the relative moderate poor sinterability and its oxidation resistance only up to 1000°C, limits the use of TiB_2 for aerospace application.
Thanks to its high hardness and moderate strength TiB_2 is used for armour and cutting tools.

Borides of Hf and Zr were investigated in early 1950s as nuclear reactor material. In the following two decades many studies were performed by ManLabs under a research program founded by Air Force Materials Laboratory: they showed the potential of diborides as nosecones and leading edge materials (25). The relatively good oxidation resistance of refractory diborides compared to others refractory intermetallics compounds (carbides, nitrides and silicides) has focused many research efforts into detailed investigation on transition metal diborides. Among them Hafnium and Zirconium Diborides were identified as the most promising candidates for high temperature applications in the extreme conditions involved during atmospheric re-entry.

Zirconium and Hafnium are very similar chemical elements so their borides are similar too: their thermal conductivities are very high and this is a favourable factor in applications where thermal stresses are developed: thanks to high thermal conductivity the borides can homogenize the heat distribution and equilibrate the temperature along the thickness reducing the formation of residual stresses. For example in rocket motor nozzles the inner part can reach 2000°C in 0.15 second, while the external part is still at room temperature. The compromise between the nozzle thickness, the thermal conductivity and the strength will determine the success or the failure of this part.

The diborides of hafnium and zirconium are nowadays of particular interest for aerospace industry mainly in sharp leading edge applications which require chemical and structural stability at extremely high operating temperatures.

In this context the Zirconium Diboride has an important advantage respect to Hafnium Diboride due to its lower density.

ZrB_2 based multilayer ceramics were detailed investigated in this thesis in order to be used as external part component of a Thermal Protection System.

2.6.2.1 Zirconium Diboride

Among the compounds belonging to the family of transition metal ultra-high temperature ceramics ZrB_2 shows a unique set of properties (shown in Table 2.I) that make it attractive candidates for thermo-mechanical structural applications such as leading-edge part on hypersonic space vehicle, propulsion system, furnace elements, refractory crucibles and plasma-arc electrodes. In particular ZrB_2 has a lower density respect to HfB_2; this makes it more attractive especially for aerospace applications.

Properties	ZrB_2
Crystal system space group	Hexagonal
prototype structure	P6/mmm AlB_2
a (A˚)	3.17
c (A˚)	3.53
Density (g/cm^3)	6.119
Melting temperature (°C)	3245
Young's modulus (GPa)	489
Bulk modulus (GPa)	215
Hardness (GPa)	23
Coefficient of thermal expansion (K^{-1})	$5.9 \cdot 10^{-6}$
Heat capacity at 25°C (J/mol ·K)	48.2
Electrical conductivity (S/m)	$1.0 \cdot 10^{7}$
Thermal conductivity (W/m ·K)	60
Enthalpy of formation at 25°C (kJ)	-322.6
Free energy of formation at 25°C (kJ)	-318.2

Table 2.I Summary of main ZrB_2 properties.

ZrB_2 crystal structure, as most of Group IV–VI transition metal diborides, is primitive hexagonal, type AlB_2: this configuration shows layers of B atoms in an hexagonal configuration (such as graphite-like rings or nets) which alternate hexagonally close-packed Zr layers. Each metal atom is surrounded by other six equidistant metal neighbours in its plane and 12 equidistant B neighbours (six above and six below the metal layer). Each B is surrounded by three B neighbours in its plane and by six metal atoms (three above and three below the B layer).

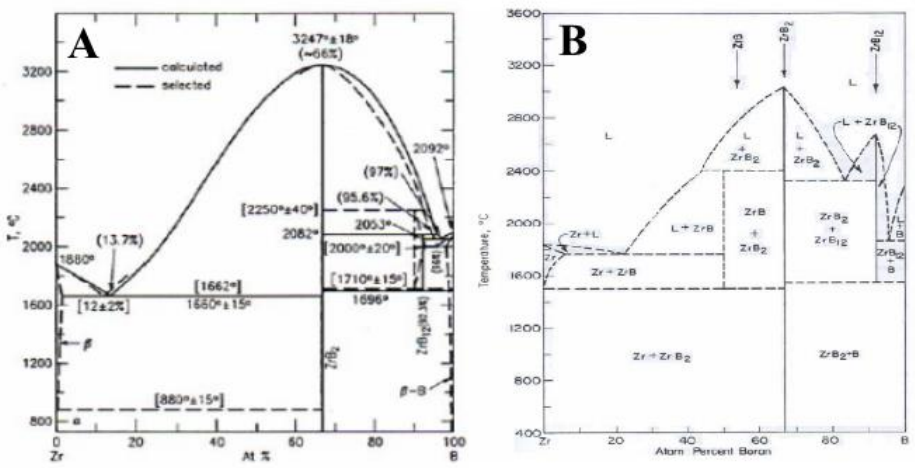

Figure 2.12 Phase Diagrams for Zr-B system from A) McHale and B) Clougherty

In Figure 2.12 is reported the phase diagrams for Zr-B (26; 27) : ZrB_2 is the main phase with a melting point of 3247°C. The very high melting point, the slow kinetic of solid state reaction and the Boron vaporization are some of the key factors which make difficult the detailed investigation of phase equilibrium diagram of Zirconium-Boron system.

Clougherty et al. (27) reported the Schedler's phase diagram of this system shows the presence of a ZrB phase and a ZrB_{12} phase which exists between 1700°C and 2680°C (Figure 2.12B). From Figure 2.12A it was evident that the solidus temperature of ZrB_{12} is 2250°C and it shows a peritectic decomposition, whereas Figure 2.12B reported an eutectic mixture of ZrB_2 and ZrB_{12} with a eutectic temperature of approximately 2300°C (28; 29).

According to Aronsson (30) when ZrB phase has been observed, considerable O, C or N might have been present in order to stabilize the cubic structure, which is generally considered to be the ZrB phase.

The ZrB_2 phase shows a very limited range of homogeneity and, as predicted by the phase diagram in Figure 4.2A, off-stoichiometric compounds will contain either free Boron or zirconium below 1500° C and may contain ZrB and ZrB_{12} in the range of 1500° to 2200° C.

ZrB_2 can be synthesize by different techniques:

- Reductions process
- Chemical synthesis
- Reactive Process

Several are the reduction processes which can be used in order to synthesize Zirconium Diboride. Carbon and Boron are the most common reducing agents, but also Boron carbide or aluminum can be used as well as combinations of reducing agents. Examples of the reactions (2.1-5) are shown below:

Carbothermal $ZrO_{2(c)} + B_2O_{3(l)} + 5C \rightarrow ZrB_{2(cr)} + 5CO_{(g)}$ (2.1)

Borotheral $ZrO_{2(c)} + 4B_{(c)} + 5C \rightarrow ZrB_{2(c)} + B_2O_{2(g)}$ (2.2)

Aluminothermal $ZrO_{2(c)} + 3B_2O_{3(l)} + 10Al \rightarrow 3ZrB_{2(c)} + 5Al_2O_{3(c)}$ (2.3)

Boron Carbide $7ZrO_{2(c)} + 5B_4C_{(c)} + 10Al \rightarrow 7ZrB_{2(c)} + 3B_2O_{3(g)} + 5CO_{(g)}$ (2.4)

Combined $2ZrO_{2(c)} + B_4C_{(c)} + 3C_{(g)} \rightarrow 2ZrB_{2(c)} + 4CO_{(g)}$ (2.5)

Carbothermal reduction is generally used to produce commercial ZrB_2 (and HfB_2 too): this process is strongly endothermic and thermodynamically favourable at temperature higher than 1500°C.

Moreover most of reported reactions also produce significant volumes of various gases, which must be removed in order to proceed to complete them. B_2O_3, carbides and Carbon are common impurities present in the final powder.

Reduction with B_4C (Reaction 2.4) has also been used to produce diborides and diboride composites. Also in this case the reaction is endothermic, but it become favourable at

temperatures lower than the reduction reactions with Carbon and Boron (Reactions 2.1, 2.2 and 2.5).

Chemical syntheses adopted to produce diborides include solutions, reactions with Boron-containing polymers and pre-ceramic polymers.

ZrB_2 can be synthesized by reacting anhydrous chlorides with sodium borohydride ($NaBH_4$) above 500°C under pressure; using this process it is possible to obtain TiB_2, HfB_2 as well as ZrB_2 crystalline particles with size 10–20 nm.

Among the reactive process the simplest method to produce ZrB_2 is the reaction of elemental precursor powders:

$$Zr + 2B \rightarrow ZrB_2 \qquad (2.6)$$

The use of direct reaction was used only in the past and nowadays is not common due to difficulty to have high pure Boron available. Moreover the high Oxygen affinity of Zirconium implies that the reaction must be carried out in inert or reducing atmospheres in order to prevent the formation of oxide impurities.

The reaction is favourable in a wide range of temperature, but it results very exothermic so, if conducted in an uncontrolled manner, the heat can ignite a self-propagating reaction and generate temperatures so high to promote local melting of the Zr (T_m is 1850°C).

The main use of this reaction (Eq 2.6) is to synthesize ZrB_2 by self-propagating high-temperature synthesis (SHS), which is a kind of combustion synthesis: the involved high heating and cooling rates produce high defect concentrations in the resulting material, which can improve sinterability of ZrB_2 respect those obtained by more conventional reduction process. Recently it has been developed a method adopting a slower heating rate and longer isothermal conditions to react fine powders of Zr and B without the ignition of SHS reactions. In this way it is possible to obtain ZrB_2 powder at temperature of about 600°C.

Due to the high melting point and the covalent character of the bonding the sintering of ZrB_2 required very high temperature just to obtain a densification degree between 70% and 90%; different methods have been used for the densification: hot pressing, spark plasma sintering, reactive hot pressing and pressureless sintering.

Historically *Hot Pressing* was the most common method (31; 32); the sintering of ZrB_2 required temperature higher than 2000°C and moderate pressure between 20 and 30 MPa; the attempts to reduce the sintering temperature up to 1800°C implied the use of very high pressure (more than 800MPa).

The main factors which influence the sintering of ZrB_2 by hot pressing are:

- The particle grain size. It has been found that hot pressing of coarse ZrB_2 powder (average grain size 20μm) at temperature of 2000°C and a pressure of 20MPa lets to reach a relative density of only ~73% (33), while a relative density of ~91% was obtained using a finer ZrB_2 powder (d≈2.1μm) under the same sintering conditions (34). Furthermore, it was possible to obtain fully dense material using a starting attrition-milled ZrB_2 powder (average particle size of $d \leq 0.5\mu m$) and performing an hot press treatment at 1900°C and 32MPa for 45 minutes. The lower HP temperature was attributed to reduction of starting particle size from microns to sub-microns value.
- Oxygen impurities such as B_2O_3 and ZrO_2 are often present on the starting powder surfaces and it have been shown to inhibit densification and to promote grain growth in the non-oxide ceramic systems. Various sintering aids (discussed later in Section 5.1) act with impurities improving the sintering process.
- Presence of sintering aids.

Research in the late 1960s on metals (Zr, Hf, Cr, Y, and Al) and ceramic (SiC,$MoSi_2$, and TaB_2) additions to ZrB_2 showed not only an enhancing in densification, but also a significant improving of oxidation and thermal stress resistance (especially in the case of diborides containing SiC, C, or SiC plus C).

Recent researches using commercial ZrB_2 powders and then sintered by HP has typically included non-reactive additives such as SiC or liquid phase forming additions such Ni, Si_3N_4, or $MoSi_2$. The high HP temperatures and pressures of historic studies are not necessary using finer starting powders (with sub-microns dimension) and the addition of aids which are able to minimize grain growth, produces a liquid phase or result in solid solution formation. The sintering temperature can be reduced thanks to the use of Si_3N_4, AlN, $MoSi_2$ and Ta_5Si_3 but pressures of 20–50 MPa were in any case required

Spark Plasma Sintering is one of the most recent advanced processing techniques developed for densifying ceramic materials (35; 36). Although SPS is similar to Hot Press technique, in place of indirect heating, the applied electrical field heats the die and the powder compact.

The main advantages in adopting SPS are: enhance densification of poorly sinterable ceramics, by the simultaneously application of a uniaxial load and a direct or pulsed electric current to a powder compact; moreover the grain growth of starting materials results reduced thanks to a shorter sintering time (it requires some minutes) compared to Hot Pressing or Hot Isostatic Pressing.

Guo et al. reported the processing the ZrB_2–ZrC–SiC system with different relative amount of the three compound : fully dense compacts with fine and homogenous microstructure were obtained after a SPS cycle at 1950°C applying a pressure of 30MPa for 2 min (37).

The reason why SPS technique can enhance densification of ZrB_2 is still the subject of intense debate. However *Guo* suggested (38) that enhancement is most probably due to an efficient heat transfer, the use of comparatively high pressure, the presence of an electrical field (use of DC pulses) and the presence of local spark discharges generated between the powders under high-energy electrical pulses.

Reactive Hot Pressing has been identified as a potential route to produce ZrB_2 ceramics with a very low level of impurities using lower sintering temperature.

There are two processes involved in RHP: *in situ* reaction of precursor powders and the densification; in this way both synthesis and densification can be combined into single-step.

Recently Reactive Hot Pressing has been used to produce both ZrB_2 ceramics by using Zr and B precursors (39) as well as to fabricate the ZrB_2-based composites with the addition of SiC and/or ZrC by using Zr, Si and B_4C precursors (40).

In particular the presence of SiC had a significant effects on both the densification temperature and the resulting microstructure (40): Zr, B, and SiC as precursors submitted to a RPH treatment at 1650°C let to obtain a sintered material with a relative density of 95%. In addition to the reduction of sintering temperature respect to those required to obtain ZrB_2 produced by the same method or using conventional Hot Press, the microstructure showed much smaller ZrB_2 grain size. The reduction in sintering temperature for ZrB2–SiC by RHP may be linked to two causes: firstly the minimization of oxide impurities such as B_2O_3, ZrO_2 and moreover the use of fine crystallite/ particle sizes.

Conclusively the Pressureless Sintering is the last method considered to densify ZrB_2 based ceramics. This method has been chosen for the sintering of multilayer in this work of thesis; a detailed study on the results obtained using this process will be discussed in Chapter 5.

Due to the high pressures required for densification, a sintering process which not implied the assistance of pressure was considered unlikely or almost impossible until the late 1980s, when studies of pressureless sintering actually began to show results. Compared to Hot Pressing, the PS process showed various advantages: the possibility to produce almost-net-shape ceramic parts with complex geometries using standard powder-processing methods; this imply a reduction of processing costs. However this method inevitably required the use of sintering aids (Section 5.1).

Following the XRD measurement were performed on the starting powder (Figure 2.13) to verify the presence of impurities on its surface.

All peaks correspond to ZrB_2 so there aren't other detectable phases on the starting powder.

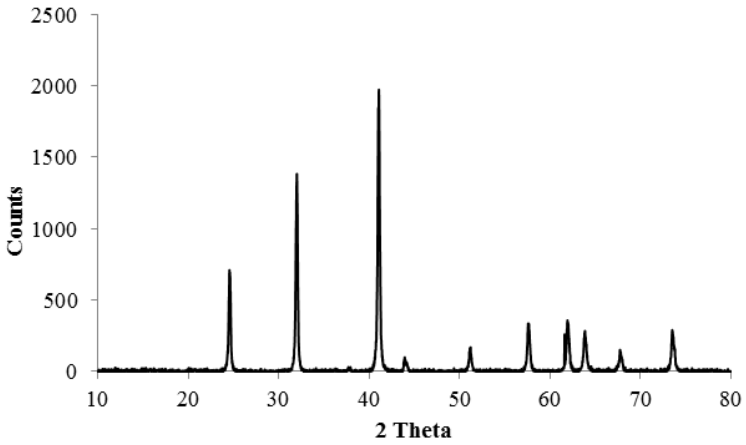

Figure 2.13 XRD on starting ZrB_2 powder.

Chapter 3
Material processing: Tape casting

3.1 Tape casting technology

The development of tape casting technique for the ceramic film production comes from the 1940s; firstly this method was well known and had applications in other contexts such as paper, painting (to test the covering power of paint formulations) and plastics industries (41).

Glenn Howatt patented this technique to produce thin ceramic sheets with controlled thickness (42) "Forming ceramic materials into flat plates, especially useful in the electric and radio fields": This is nowadays the main application even if it extends very far beyond the uses imagined in 1952.

This method involved the preparation of a suspension based on a mix of ceramic powders and organics components (dispersant, binder and plasticizer) in a proper solvent, which was spread or "cast" on a flat moving support. After the casting phase, the solvents were slowly evaporated in order to obtain the so called "green ceramic tape" in form of a thin and flexible sheet.

The thickness for green tapes usually goes from 5 microns to some millimetres (43).

The tape casting technique could be applied not only for ceramic sheets production but, adopting proper modifications, also to metals.

For example slip casting is probably the processing method with greater similarities with tape casting because of the starting conditions are the same but it involves the use of both ceramic or metallic powders. However, they mainly difference in the drying conditions: slip casting uses a Paris mold in order to absorb the water vehicle while in tape casting a plastic carrier film is used and the drying is conducted by solvent evaporation from the surface; moreover in this technique the use of nonorganic solvents is very common in order to allow a fast drying process.

The literature reported that for his first applications Howatt used a porous plaster to apply water as liquid media; then in 1950s the American Lava Corporation introduced the favourable use of a plastic carrier or "non-absorptive moving polymer carrier" which allowed the mass production and also the storage of the green tape rolls.

Figure 3.1shows the basic apparatus used for tape casting; it is constituted by:

- The reservoir where the slurry is placed before the casting phase;
- The doctor blade which is the most important component; "doctor" indicated a scraping blade able to remove the excess of substance from a moving surface being coated (43).

Doctor blade indicates the moving port of the slurry reservoir which, once opened, allows the slurry being cast on a moving carrier polymer film and in addition regulates the amount of the

slip by removing the excess of suspension during the process. The thickness of the tape is fixed by selecting the doctor blade opening gap.

- The slip with selected chemical composition
- The carrier material

The casting rate is fixed and controlled in order to obtain a homogeneous film.

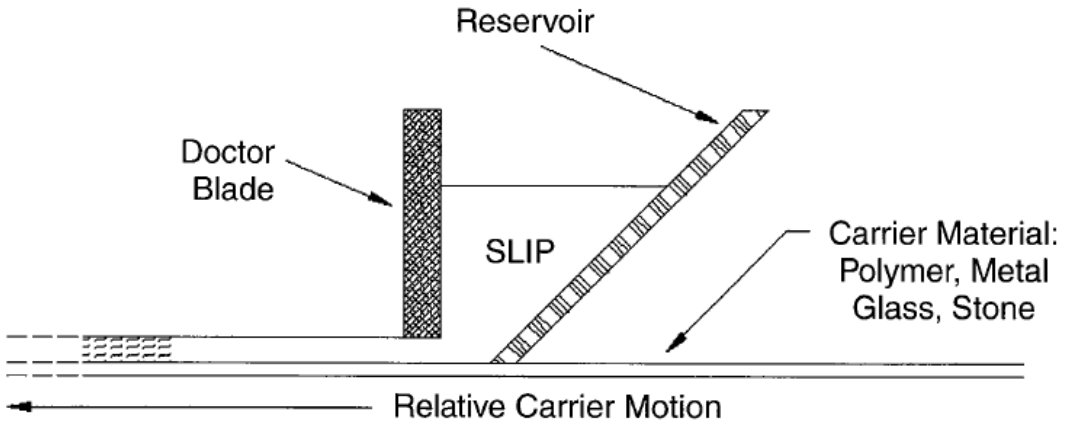

Figure 3.1 Basic scheme of a typical tape casting apparatus

There are a lot of parameters to take in account during the tape casting process: the slurry formulation, rheological properties of the slip, the gap of the doctor blade, the speed of the carrier, the reservoir depth, the shape of the doctor blade and the drying chamber (that is strongly dependent on the type of solvents used in the formulation); all these factors greatly influence the properties of the resultant green tape.

It is one of the best methods adopted in order to obtain a large, thin and flat ceramic layer with low variation of density along the casting direction and an homogeneous pore distribution (if present); it can be used for the production of multilayer structures with all similar layers or alternating layers with different chemical composition. An important advantage of tape casting is its low cost-effective application both for industrial and laboratory testing techniques.

This method shows a linear relation between the slurry, the green tape and the sintered product: the homogeneity and the stability of the slurry determine the properties of the green body such as the packing of the particles; moreover they have influence on the sintering process and then on the characteristics of the final products (44).

Clegg et al. (45) originally reported the processing and characterization of SiC/C multilayer mainly in term of mechanical properties: SiC powder with an addition of 0.4 wt.% B was firstly mixed, pressed into a 2-mm-thick-sheet and then rolled into flat sheets (about 200 μm in

thickness). After cutting, this thin sheets were coated with graphite, stacked and pressed to form a plate 2 mm thick. After debinding and sintering treatments, a SiC/C multilayer was obtained; its relative density was measured around 98%.

The main difference between a monolithic and laminate material was found in term of load/deflection behaviour: the former behaved in a linear elastic trend until catastrophic failure. On the other hand the laminate deformed with a linear elastic fashion until the crack reached the same stress intensity as the monolithic SiC, and then the cracks deflected along the SiC-C interface. So the apparent toughness increased from 3.6 to 15 $MPa \cdot m^{1/2}$, and the work of fracture increased from 28 to 4625 J/m^2.

This is the main advantage of a multilayer structure respect to a monolithic one; in this PhD thesis laminates based on ZrB_2/SiC system were processed and characterized in term of physical, mechanical and thermal properties. Moreover, thanks to the possibility to design multilayer structures with different configuration, a structure containing composite layers in between SiC ones was also investigated.

3.2 Materials and processing

The different components which form the slurry highly influence the properties of both green tape and final sintered products; for this reason it is necessary to study in details all aspects linked to each constituent. In the following sections the materials selection process and the properties of each of them will be discussed.

3.2.1 Powders

In any fabrication process the most important element is the starting powder because it mostly influences the final product properties: after the removal of organic components and the densification process, the powders are the only elements of the batch left and they will define the products performance (41). The criterion for its selection mainly depends on the requirements needed for the different applications and then the potentialities for using in specific manufacturing techniques. Especially in the case of tape casting it is necessary a complete characterization of these powders in order to provide a proper chemical formulation.

The most important criteria to be considered are: chemical purity, particle size, distribution and shape, surface area, density, agglomeration/segregation degree, homogeneity in composition, sintering activity, ability to be mass-produced, compatibility with other slip components and costs of production.

In fact the optimization of the slurry formulation and its preparation is necessary in order to avoid inhomogeneity and segregation and moreover to promote the packaging of the particles in the next phases.

The presence of impurities can inhibit and modify the sintering mechanism; for this reason it is important to know and eventually check the level of impurities present on the starting powder.

The effect of particle size and distribution have been widely discussed in literature (46; 47; 48).

The tape casting process takes advantage of gravity and shrinkage of organic components during drying phase in order to generate a packed system; in order to obtain the highest possible green bulk density it is fundamental the selection and control of the particle size and distribution.

Mc Geary (49) reported a detailed theoretical study on the packaging of the powders: he predicted a maximum packaging of 74 vol.%, for mono-size particles with ideal sphere shape without Van der Waals interactions between particles. The arrangement have to be octahedral or tetrahedral, with a coordination number of 12. For coordination number of 10, 8 and 6 theoretical calculation of the packing densities would be 69.8 vol.%, 60.5 vol.% and 52.4 vol.% respectively. Experimental calculations indicates a packaging around 58 to 65 vol.% when the coordination number is 8. For liquid suspensions, a very good approximation for packing density values is established around 40-45 vol.% with particles of approximated 1 μm of diameter (50).

Shanefield (51) showed that in commercial powders with a standard particle size distribution, the best packaging factor correspond to about 55% of theoretical.

This relative low value was due to the fact that in most of cases the powder processing method favoured the obtaining of very fine particles without taking into account that to a finer powder corresponded an higher surface energy and so a greater driving force during sintering process.

In this thesis it will be showed and underlined (Section 5.3) the importance and the influence of starting powder particle size in preparation of ZrB_2/SiC based multilayer integrating layers with different composition.

The surface area is another very important parameter because it gives an indication on the best interaction factor among components in order to have a good dispersion, lubrication or binding qualities: in fact there is a direct relation between the total powders area and the amount of organics needed. Moreover the selection of the proper dispersant/solvent combination, as well as the proper dispersant (and its concentration), are all critical factors for powders with very high surface-area (43). In general powders with high surface area, that means above 20 m^2/g, are much more difficult to work with, the ideal range is between 5 and 15 m^2/g.

There are different powders processing methods such as the mix of oxides in a solid solution carried out by calcination of premixed oxides, hydroxides and carbonates in a temperature range

of 500-1000°C. Precipitation and co-precipitation are other important techniques through it is possible to obtain hydroxides and/or oxalates from water-based solutions (Bayer process for the fabrication of Al_2O_3).

Almost all these mentioned techniques leave them in an agglomeration state so it will be necessary a second step in order to de-agglomerate them: a reduction of the particle size is so required in order to avoid dispersion problems in the slip, inhomogeneity and/or lower consolidation of the green tape and obtain a final sintered product free of porosity.

This dispersion milling phase could be necessary also in order to homogenize the particle size of different powders used in a unique system. In general, this process can be carried out by ball milling (wet or dry), vibratory ball (wet and dry too) , attrition milling in wet ultrasonic dispersion technique and ring gap mill.

The density of the powders is another important factor in powder selection. During tape casting process is also necessary to maintain an high quantity of particles in suspension and, depending of the particle weight, is possible to determine the particle size required for a specific formulation.

3.2.2 Solvents

Tape casting is a fluid forming process and the component which lets the powders behave as a liquid and flow on a support is the solvent; this liquid element is also used in order to homogeneously distribute the other ingredients in the slurry producing a uniform mixture (52)

The solvent or mixture of solvents used to formulate the slurry composition have to:

- Dissolve the organics components of the slurry such as binder and plasticizers.
- Disperse the powders (ceramic or intermetallic ones).
- Provide an uniform distribution of all other ingredients in order to obtain an homogeneous mixture of them.
- Give to the suspension the desired rheological properties such as a suitable viscosity.
- Provide a quick evaporation at moderate temperature (often the drying phase is conducted at room temperature).
- Ensure a good consolidation of the tape.

Another factor could influence the solvent selection is the production costs and the effects on health and environmental impact. Some solvents such as Xylenes, MEK, toluene and benzene have been banded for industrial use in same countries because of their carcinogenicity and in addition for their long term effects on the human body.

All organics present in the slip need to be dissolved, for this reason it is widely used a mixture of solvents in order to increase the ability to dissolve (53) and at the same time to control the drying

rate, the costs and the safety. Some studies determined that when using a mixture of two types of solvents, respectively classified as "kinetics solvents" and thermodynamic solvents", it is possible to use lower amounts of solvents compared to the amount required using only one; this is due to the combined effect of an efficient interaction and a faster evaporation.

This is the case of the so-called azeotropes, introduced by Boch and Chartier in 1988: they are a mixture of solvents with the suitable feature to acts as one; they show an exceptionally good solubility and the evaporation rate is quite fast.

Table 3.I shows the most used solvents for tape casting.

Solvent	Boiling point [°C]	Evaporation rate [n-butylacet.=1]	Heat of vaporization [J/g]	Viscosity at 25°C [mPa s]	Polarity Et(30) [kJ/mol]	Relative permittivity	Surface tension [mN/m]
Water	100	0.16	2260	1	264	80	73
Methanol	65	3.70	1100	0.6	232	33	23
Ethanol	78	2.65	860	1.2	217	24	23
Butanol	118	0.44	578	2.9	210	18	22
Benzyl alcohol	205	<0.01	415	5.8	213	13	35
Isopropyl alcohol	82	2.08	578	2.4	204	18	22
Ethylene glycol	198	<0.01	800	20	236	37	48
Ethyl acetate	77	4.95	360	0.4	160	6	23
Butyl acetate	127	1.00	310	0.5	155	5	26
Methyl ethyl ketone	80	4.59	444	0.4	173	18	25
Acetone	56	7.70	524	0.3	177	21	25
Trichloroethylene	86	4.90	243	0.4	150	3	25
Toluene	110	1.96	352	0.6	142	2	29
p-Xylene/o-xylene	140	0.55	327	0.7	141	2	28
Cyclohexanone	155	0.24	427	0.8	171	18	35

Table 3.I Most common used solvents for tape casting formulation.

Most of tape casting slurries are prepared with nonaqueous solvents and, among them, the organic ones are the most used.

Water is recommended because is very cheap and it is one of the most environmental friendly solvents, nevertheless it is not the most common used because of the difficulty in finding water-soluble binders and plasticizers. In addition adopting aqueous suspension formulation the casting speed increases and the evaporation rate (drying step) decreases: it affects the production cost because of a reduction in the production capacity.

The formulation of the slip starts with the selection of the powder because, as it was mentioned previously, it has a significant influence on the final product properties; after that it is necessary to choose the binder(s) and then, the liquid to dissolve the selected binder(s).

The chosen solvents must not adversely affect the powders (43) and all organics present in the slip need to be dissolved as well. For this reason the investigation on the interactive force between the liquid media and the rest of the suspension components is required; these forces can

be classified based on the atomic origin: Ionic force, dipole/dipole force, hydrogen bonding forces and Van Der Waals forces.

These kind of interactions can affect the performance of the solvents; so it's important to choose a liquid media showing a good compatibility with the binder. For example they should have similar functional groups because their polarity have an effect on the manner in which they interact (41).

3.2.3 Surfactants

The role of surfactant in ceramic processing is very important; the literal meaning is SURFace ACTive AgeNT. They include different chemical aids like dispersants, deflocculants, wetting agents, flattening agents, flocculants and many others. In general it is an additive which actively modifies the particles surface to give them the desired properties such as a surface charge, a surface energy or a specific chemical activity. In this case, the term surfactant is regarding to the dispersant agent used to control the natural agglomeration of the ceramic powders into the slurry (3), so its addition help the dispersion of particles and hold them in an homogeneous suspension. The dispersant action can be performed by steric hindrance or ionic repulsion.

The natural tendency of forming powder agglomerations is due to attractive and repulsive forces acting on small particles which lead them to stay together.

These forces are the Van der Waals ones which are attractive; they are generated by the interaction of atoms with permanent or induced electron/nucleus dipoles on the particles surface.

On the other hand the repulsive forces can have both electrostatic and steric nature. The first ones occur when the particles have the same the electric charge so they magnetically repel one each others. It is most common using polar solvents such as water-based slurries.

The second ones are predominant in non-polar organic solvents, where the electrostatic forces should be smaller. The mechanism involves the separation of particles by putting a coating on one particle which physically avoids another particle coming into contact with it. Organic long chained macromolecules are often used in both aqueous and nonaqueous system to favour this mechanism.

Most of the dispersants used in solvent-based tape casting are of the steric hindrance type: the idea is to obtain an electrosteric stabilization of the particle powders in the first step of the process. This mechanism can be briefly explained as follows: there are macromolecules formed by *hydrocarbons with acid or basic head groups or of amphipathic copolymers which attach themselves to the particle surface while the rest of molecules are extended into the liquid medium* (41). These hydrocarbon chains form a network surrounding each particle and keep them separated from the others.

The menhaden fish oil (MFO) is the most used surfactant for tape casting (it is also used in this work of thesis), due to its effectiveness (the deflocculating ability is due to the large variety of fatty acid esters it contains), cost and environmental compatibilities (it is a natural additive). It can be formed by more than 20 types of fatty acids such as linoleic, palmitic, myristic, stearic (41); the particle surfaces are attached to the long-chain of acid carboxylic groups.

Another example of common used dispersant/deflocculant is the Phosphate Ester.

A second function of dispersant is its action as deflocculant: the agglomerates tend to trap air in powder interstitial spaces; if these particle groups are not broken the air could form bubbles in the green tape or even pores in the sintered material.

It is well-known that binder overlaps the surfactant effects; nevertheless the use of a dispersant improves the working place for the binder that can act on each particle, just separated by the dispersant/deflocculant, instead of envelop an agglomerate and makes it a particle group.

3.2.4 Binder

The binder supplies the network which hold the entire chemical system together in the casting process; when the solvents evaporate, the green tape forms a matrix with this organic component. Then when the powders are entrapped into the chains, they can produce a network between them leaving a residual porosity resultant from the drying process.

Being the only continuous phase in the green tape the binder has an important effect on its properties such as flexibility, strength, plasticity, laminability, durability and smoothness (43).

Binder is the one of the most important component in a slurry formulation and then in the tape processing route. For this reason it is necessary to identify all the parameters to select a proper casting binder such as solubility, viscosity, cost, strength, Tg or ability to modify Tg, firing atmosphere of the powder, ash residue, burnout temperature and others (41; 43).

There are many different binders widely used for slip formulation; they can be classified in two groups: polyvinyls (vinyl) and polycrylates (acrylic). Both of them show a good film forming capability, but they differ in the burnoff/removal properties under different atmospheres. In general, there are long-chain polymers or precursors (monomers or emulsion particles) that become long-chain polymers during drying (41; 43).

There is a third group of binder called cellulose which is less common used, especially in the formulation with water as a solvent.

3.2.4.1 Vinyl

Vinyl binders include many compounds widely diffused and known both in consumer market and industries. Among them polyvinyl chloride (PVC) is the most commercially known, it has

applications in many different industries such as fabrication of water and sewer pipes or lawn forniture.

Moreover polyvinyl alcohol (PVA) used in food and textile industries and polyvinyl butyral (PVB or Butvar) used in the textile industry and for the production of safety glass are usually used in the slurry formulation, even more than PVC.

Depending on the furnace gaseous atmosphere used in the process, the vinyl can react: in oxidizing atmosphere, the burn-out could be complete because these polymers burn at high temperature and require Oxygen from the gaseous atmosphere; the residual Carbon from this process interacts with Oxygen to form CO and CO_2. Wet hydrogen, nitrogen and cracked ammonia atmosphere can also provide good removal of the binder.

In presence of non-oxidizing atmosphere the decomposition of the binder releases Carbon (ash) (41).

3.2.4.2 Acrylics

The main advantages in using acrylics binders are: the cost effectiveness, non-ash residue in neutral or reducing atmospheres, strength, solubility, and ability to modify Tg.

Acrylics show a different decomposition mechanism respect to vinyls; in fact they break down, unzip their chain and evaporate (43). This mechanism is favourable in reducing or neutral atmosphere with only little amount of Carbon residue formation.

Polymethyl methacrylate and Polyethyl methacrylate give a very good strength to the green tape at low concentrations.

Both Vinyl and Acrylics can be plasticized by several additives.

3.2.4.3 Cellulose

These polymers have been mostly used in water-based slurries because of most of cellulose polymers are water soluble. There exists several considerations about these compounds; the first one is the thickening properties, since the cellulose requires more liquid medium providing a low solid loading slip that raise up the drying shrinkage, cracking and porosity of the tape. Another problem is related to the high quantity of air entrapped into the slurry that generate high amount of bubbles during casting, and high porosity or flaws in the green tape (43).

3.2.5 Plasticizer

The last organic additive is the plasticizer, which has the role of offering flexibility and/or plasticity to the green tape; this means that it is possible to bend the tape without damage or crack it.

The mechanism consists in increasing binder(s) workability and flexibility (14).

The molecular weight of a plasticizer has to be around 300 and 400 with a boiling temperature of more than 200°C, moreover it has to show chemical and physical stability, low cost and no hazardous environmental impact.

Moreover the plasticizer has to interact with the binder allowing the binder polymer chains to move inside the tape matrix without breaking the matrix itself.

Plasticizers are classified in two types depending on the mechanism that can provide flexibility and/or plasticity to green tape.

The first one, "Type I" is a plasticizer that *soften the polymer chains between particles allowing them to stretch*; while plasticizers of the "Type II" can add plasticity (plastic deformation) to the green tape matrix (43).

The first class of plasticizer is a chemical which soften the polymer chains between particles allowing them to stretch more easily. They modify the glass transition temperature (Tg) by shortening the polymer chains allowing to have greater flexibility at a given temperature; moreover the plasticizer is able to dissolve the binder: the addition of a component such as phthalates can in fact partially dissolve it.

The addition of different amounts of Type I plasticizer has different effects on the green tape: large amount produces a tape with higher elasticity; in this case is possible to stack the layer without using any adhesive material because the surface is particularly sticky. However an excess of plasticizer causes the adhesion of the polymer to the carrier surface (43).

The second class of plasticizer interposes between the polymer chains hindering the formation of molecular bonds between the chains and giving them higher mobility in the dry tape: the resultant effect is the lubrication of the matrix.

Other capabilities of the Type II plasticizer are to avoid cracking problems during drying of the green tape, to reduce the yield stress and to increase strain to failure. Rheological parameters such as shear behaviour and shear viscosity will be benefited: in fact the lubrication effect increases the mobility within the slurry before drying, improving the motion of the fluid through the blade during cast. Furthermore, the lubrication makes easy the release of the film from the casting support, because the bottom side of the tape results lubricated by the plasticizer. An abusive use of a type II plasticizer may reduce the yield stress providing deformation under its own weight (43).

Chapter 4
Processing methods and experimental techniques

4.1 Processing of ZrB_2/SiC laminates by tape casting

ZrB_2/SiC based multilayer specimens were produced by tape casting technique. The processing method involves different steps such as slurry preparation, tape casting, green samples assembly, debinding and pressureless (or spark plasma) sintering.

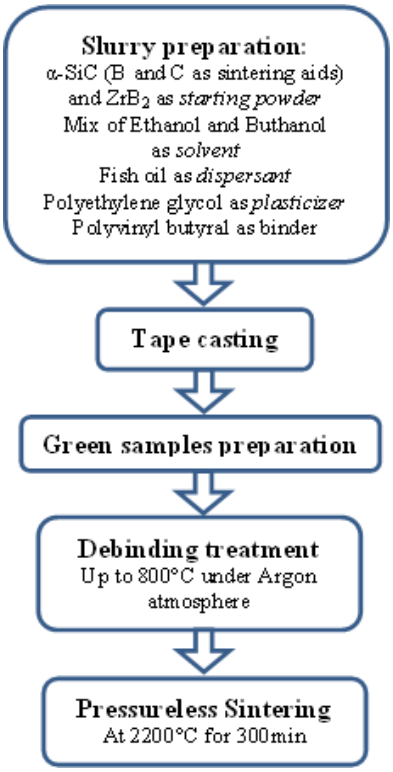

Figure 4.1 Preparation process of ZrB_2/SiC laminates.

4.1.1 Slurry preparation and tape casting

Commercially available Zirconium Diboride powder (Grade B, H.C. Starck, Germany with an average particle size of 2.25 μm) and α-SiC powder (H.C. Starck UF-15, Germany with a mean particle size of 0.55 μm) were used in this study as starting powders for the fabrication of laminates.

The effectiveness of several sintering aids was compared looking for an additive that can be widely used both for pure ZrB_2 and for composites based on ZrB_2/SiC system. These sintering aids were added to the ceramic materials using proportions suggested by the literature:

B_4C (H.C. Starck, 0,8 μm), VC (H.C. Starck Grade HV 160, 1,5- 2 μm), TiC (H.C. Starck Grade HV 120, 1-1,5 μm), Si_3N_4 (H.C. Starck Grade M11-A), $ZrSi_2$ (*Alfa Aesar, -325mesh, ≈44μm)*, C (Alfa Aesar flake 7–10 μm) and B (H.C. Starck amorphous grade I, 1–2 μm) were tested as well

as some their combinations. Carbon and Boron were always used as sintering additives for SiC; they were successfully added in order to improve both its densification and mechanical properties of resulting materials (16; 17).

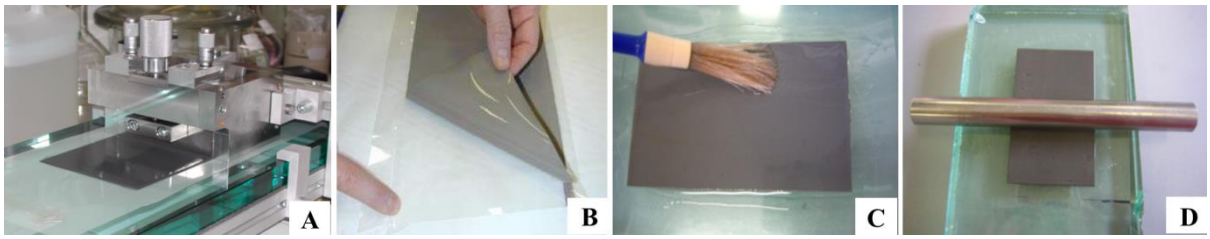

Figure 4.2 Multilayer preparation: A) Casting of the slurry, B) Green tape, C) and D) Stacking of layers

Slurry components		Composition of SiC slurry (wt%)	Composition (wt%) of SiC/ZrB_2 slurries designed to obtain composites with SiC decreasing from 90 to 10 vol%	Composition of ZrB_2 slurry (wt%)
Solvents	Ethanol	19.9	Progressively decreasing from 19.3 to 15.6	15.3
	Buthanol	30.5	Progressively decreasing from 29.6 to 24.1	23.5
Dispersant	Fish oil	0.1	0.1	0.1
Powders	SiC	33.6	Progressively decreasing from 29.3 to 2.6	-
	B	0.3	Progressively decreasing from 0.3 to 0.03	-
	C	1.0	Progressively decreasing from 0.9 to 0.1	-
	ZrB_2	-	Progressively increasing from 6.3 to 45.9	49.9
Binder	Polyvinyl Butyral	9.6	Progressively decreasing from 9.3 to 7.6	7.4
Plasticizer	Polyethylene Glycol	5.0	Progressively decreasing from 4.9 to 3.9	3.9

Table 4.I Composition of the slurries submitted to tape casting

The above mentioned ceramic powders were dispersed in a mix of Ethanol (≥99.8%, Sigma-Aldrich, Germany) and Buthanol (≥99.4%, Sigma-Aldrich, Germany) as solvents and Fish oil (Afom medical, Italy) as powders dispersant and then were firstly mixed for 24 hours in an alumina jar with alumina milling balls. Afterward, plasticizer (polyethylenglycole, Bisoflex 102 Cognis) and binder (polyvinilbutyral, Butvar B76 Solutia) were added into the above slurry and further mixed for 48 h.

Slurries with composition from pure SiC to pure ZrB_2 and composite with different ZrB_2:SiC ratio were processed as shown in Table 4.I.

After degasing, the slurry was transferred in the reservoir of the tape casting machine and casted on a moving Mylar support (Figure 4.2-A), The layer thickness was controlled by selecting proper blade gaps (the standard value is 1,0 mm) as well as casting rate (usually 100 mm/min).

4.1.2 Green sample preparation

The as casted slurry is let to dry on the flat surface of tape casting apparatus in order to remove the organic solvents by controlled evaporation in saturated of solvents air at room temperature. The width and thickness of green layer were 100 mm (using the small machine) or 200 mm (in case of use of big apparatus) and an average thickness of about 200 - 250 µm.

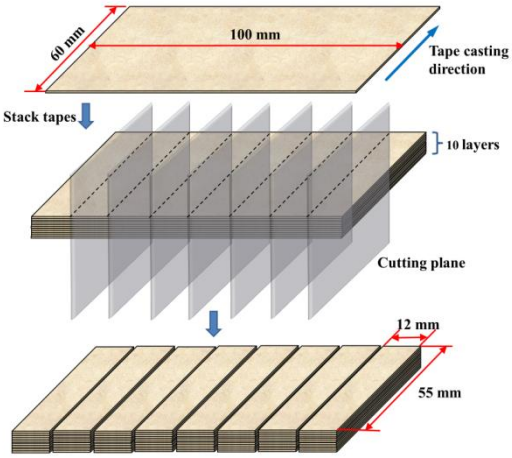

Figure 4.3 Preparation process for green specimens for bending test

The green tapes of SiC, ZrB_2 and the composites (Figure 4.2-B) were then cut in the proper shape and then carefully detached from the plastic support. The multilayered were obtained by painting a gluing solution made of water, ethanol and polyvinyl alcohol (PVA) in the proportion 10g:10g:1g before stacking next layer (Figure 4.2-C). A mandrel is passed on the sample in order to let the successive layer adhere without the formation of air inclusion (Figure 3.3-D). Ten layers are stacked in order to reach after sintering; the number of layer can be changed in function of the requested thickness for the different mechanical and thermal tests. Green samples with different shapes and dimensions were prepared (bars, plates and disks); for example Figure 4.3 shows the preparation of samples for three points bending test.

It should be noted that the roughness of lower-side (in contact with Mylar film) and upper-side (in contact with air) was different due to the presence of the Mylar film, as shown in Figure 4.2-B, the rougher upper-side was always pasted with the smoother lower-side of another tape during stacking.

4.1.3 Debinding process

Laminates were then submitted to a debinding treatment in order to remove the organic components (binder and plasticizer deriving from the slurry and PVA coming from the gluing solution). Debinding is carried out by heating up to 800 °C into an oven under an inert Argon atmosphere in order to prevent oxidation (Figure 4.4).

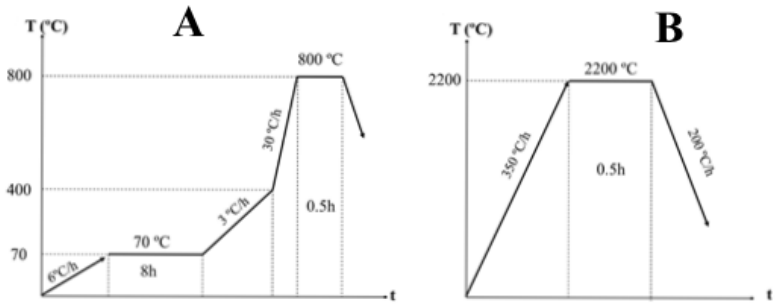

Figure 4.4 A) Debinding treatment and B) Pressureless sintering cycle

The specimens were debinded on a graphite support and a graphite weight is put over them in order to avoid sample deviation from planarity. Slow heating up is necessary in order to limit the rate of gaseous evolution due to organics decomposition thus preventing bubbles formation or specimen rupture which may be induced if the gaseous evolution is too rapid and violent.

The decomposition behaviour of binder, plasticizer and PVA was tested by TGA from room temperature to 800 °C at a constant rate of 1 °C/min in flowing Argon atmosphere (50 ml/min); the results are shown in Figure 4.4.

Most of the organic components would be decomposed before 400 °C (Figure 4.5). Moreover, the organic materials will decompose faster and completely at comparatively lower temperature under slower heating rate (3 °C/h).

It must be noted that the decomposition of organics was not complete and a certain amount of carbonaceous species remain in the sample. By thermogravimetric investigation we observed that at 800 °C the weight losses of a SiC multilayer specimen is about 72.2 wt%. Thus allowed to estimate that binder, plasticizer deriving from the slurry and PVA coming from the gluing solution (it was considered the dry green tape composition as reference) all together left a residual carbonaceous species amount of about 1.8wt%.

In order to calculate the amount of free Carbon we have to consider both the Carbon introduced into the slurry and the debinding carbonaceous residue. Consequently we can estimate the amount of free Carbon equal to about 5.4 wt%.

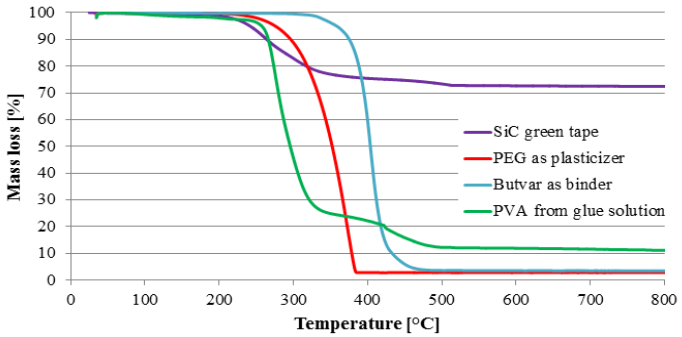

Figure 4.5 TGA showing decomposition of binder, plasticizer and PVA.

4.1.4 Pressureless Sintering

Finally the as debinded specimens were transferred into the sintering furnace and pressureless sintered at 2200 °C under argon atmosphere for 30 minutes (Figure 4.4B); the sintering temperature and time were based on the preliminary experiment (54).

Usually the densification process of ceramic composites and multilayer required pressure assistance as well as high temperature which necessarily implied shape and size limitations and high equipment cost; so these methods were difficult to extend towards large industrial applications. In order to overcome these limitations pressureless sintering was adopted in present work.

During debinding, the samples are sintered on a graphite support and a graphite weight is put over it in order to avoid sample deviation from planarity, in addition a small amount of coarse SiC powder is used as lubricant between graphite support-sample and sample-graphite weight in order to avoid unwanted adhesion.

4.1.5 Spark Plasma Sintering

An alternative process for the sintering of multilayers was the Spark Plasma Sintering. SPS was found to compact powders satisfactorily through the simultaneous application of direct current pulses of high intensity and pressure. The electric current induces a temperature elevation within the sample by Joule's effect. The whole process lasts just a few minutes.

The consolidation experiments were performed at TECNALIA in a FCT Spark Plasma Sintering furnace (model S8451). This equipment can supply a direct current of 10000 A of intensity under a maximum tension of 10 V. The DC current was applied with pulse time of 10 ms and a pause time of 5 ms. The sample was placed in a graphite die between two graphite punches. The diameter of the samples was 20 or 30 mm. During the tests, the chamber was maintained under vacuum (10^{-2} Pa). Temperature was controlled by a pyrometer that measures the temperature in the interior part of the graphite punch. The maximum temperature was between 1700-1900 ºC during 1 min of holding time. The load (50 MPa) was applied during the heating.

In this work of thesis SPS was performed on SiC and ZrB_2 based material (only on few laminates) in order to compare the microstructure of the two basic compounds sintered by two different techniques.

4.2 Experimental methods

4.2.1 Density measurements

The density is one of the most important properties of a material; because of its great influence on the other mechanical characteristics, it is considered a fundamental tool for defining structural properties that are required for a specific application and so assuring a good performance of the material.

It is directly linked with the sintering process: it is a measure of how much the particles of the powder were sintered to form the "monolithic" material and consequently how much is the porosity left.

There are different methods to measure the densification of any material; in this work geometric, bulk and apparent density were measured. For each series of samples at least four specimens are selected for the measurements.

All the values are reported respect to the theoretical density which is calculated by the rule of mixtures.

The *geometric density* was evaluated by measuring weight (by an electronic balance suitable to weigh accurately to 0.0001 g) and dimensions (by a digital caliper) of samples considering them in a geometrically regular parallelepiped bars.

The *bulk density* correspond to the ratio between the dry mass of the sample and its exterior volume, including pores (1).

The procedure to measure the bulk density involves different steps: firstly, after drying the specimen to constant mass by heating it in an oven, the *dry mass* D is measured. Then the test samples are placed in a pan of distilled water and boil for at least two hours taking care that water cover them for all the time. The specimens are placed in a wire loop that is suspended from one arm of the balance in water and the *suspended mass* S for each sample is measured. The last measurement of the *saturated mass* M is performed after blotting the specimens lightly with a moistened cotton cloth in order to remove all excess of water from the surface.

We can calculate the exterior volume V as follows:

$$V = M - S \qquad \text{(Eq. 4.1)}$$

So the bulk density corresponds to the ratio between the dry mass of the sample and its exterior volume.

$$\text{Bulk density} = D/V = D/(M-S) \quad \text{(Eq. 4.2)}$$

The *apparent density* is measured by using Ultrapycnometer 1200e from Quantochrome. It lets to measure the volume of solid materials by employing Archimedes' principle of fluid (gas in our case) displacement and the technique of the gas expansion. Helium is used its small atomic dimension enables entry into pores, also with very small size.

The procedure to measure the apparent density is very simple and automatic: sample(s) is introduced in a cell with proper dimension (there are different size in order to measure sample with different bulk), the helium is introduced in the system and a software calculate the difference in volume between the empty and the full cell. The weight of test sample is introduced manually.

By opening the valves to the sample cell, the system is brought to ambient pressure P_a after being purged with Helium; the state of the system is defined as:

$$P_a \cdot V_c = n \cdot R \cdot T \quad \text{(Eq. 4.3)}$$

Where n in the number of moles of gas occupying volume V_c (the empty sample cell volume) at P_a, R is the gas constant and T_a is ambient temperature in Kelvin.

When the solid sample of closed volume Vp is placed in the sample cell, Equation 4.1 can be written:

$$P_a \cdot (V_c - V_p) = n_1 \cdot R \cdot T_a \quad \text{(Eq. 4.4)}$$

When pressurized to some pressure above ambient, the state of the system is given by:

$$P_2 \cdot (V_c - V_p) = n_2 \cdot R \cdot T_a \quad \text{(Eq. 4.5)}$$

Where P_2 indicates the pressure above ambient and n_2 represents the total number of moles of gas contained in the sample cell. When the valve opens to connect the added volume V_A to that of the cell (in order to make a measurement in term of pressure difference), the pressure will fall to a lower value P_3 given by:

$$P_3 \cdot (V_c - V_p + V_A) = n_2 \cdot R \cdot T_a + n_A \cdot R \cdot T_a \quad \text{(Eq. 4.6)}$$

Where n_A is the number of moles of gas contained in the added volume when at ambient pressure.

The term P_aV_A can be used instead of n_ART_a in the following equation:

$$P_3 \cdot (V_c - V_p + V_A) = n_2 \cdot R \cdot T_a + P_a \cdot V_A \quad \text{(Eq. 4.7)}$$

Substituting $P_2(V_c\text{-}V_p)$ from equation 4.10 with n_2RT_a Equation 4.7 changes:

$$P_3 \cdot (V_c - V_p + V_A) = P_2 \cdot (V_c - V_p) + P_a \cdot V_A \quad \text{(Eq. 4.8)}$$

$$(P_3 - P_2) \cdot (V_c - V_p) = (P_a - P_3) \cdot V_A \quad \text{(Eq. 4.9)}$$

Then

$$V_c - V_p = \frac{(P_a - P_3) \cdot V_A}{(P_3 - P_2)} \quad \text{(Eq. 4.10)}$$

This last equation (4.10) is further reduced by adding and substracting P_a from P_3 and P_2 in the denominator, giving:

$$V_p = V_c - \frac{(P_a - P_3) \cdot V_A}{(P_3 - P_a) - (P_2 - P_a)} = \frac{V_A}{1 - \frac{(P_2 - P_a)}{P_3 - P_a}} \quad \text{(Eq. 4.11)}$$

Since P_a is made to read zero, that is, all pressure measurements are relative to a P_a, Equation (4.11) becomes:

$$V_p = V_c + \frac{V_A}{1 - (P_2 / P_{3)}} \quad \text{(Eq. 4.12)}$$

Equation (4.12)is the working one used by Ultrapycnometer 1200e to measure the volume of sample and the closed pores.

This equipment is used, not only to estimate the apparent density of laminate, but in addition to calculate the density of starting powder.

4.2.2 Mechanical properties test

4.2.2.1 Elastic modulus

Different tests can provide a measure of Young's (or elastic) modulus. It is a relationship between tensile elastic stress and its corresponding strain, following Hooke Law. The method used in this work is called "Impulse Excitation of Vibration" and involves the analysis of transient natural vibration on RFDA MF basic instrument, IMCE n.v. Belgium (Figure 4.6).

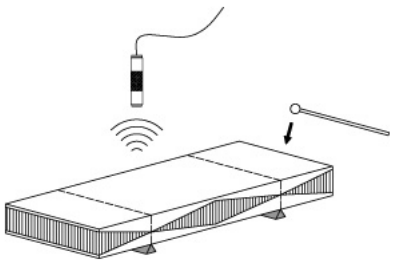

Figure 4.6 RFDA equipment for Young's modulus measurement.

The equipment measures the flexural vibration frequency and calculates the Young's modulus using the mass and the dimensions of the sample; following the formula uses for a rectangular bar (according to ASTM E1876 and ASTM C1259-01):

$$E = 0.9465 \left(\frac{m f_f^2}{w}\right) \left(\frac{l^3}{t^3}\right) T_1 \quad \text{(Eq. 4.13)}$$

where E is the Young's modulus, f_f is the Flexural frequency, m is the sample mass, l, w and t respectively its length, width and thickness; T_1 is the correction coefficient that accounts for the finite dimensions of the bar, the Poisson's ratio, etc:

$$T_1 = 1 + 6.585(1 + 0.2023\mu^2)\left(\frac{t}{L}\right)^4 - \left[\frac{8.340(1+0.2023\mu+2.173\mu^2)\left(\frac{t}{L}\right)^4}{1+6.338(1+0.1408\mu+1.536\mu^2)\left(\frac{t}{L}\right)^2}\right] \quad \text{(Eq. 4.14)}$$

where μ is the Poisson's ratio.

If the ratio L / t is greater than 20, T_1 can be simplified to the following:

$$T_1 = 1 + 6,585\left(\frac{t}{L}\right)^2 \quad \text{(Eq. 4.15)}$$

and E can be calculated directly.

If L/t is smaller than 20, either the Poisson's ratio is known or T_1 can be calculated with an iterative process.

The vibration signal emitted by the sample is captured using a microphone and sent to the RFDA (Resonant Frequency and Damping Analysis) software which display the resonant frequency.

4.2.2.2 Bending strength

Three-point bending tests (Figure 4.7) were performed adopting 40mm outer span and a cross-head speed of 0.1 mm/min (Sintech 10 D equipment, UNI EN 658.3standard).

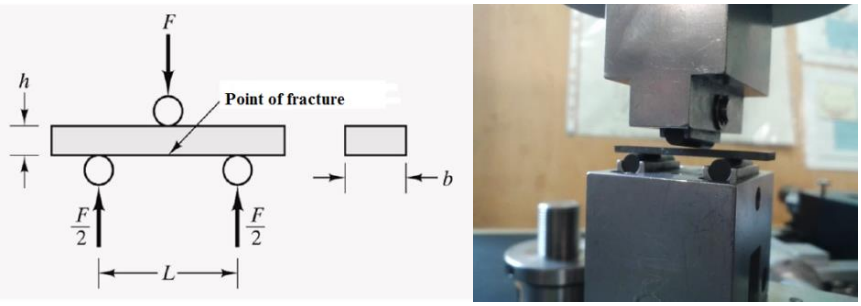

Figure 4.7 Configuration for three point bending test.

Samples are in form of bars with a rectangular cross section and specific dimensions which depends on the length of span of the flexural fixture according with ASTM-C 1161-94(1996). The specimen is placed between the span and then is applied a concentrated load in one central point; the sample is in compression at the surface positioned in the load part and is in tension in the rear surface part. This test gives information about the flexural strength by the following equation:

$$\sigma = \frac{3PL}{2bd^2} \quad \text{(Eq. 4.16)}$$

Where σ is the flexural strength, *P* the load, *L* is the span length, *b* is the width of the sample and *d* is the thickness of the specimen.

4.2.2.3 Microhardness measurements

Indentation is the method used to determine the hardness of materials that consist in quantifying the resistance of a surface to the penetration by a harder object.

Several methods have been developed and the main ones are Rockwell, Brinell, Vickers and Knoop; recently also nanoindentation techniques have been developed. Each method requests a specific geometry and size of the indenter, a specific equation, and presents also specific load conditions.

All these tests can be useful to give information about the effect of a specific fabrication process or a thermal treatment; moreover they are often used for quality control and correlation with other properties of the materials.

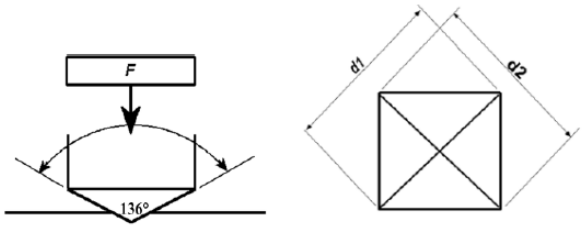

Figure 4.8 Configuration for microhardness test

In this thesis, Vickers hardness test (ASTM E92-72) was used (Figure 4.8). Specifically microhardness (HV) of ceramic multilayer was measured using a LEICA micro HV indenter with a load of 50g or 100g for a dwelling time of 10 s. At least 10 measurements were performed for each specimen, in order to obtain statistically representative results. The test consists in penetrate a surface under investigation by an indenter, in this case a diamond pyramid with square-base that forms an angle of 136° with the opposite side. The force applied is known and, by measuring the surface area of the imprint (the operator measures the imprint diagonal length) the microhardness can be calculated by the simple geometrical formula :

$$HV = \frac{1.864 \cdot P}{L^2} \qquad \text{(Eq. 4.17)}$$

Where P is the applied load and L is the length of indentation along its long axis.

Vickers hardness test should be independent of the load, except in case of small loads (55).

4.2.3 Oxidation test

Thermogravimetric Analysis (TGA) lets to heat a material with a controlled rate in a specific atmosphere and record the variations of the weight occurring. The used equipment mainly

consists in a heated chamber with an electronic microbalance where the sample is placed, a control thermocouples, a vacuum system, gas entrance and outlet and a cooling system.

This equipment can reach 1600°C and can operate in different gaseous flux such air, nitrogen, or argon.

Small samples with size of about 3×3×1.8 mm were cut by sintered ceramic bars and submitted to oxidation test. TGA were carried out on a Mettler-Toledo TGA/SDTA851e equipment: each sample underwent two subsequent oxidation cycles which consist of heating up to 1600°C (constant rate of 10°C/min in flowing air of 50 ml/min) and cooling down to room temperature (cooling rate 18°C/min).

Moreover TGA were also performed on green tape made of 100%SiC and 80vol%ZrB_2+20vol%SiC in order to study the decomposition of the organic components in ceramic films with different composition and in addition to compare it with the degradation process of the pure Polyethylenglycol and Polyvynilbutyral. The treatment was done in similar conditions respect to the debinding cycle: from room temperature to 600°C (complete degradation of organic compounds) with a constant rate of 1°C/min in flowing argon of 50 ml/min.

Laminates (bars 55x12x1.8 mm in size) were also submitted to long-period oxidation treatment: this isothermal oxidation test was performed under static air at the temperature of 1600° C for 24 hours in a Carbolite HTF1800 oven. A refractory frame with SiC fibers stretched between refractory supports was put inside the large furnace chamber. The specimens were hung by positioning them on the SiC fibers in order to avoid any contact with the walls of the oven. After long time oxidation the morphology and the microstructure of the specimens were investigated and compared to that of the as-processed materials. Most of these specimens (especially those with the higher content of ZrB_2) swelled and lost their regular shape because of the emission of gaseous oxidation products and the formation of borosilicate glassy phase (with low viscosity at 1600°C) during this oxidation treatment. For this reason it was not possible to perform mechanical tests on these oxidized specimens according to current standards, which would be required for investigating the mechanical feature changes resulting from oxidation. In fact machining would be necessary in order to recover the geometrical shape needed for mechanical test, but machining would also remove the external part of the oxidized specimens and therefore would change the overall composition of these specimens. Therefore less severe oxidation conditions were adopted in order to keep a suitable geometrical shape for oxidized specimens. The 24 hours isothermal oxidation treatment was thus repeated at 1500° C on the laminates less sensitive to oxidation owing to a limited content of ZrB_2 (laminates with composition: 100 %

SiC, 80%SiC-20%ZrB_2 and 60%SiC-40%ZrB_2). The mechanical features of these last specimens were investigated.

4.2.4 XRD analysis

The composition of laminates is checked by X-ray diffraction (Philips PW 1710, Cu-Kα radiation) between 20 and 80° (2θ). The X-ray pattern of the sample surface was compared with that of the powders obtained by milling the samples in order to investigate any possible composition difference between the surface and the core of the specimens, possibly resulting from surface contamination.

XRD method is based on the Bragg Law:

$$n\lambda = 2d \sin \theta \qquad \text{(Eq. 4.18)}$$

where n is an integer number (generally 1), λ is the wavelength of the incident X-Ray radiation, θ is the incident angle and d is the distance between identical planes reflecting the radiation.

When a photon incises with angle θ on several atom planes separated by the distance d, a diffraction will take place thanks to the constructive interference between the photons and the atoms. From the distances d relative to each family of planes of a material and considering in addition the intensities of the diffracted beams, it's possible to know the lattice parameters and the atoms disposition in the crystal cell. All the diffractions of all the lattice planes create a pattern of diffraction signals that is specific for every material (56).

Since always $\lambda < 2d$, the wavelength must be rather low; for this reason X radiation is used to excite the sample.

X-Pert HighScore is the software used in this thesis in order to elaborate the intensities in function of the diffraction angles and then identify and estimate the promising phases from the PCPDFWIN database (containing an extremely high quantity of identified and standard patterns). It is possible making a comparison between the experimental X-ray pattern and the reference ones.

For analysis of very small area on multilayer laminates after oxidation test, X-ray microdiffraction analysis was performed by using Rigaku D/MAX diffractometer (Cu-K_α radiation with λ=1.54056 nm and at a generator voltage of 40 kV and generator current of 20 mA) at a fixed 10° angle ω and rotate φ angle between -30° and 30°. Angles between 10° and 90° (2θ) were then considered in order to elaborate the XRD spectra. This particular device worked with a collimator (100 and 300 μm is used in this work) which allow to obtain a collimated X ray radiation for the analysis of small samples or of small area with precision and accuracy.

4.2.5 Microstructure observation

The polished surface was observed both by optical microscope (Reichert Microscope, Austria) and Zeiss Assing Supra 25 Field Emission Scanning Electron Microscope; the SEM is equipped with an high-resolution EDS probe Oxford 7353 EDS, in addition to the SE and BSE detectors.

The fracture surface was observed on Zeiss Supra 25 Field Emission SEM.

The size of crystal grains can be put in evidence by SEM observation of the fracture surface of specimens submitted to mechanical test or by SEM and optical microscope examination of the cross section of the specimens, after polishing and thermal etching.

Scanning electron microscopy (SEM) lets the observation of heterogeneous organic and inorganic samples on a micrometric and nanometric scale obtaining three-dimension like images. The samples are irradiated with a highly focused electron beam; the interaction between electrons and specimen surface could generate different signals such as secondary electrons, backscattered electrons and characteristic X-rays. These can be obtained in dependence of the specific emission volumes within the sample and can be exploited to investigate different samples properties, e.g. topography, composition, crystallography, etc.

The equipment is divided in four main parts: the *electron column* (the most conventional gun is a tungsten wire of 0.25 mm of diameter as electron source, where the tungsten filament is heated to approximately 2500°C), the *specimen chamber*, the *vacuum pumping system* and the *electronic control of the imaging system*.

The electrons are attracted to the anode by a positive voltage (in a range from 5 to 30 kV) which can be controlled manually by the operator and it is usually around 10-20 kV.

The vacuum system usually works at 10^{-3} Pa and provides the conditions for the beam to be scattered by gas atoms. The magnetic lenses have the function to focus the electron beam on the sample surface; it can be adjusted by the current changing the working distance.

The signals of greatest interest for the image elaboration in this research activity are mainly the secondary electrons (SE) because their variations are strictly linked to changes in surface topography and they give information on sample surface morphology. They have low energy, and by putting an electrically charged grid near to the sample, it is possible to convoy them all toward a sensor, that counts their number. The secondary electron emission is confined to a very small volume near the beam impact area and it allows to obtain images with very high resolutions.

Moreover it is possible to perform chemical analysis with SEM equipment by measuring the energy and intensity distribution of the x-rays generated by the electron beam. One of the most common x-rays detectors are the so called Energy-Dispersive X-ray Spectrometer (EDS). In

EDS, the impact of a X photon on the sensor generates an electron-hole couple with an energy proportional to those of the photon.

After passing through a thick beryllium window (8 μm) the X-rays are detected by a Silicon diode; this is generally cooled to reduce noise. The analysis of the spectrum can ensure from a qualitative to a semi-quantitative characterization of the specimens. The qualitative identification of the elements is possible assuming that each element emits an X-ray with a specific wavelength. On the contrary, the quantification of the elements is quite difficult: the calculations are much more complex, because it is essential not only to integrate the peaks, but also to calculate the background signal, use correction for atomic number, fluorescence, adsorption (the so called ZAF correction) and tare the system with a known standard. The surface must also be extremely flat to avoid morphology effects on the signal.

4.2.6 XPS techniques

XPS is based on Photoelectric effect, so it involves the excitation of sample with photon which is absorbed by an atom in a molecule or a solid leading to the ionization of it and the emission of a core electron. The analysis of the kinetic energy distribution of the emitted photoelectrons is used to investigate the chemical composition and the electronic state of the sample surfaces.

In this thesis the scale growing on oxidised ceramic laminates is studied by X-ray photoelectron spectroscopy (XPS PHI 5000 VersaProbe) with a monochromatic Al-Kα radiation. XPS analyses were performed by using an X-ray spot about 100 μm in diameter. Dedicated neutralization system was employed in order to avoid charging effect on the samples during analyses. It consists in an electron gun, combined with positive Argon ion gun, in order to increase his efficiency. Calibration of XPS equipment was performed by matching the literature binding energy values of Au 4f7/2, Cu 2p3/2 and Ag 3d5/2 peaks.

4.2.7 Dynamic light scattering

The processing of laminates integrating composite layers in between SiC ones presented difficulties coming to the use of starting powders with very different particle size (ZrB_2 has average dimensions of 2,25 μm while SiC only 0,55 μm); this cause the development of stresses and the consequent failure of the multilayer.

In order to overcome this problem it has been made a milling of ZrB_2 starting powder in order to homogenize ZrB_2 and SiC particle size and then evaluate the effects on the material densification degree and mechanical properties.

The milling is performed by using an high energy milling system equipped with Tungsten Carbide elements.

The investigation on dimensional distribution of particle size is performed by Dynamic light Scattering (Zetasizer Nanoseries ZS90, Malvern Instrument).

The measurement is based on the interaction between a monochromatic and coherent radiation and the particles : when a laser beam passes through a dispersion of particles in a liquid produces a signal of scattered light . In dynamic light scattering, the speed at which the particles are diffusing due to Brownian motion is measured. Bigger are the particles slower the Brownian motion as shown in Figure 4.9.

By measuring the rate at which the intensity of the scattered light fluctuates when detected (using a suitable optical arrangement) and comparing the sample's scattering pattern with an appropriate optical model, it is possible to estimate the particle size distribution.

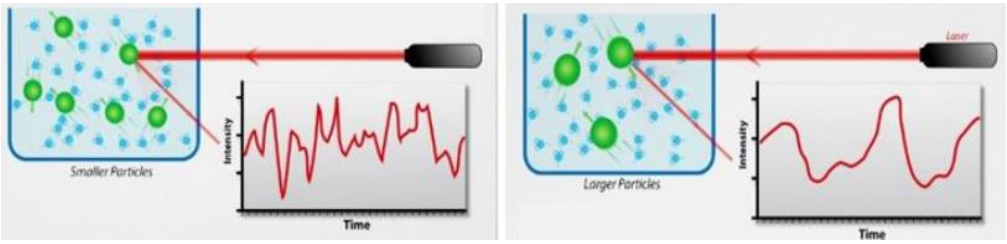

Figure 4.9 Intensity of scattered light in function of the particle size.

4.2.8 Emissivity test

The EMF facility is shown in Figure 4.10; the measurements consisted of the following steps:

- The sample was placed in the sample holder on one side of the blackbody cavity.
- The vacuum vessel was evacuated and then filled with the selected inert gas (argon for our investigation)
- The cavity was then resistively heated up to the desired temperature; varying the electrical current it was possible to measure the emissivity at different temperatures; it was constantly monitored by a pyrometer.

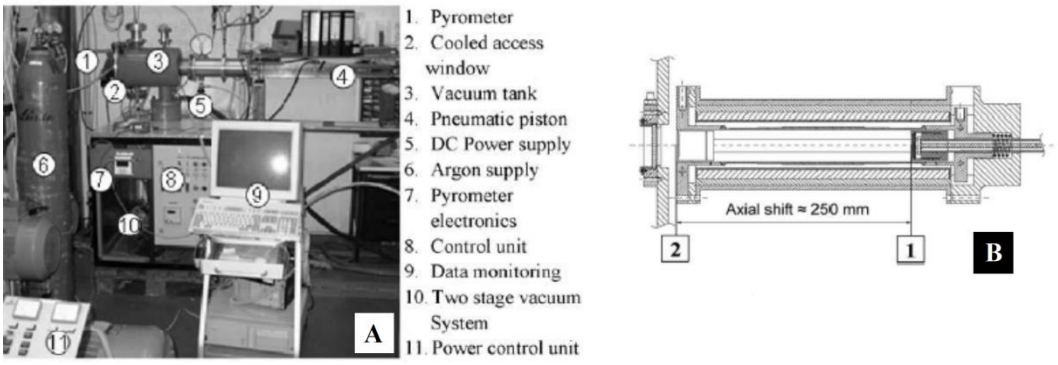

Figure 4.10 A) EMF facility and B) Moving piston

Thanks to the exchange of radiation the sample reached a thermal equilibrium with the cavity, so when the temperature was stable, the sample was shift on the opposite site of the cavity where a second temperature is taken.

According Stefan Boltzmann law:

$$S_{Pos\,i} \approx \sigma \cdot \varepsilon_{Pos\,i} \cdot T^4_{Pos\,i} \quad \text{(Eq. 4.18)}$$

Where $S_{pos\ i}$ was the signal of pyrometer in i-position [V] , σ was the Boltzmann constant [Wm^2K^{-4}] and $T_{pos\,i}$ was the measured temperature at that position [K].

The ratio between signals was:

$$\frac{S_{pos\,2}}{S_{pos\,1}} = \frac{\varepsilon_{pos\,2} \cdot T^4_{Pos\,2}}{T^4_{Pos\,1}} \quad \text{(Eq. 4.19)}$$

As the shift is isothermal ($S_{pos1}=S_{pos2}$), the emissivity can be calculated by the ratio of the two signals or by the apparent temperature drop:

$S \approx T^4 \rightarrow S_a \approx T_a^4$

$$\varepsilon_{pos\,2} = \frac{T^4_{a,Pos\,2}}{T^4_{a,Pos\,1}} \quad \text{(Eq. 4.20)}$$

Following the experimental conditions are reported:

Power supply

Applied current: 30 – 520 A

Generated power: 100 – 4900 W

Blackbody cavity

Dimensions: 40-50 x 250 mm

Material: Graphite, roughness 0.2

Gas environment: Argon 4.8 (99,998% purity) at 1.2 bar

The choice to do the tests under Argon atmosphere was due to the fact that inert atmosphere minimize the oxidation process in addition to keeping more stable and reproducible the measurement conditions.

Piston

Moving speed: 1.15 m/s (time from position 1 to 2 < 0.2s)

Girl pyrometer IRM5 (100 – 3000 °C)

Measurement rate: 5 Hz

Calibration: from 100 to 1500 °C at 2-22 m

Resolution: < 1.5 mV (0.4 K)

Chapter 5
Multilayer based on ZrB_2/SiC system: processing and mechanical properties

Transition metal borides such as ZrB_2 and HfB_2 have a melting point higher than 3000°C ant it makes them candidates for use as structural materials at temperature above 1800°C. Within the family of Ultra-High Temperature Ceramics, they show a unique set of mechanical and physical properties, including high melting points, high thermal and electrical conductivities and chemical inertness against molten metals (57; 19; 58). ZrB_2 is reported to have excellent resistance to thermal shock and to oxidation compared to other non-oxide structural ceramics (59); moreover it shows the lowest theoretical density among UHTC (d_{ZrB2}=6,09 g/cm^3 compared to d_{HfB2}:11,2 g/cm^3) which makes it attractive especially for aerospace application.

The use of this single-phase material for high-temperature structural applications is limited by its low intrinsic sinterability and poor oxidation resistance (60; 61).

Some compounds are so added in the slurry formulation as sintering aids in order to improve densification degree, mechanical properties and oxidation behaviour; obviously all these material characteristics are closely linked to the chemical composition, the microstructure and the added intergranular second phase.

5.1 Sintering aids for ZrB_2

Many studies have been done on different compounds in order to use them as sintering aids for ZrB_2; these additives can be divided into two main groups on the base of their activity mechanism:

-*Liquid phase formers* such as refractory metals and disilicides of transition metals.

The addition of metals such as Ni, Co, Fe in an amount higher than 2wt% increased the densification degree thanks to the formation of a liquid phase (62; 63; 64). It has been reported that the addition of $MoSi_2$ was beneficial for the densification and microstructure of the ZrB_2-based composites (65): this sintering aid hindered the ZrB_2 grain growth. Moreover thanks to its ductility at temperatures over 1000°C, the $MoSi_2$ phase can accommodate among the ZrB_2 particles filling the voids left by the ZrB_2 skeleton and favouring the formation of a material free of porosity. In addition *Silvestroni et al.* showed that ZrB_2 samples containing $MoSi_2$ in the range from 5 to 20% tested at 1200°C and 1500°C in air were found to be coated by a protective silica layer formed as a consequence of $MoSi_2$ oxidation (66; 65).

This silica layer could have acted as a grain lubricant for particle rearrangement during the initial stage of densification, and formed liquid phases, through reaction with surface oxides present in the starting powders (as Boron oxide).

$ZrSi_2$ addition lowered the sintering temperature of ZrB_2 ceramics: according to *Guo et al*. (67) the SiO_2 present on the surface of $ZrSi_2$ reacted with B_2O_3 on the ZrB_2 starting powder to form an intergranular liquid phase that favored grain rearrangement as well as improved the packing of particles.

- *Reactive agents* such as carbides and Carbon. Oxide impurities present on the surface (mainly ZrO_2 and B_2O_3) of starting powder have been shown to inhibit densification and also to promote grain growth in the non-oxide ceramic system; these kind of aids reacted with the oxide impurities improving the densification process.

	Sintering Addtives [%wt]	Sintering condition [%wt]	Geometric Relative density [%]	Bending Strenght [MPa]	Elastic modulus [GPa]	Reference
ZrB_2 (no aids)		2200°C/30 min	83.0±1.8	165±14	337±15	Experimental
ZrB_2	4C		83.2±1.5	229±16	304±8	Experimental
	5TiC		91.9±1.2	267±40	438±17	Experimental
	$10ZrSi_2$	1700°C/60min	49.1±2.0	42.2±0.9	-	Experimental
		1850°C/5 min	82.6±5.3	181±20	311±9	Experimental
		1700°C/60min +2200°C/30 min	84.4±5.0	94±22	317±9	Experimental
		1650°C/60min	*95.7*	-	*405*	*(14)*
80vol%ZrB_2 + 20vol%SiC	0,1B +0,3C	2200°C/30min	92.9±1.0	277±15	444±9	Experimental
	1B	2200°C/30min	84.6±1.5	153±17	377±8	Experimental
		2100°C/120min	*>99*	*519±31*	-	*(29)*
	$0,4B_4C$ +3C	2200°C/30min	84.0±2.0	238±15	352±9	Experimental
		2200°C/120min	*98.2*	*382±24*	*405±34*	*(38)*
	$1B_4C$ +3C	2200°C/30min	85.0±2.5	221±16	362±8	Experimental
		2200°C/120min	*99.8*	*301±4*	*391±11*	*(38)*
	2,7VC+0,1B +0,3C	2200°C/30min	93.7±1.3	167±29	426±20	Experimental
	3,5VC+0,1B +0,3C	2200°C/30min	88.2±1.5	214±26	419±15	Experimental
	5,2VC+0,1B +0,3C	2200°C/30min	86.6±1.5	186±23	390±12	Experimental
		2200°C/120min	*99.0*	*511±70*	*454±9*	*(20)*
	5TiC+1B +3C	2200°C/30min	83.6±1.7	236±60	314±23	Experimental
	$2,3Si_3N_4$ +0,1B +0,3C	2200°C/30min	91.2±1.2	191±31	434±11	Experimental

Table 5.I: Properties of ZrB_2 and ZrB_2/SiC laminates: comparison between experimental and literature data.

Both of Boron carbide (68; 69) and Tungsten Carbide (70; 60) reacted with ZrO_2. The addition of 4wt% B_4C produced almost fully dense ZrB_2 at 1850°C in vacuum without pressure assistance. On the other hand the addition of 4wt% WC lets to reach density of ≈95%, but only

for sintering temperature higher than 2100°C. This difference in sintering temperature was due to the different onset of the reactions of aids with the surface impurities. The densification process was more effective for a combination of B_4C and C than for B_4C alone (71; 72).

Vanadium Carbide resulted more efficient in removing the surface oxide impurities of ZrB_2 compared to WC (73).

The most common additive for ZrB_2 was Silicon Carbide; its addition improved the sinterability, inhibited grain growth and increased the oxidation and ablative resistance (57; 74; 75; 76).

Starting from the *state-of-the-art* on sintering additives used to obtain pure ZrB_2 and ZrB_2/SiC based materials with very high densification degree (a pressureless sintering process is used), this work focused the attention on few of these compounds verifying the effects of their addition on multilayer ceramics.

The outcomes of the screening of sintering additive were summarized in Table 5.I. The densification of ZrB_2 without any sintering aids resulted in a material with high residual porosity which justified the low mechanical properties such as elastic modulus and bending strength. On the contrary of what reported by *Mishra et al.* (77) the addition of Titanium Carbide in an amount of 5wt% was not detrimental for sintering of ZrB_2: the relative density reached almost 92% and the mechanical properties increased significantly. The addition of 4wt% of Carbon improved the physical and mechanical properties of sintered material; it probably is able to inhibit the grain growth of ZrB_2 (77).

On the base of promising results obtained by *S.-Q. Guo et al.* (67) showing an almost full dense ZrB_2 material in presence of Zirconium Disilicides as sintering aids and pressureless sintered at 1650°C for 60 minutes, the effect of the addition of this compound has been studied.

Laminates containing 10vol% $ZrSi_2$ have been sintered at 1700°C for 60 minutes: the results was a very low densified multilayer with poor structural integrity. Laminates with the same composition were then sintered at 1850°C for 5 minutes and in two-steps process respectively at 1700°C for 60 minutes plus 2200°C for 30minutes. Only the sintering process in two steps let to obtain material with acceptable properties, even if lower than those obtained with other sintering aids such as Titanium Carbide: besides the geometrical density (82.5%) the apparent one was measured obtaining a value of 92.3%. In addition to a relevant improvement in densification degree, the mechanical properties such as elastic modulus and microhardness increased significantly. Only the bending strength resulted underestimated, probably due to the residual porosity of the material.

Relative geometric density (respect to the theoretical one) in the range 83.5-94% were obtained for ZrB_2/SiC composite laminates using different sintering additives: B+C; B;VC+B+C;

Si_3N_4+B+C. These values were lower than those expected for monolithic ceramics: they can be easily explained considering both the surface roughness which greatly affected the calculated geometric density of such a thin specimens, and the approximation of the sample shape to a regular parallelepiped didn't take into account the mistake coming from the measure of the dimensions.

The addition of a mixture of Boron and Carbon (the amount was calculated respect to SiC amount) allowed to obtain not only a very high value of relative density, but also the highest bending strength and elastic modulus. The addition of these two compounds in a small amount was reported to be necessary to activate the sintering process of SiC as well as to improve the physical and mechanical properties of the composite (78; 16; 17; 79).

It is generally believed that during the sintering process Carbon reacts with impurities containing Oxygen (for instance with the SiO_2 covering the surface of SiC particles) thus limiting the presence of oxides that can melt at high temperatures.

Stobierski et al. (16) reported that the rule of Carbon in the sintering process of Silicon Carbide was different in function of the temperature. In the range 1400°C-1600°C, so at temperature much lower than SiC sintering one, the presence of Carbon promoted the chemical bonding of the volatile products such as Si and SiO and only Carbon Monoxide is transferred to the gaseous phase. At higher temperature, between 1600°C and 2000°C the rule of Carbon was mainly to limit the weight losses and arrest the grain growth process. Boron is believed to active the sintering process by promoting the formation of a Boron-Silicon-Carbon liquid phase when its addition was higher than 0,5% (17); however the liquid phase was only in a very little amount. In fact for high temperature required in specific TPS applications, the formation of a liquid phase should be controlled and limited since the protection systems operate at temperatures even exceeding 2000°C and have to keep suitable mechanical features also in this extreme condition.

The presence of VC in addition to Boron and Carbon let to obtain a laminate with very good relative density, high elastic modulus, but quite low bending strength.

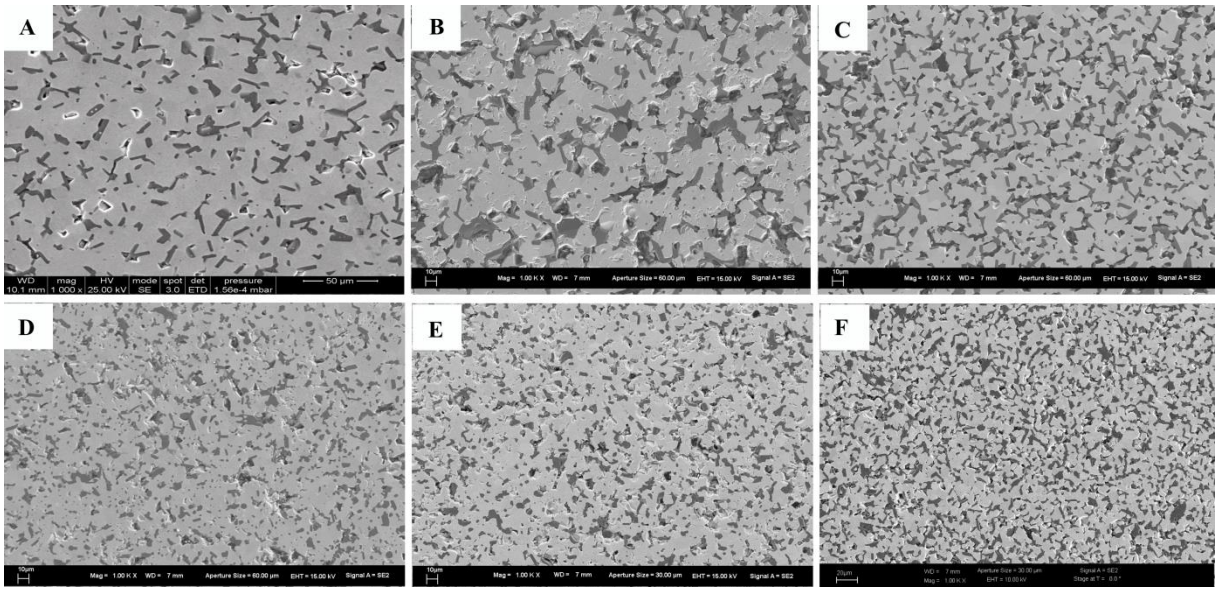

Figure 5.1 Micrographs by SEs-SEM (polished cross section) of the specimens with composition 80vol%ZrB_2 + 20vol%SiC plus different sintering aids :A) 0.1%Boron+0.3% Carbon; B) 1% Boron; C) 1% Boron Carbide+3% Carbon; D) 2,7%VC+0.1%Boron+0.3% Carbon; E) 5%Titanium Carbide+0.1%Boron+0.3% Carbon; F) 2,3%Silicon Nitride 0.1%Boron+0.3% Carbon

The addition of a mixture of Boron and Carbon was then adopted for processing specimens containing ZrB_2 and SiC.

The comparison of SEM micrographs of laminates with composition 80vol%ZrB_2+20vol%SiC plus different sintering aids (Figure 5.1) puts in evidence differences in microstructure: ZrB_2 grain growth resulted particularly evident in presence of 1% Boron where the final grain size were four times bigger than the starting powder dimensions. It was in agreement with the microstructure of material with equal chemical composition reported by *Wang et al*. (80): composite samples with 1% and 2% amount of Boron and sintered at 2100°C showed fine microstructures with similar components grain size. Increasing the sintering temperature to 2200°C, both the ZrB_2 and SiC grains grew up: for addition of 2% of Boron the average ZrB_2 grain size was 34% larger compared to that observed for the addition of only 1% Boron. The distribution of SiC and additives resulted homogeneous in all the microstructures; the black spots corresponded to residual porosity.

5.2 Laminates based on ZrB_2/SiC system

In this research activity a systematic study on laminates with different ZrB_2/SiC relative amounts has been done with the aim to optimize the composition in function of the physical and mechanical properties. Ceramic laminates were prepared using SiC and ZrB_2 in percentages ranging from 100%SiC to 100% ZrB_2.

5.2.1 Microstructure

The size of crystal grains was characterized by examining polished, chemically or thermally etched cross-section reported in Figure 5.2.

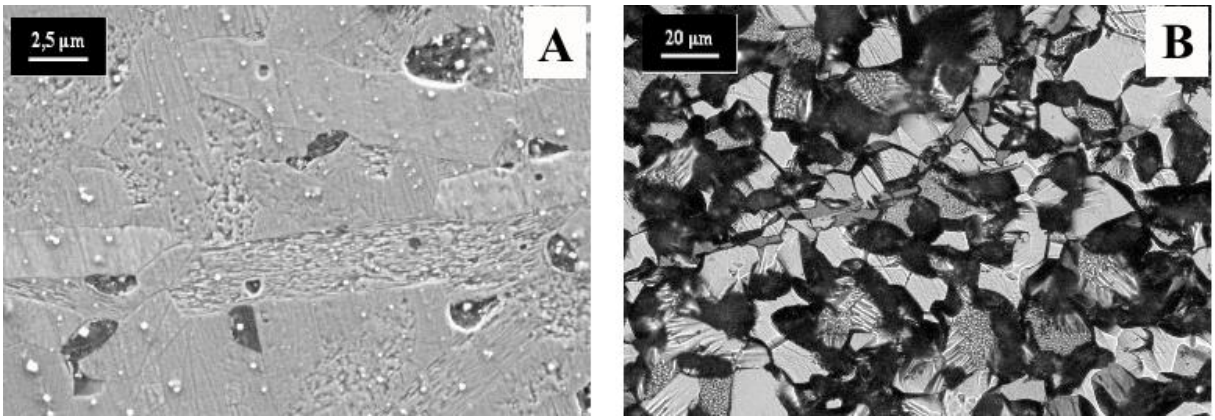

Figure 5.2 Optical micrograph of polished cross section of laminates with composition A) 100%SiC and B) 100%ZrB_2.

A wide grain size distribution was observed: the microstructure of SiC multilayer consisted of few small polygonal grains with an average grain size of 2 µm and many rod-like grains with length between 6 µm and 20 µm and aspect ratio ranging between 3 and 7.

In the case of ZrB_2 laminate only polygonal grains were observed with a maximum grain size of ≈ 24 µm and a minimum of ≈9 µm.

Evident crystal grain growth occurred during sintering at 2200°C, in particular in the case of SiC multilayer; it has been observed also in the composite microstructures, but the growth of ZrB_2 grains seems lower on average. In this last case both polygonal crystals (with size ranging between 2 µm and 24 µm) and rod-like grains (length up to 20 µm) were observed.

Figure 5.3 shows the microstructure of laminates in the entire range of composition from pure SiC to pure ZrB_2.

The microstructure of specimens with a 100%SiC (Fig. 5.3A) and 100%ZrB_2 (Figure 5.3D) was not completely homogeneous because of the presence of graphite and residual porosity. On the other hand the microstructure of composite laminates was based on an homogeneous mixture of SiC and ZrB_2 crystals (Fig. 5.3B and Fig.5.3C): the SiC grains resulted elongated and were regularly dispersed in ZrB_2 grains. Residual porosity in composite laminates was more likely found at the interface between SiC and ZrB_2.

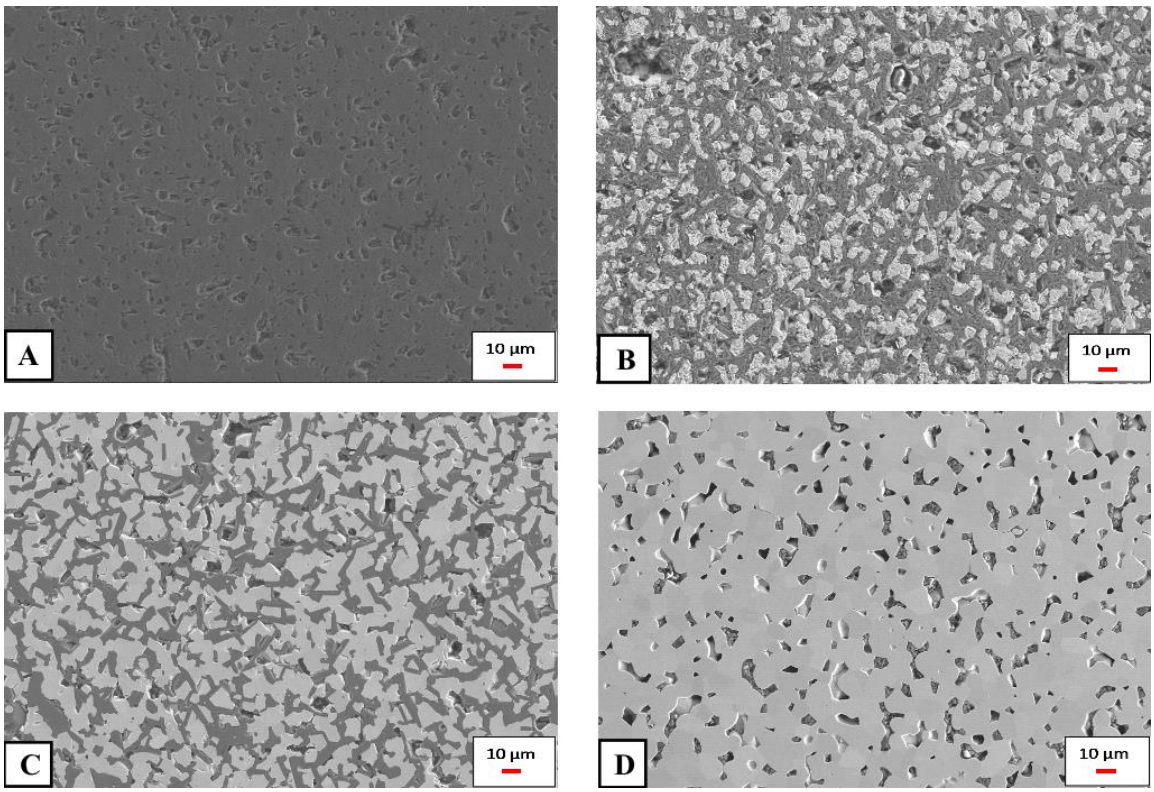

Figure 5.3 SEM images of polished surface of laminates with composition: A): pure SiC; B): 60%SiC-40%ZrB_2; C): 40%SiC-60%ZrB_2; D): pure ZrB_2.

EDS analysis (Fig. 5.4) proved that the light grey phase consisted of ZrB_2 while the black one mainly consisted of SiC; the graphite inclusions were present too and they appeared in a dark color. Any reactions occurred between the two main component during the densification, in fact there was not observed the formation of other phases.

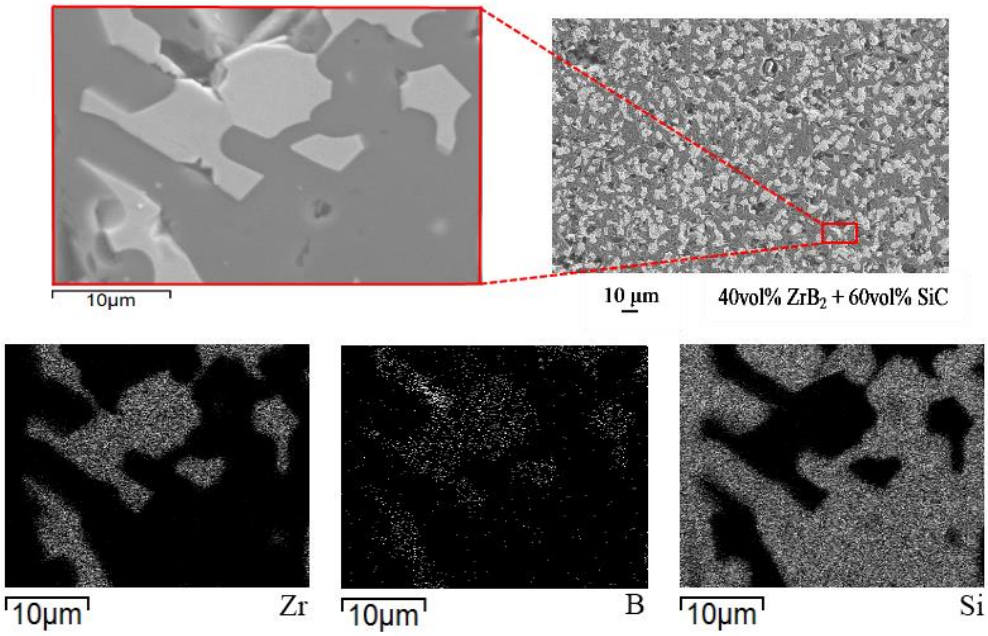

Figure 5.4 Elements EDS maps of cross section surface of laminate with composition 60%SiC-40%ZrB_2

5.2.2 XRD

The X-ray diffraction patterns of laminates with different ZrB_2:SiC ratio were reported in Figure 5.5; they showed the presence of peaks mainly belonging to SiC and ZrB_2 phases, whose relative intensities were strictly dependent on ratio between the two main components .

Also the peak corresponding to graphite can be observed in most of the sample surface X-ray diffraction patterns. The highest intensity Carbon peaks were observed for pure SiC laminates: actually 3 wt% of Carbon and 2wt% of Boron, calculated with respect to the SiC amount, have been added as sintering aids to the slurries of pure SiC and of composite one. A very low intensity peak of graphite peak was also observed in the diffraction patterns of laminates with a low content of SiC: its presence comes from the thermal decomposition of binder and plasticizer occurring during debinding treatment which left a carbonaceous residue (81). In addition a contamination of the sample surface with Carbon could occur also during sintering, since both the chamber and the heating elements of the sintering furnace were made of graphite. However no significant difference between the X-ray patterns of the surface and those obtained for powdered specimens was observed.

X-ray diffraction confirmed what it was just shown by EDS analysis: any reaction occurred between SiC and ZrB_2 during the sintering process.

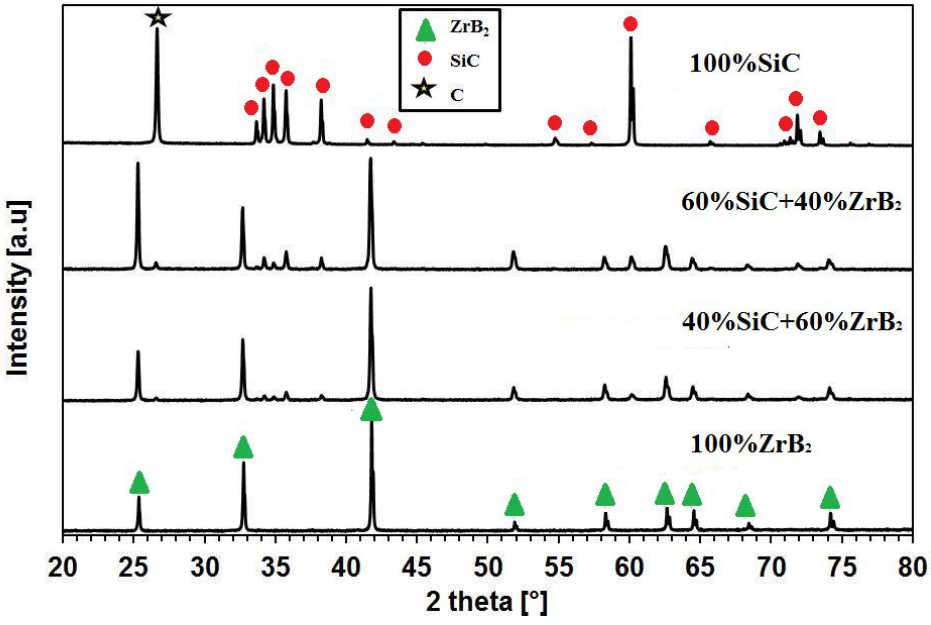

Figure 5.5 XRD diffraction pattern of laminates surface: pure SiC; 60%SiC-40%ZrB_2; 40%SiC-60%ZrB_2 ; pure ZrB_2.

5.2.3 Density

In Figure 5.6 were reported the relative geometric, bulk and apparent density of laminates with decreasing amount of ZrB_2.

The geometric density values were always underestimated with respect to the bulk and apparent ones: this was because of the error in considering the sample as a regular parallelepiped; all the multilayer were cut manually, so the opposite faces could be not perfectly parallel. Moreover the presence of surface roughness limits the precision in measuring the samples dimensions.

The residual porosity comes from the thermal decomposition of organic components occurring during debinding treatment which was not completely recovered during the sintering process. In addition an enhanced degree of microporosity was expected to remain at the interfaces between the layers stacked in a laminate structure.

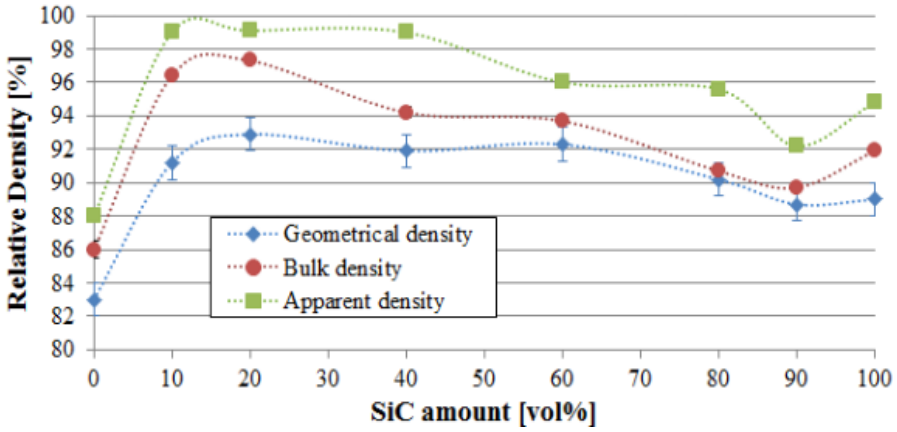

Figure 5.6 Geometric, Bulk and Apparent density for laminates with increasing amount of SiC.

The addition of C and B improved the densification of multilayer containing pure SiC, (81; 82; 79) but they also helped the sintering of ZrB_2/SiC composites where SiC was present as major component. However when the main component of the composite becomes ZrB_2 similar densification degree can be observed: the presence of SiC improved the densification of the ZrB_2 composite matrix, as was previously reported in literature (83; 75; 57) . ZrB_2 multilayer processed without the help of any sintering additive showed the lowest density value which confirmed its poor intrinsic sinterability.

5.2.4 Mechanical properties

Figure 5.7 shows the effect of the chemical composition (ZrB_2:SiC ratio) on elastic modulus, flexural strength and microhardness.

Most of literature reported elastic modulus of hot pressed ZrB_2 (it was the most used sintering process because of its poor sinterability), whose values were in the range from 350 GPa to 530 GPa in function of the porosity and the used additives.

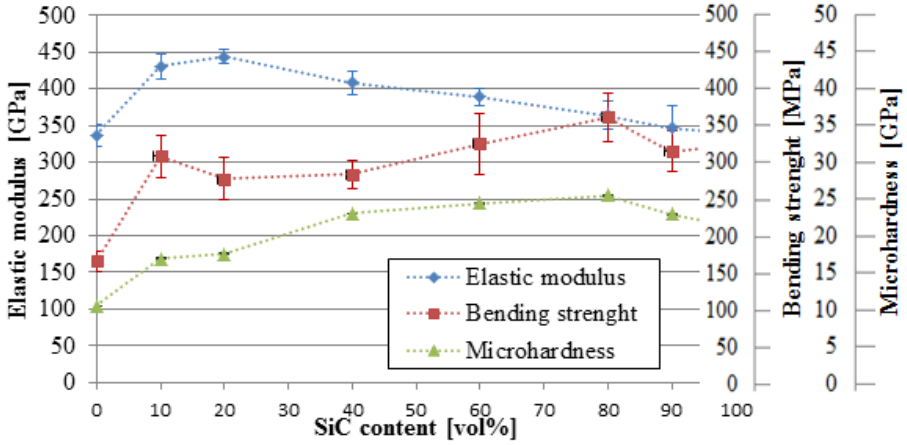

Figure 5.7 Mechanical properties laminates with increasing amount of SiC.

Some reference handbooks (84; 59) reported that Young's modulus of fully densified polycrystalline ZrB_2 (obtained by hot pressing process too) without any sintering additives was in the range 489-500 GPa.

In literature it was possible to find many characterization of ZrB_2/SiC based composite sintered by hot pressing: their elastic modulus has been shown to be in the range 450-484 GPa (85; 86; 87; 88), so slightly lower than that of pure ZrB_2.

In our investigation the elastic modulus was found to increase with a linear trend in function of the increasing amount of ZrB_2 up to 90vol%; then it decreased to the lowest value (337 GPa) for pure ZrB_2. This trend is in accordance with the density one: Young' modulus is in fact greatly influenced by the presence of porosity in the material which resulted quite high for pure ZrB_2. Moreover our laminates with composition 80vol%ZrB_2-20vol%SiC had a higher elastic modulus (444 GPa) respect than 382GPa (89) and 374GPa (90) shown for composite with the same composition obtained by pressureless sintering.

Without combining high temperature and pressure during sintering process it was not possible obtain fully dense ZrB_2; therefore the residual porosity had a great influence on the mechanical properties too, first of all on the elastic one. In order to obtain almost full dense pressureless sintered material and exploit all advantages of a so produced material in structural applications, it was necessary the addition of SiC which lets to obtain a good performance material (good physical and mechanical properties).

Even if many attempts have been done in order to make a prevision of elastic modulus for composite containing particles (many models exist for composite containing fibers) on the base of theoretical dissertation, no-one of these models resulted completely coherent with the experimental results. For this reason we can use only semi-emphirical models such as Couto equation (91; 92):

$$\frac{1}{E_c} = \frac{1-V_p^{1/2}}{E_m} + \frac{1}{\left(\frac{1-V_p^{\frac{1}{2}}}{V_p^{\frac{1}{2}}}\right)\cdot E_m + E_p} \qquad \text{(Eq. 5.1)}$$

Where E_c was the ZrB_2/SiC composite Young' modulus, V_p was the volume fraction of particle, E_m and E_p were elastic modulus of respectively matrix and particles.

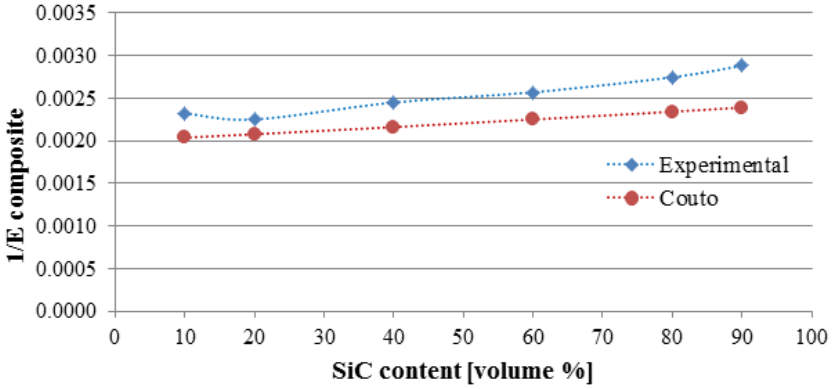

Figure 5.8 Elastic modulus of composite with different ZrB_2:SiC ratio: comparison between experimental and Couto' model values.

Figure 5.8 puts in comparison the prevision of elastic modulus obtained by Couto model and the experimental value: for all the compositions it was evident that the experimental values had the same trend (elastic modulus decreased with increasing of SiC content in the composite) respect to the model one, but they were always greater than Couto's prevision.

Moreover the bending strength and the microhardness of investigated multilayer resulted lower than those reported in the literature for hot pressed SiC, ZrB_2 and composites made of a mix of them, but the bending strength had consistent values than those of similar ceramics produced by pressureless sintering (83).

Pure SiC multilayer and composites with different relative amount of SiC and ZrB_2 showed similar bending strength values in the range 277 MPa-365 MPa without a strictly connection with the chemical composition. On the contrary, *Lu et al.* (93) showed that the positive effect of SiC in the sintering process was counterbalanced by the agglomeration of the SiC particles (which progressively increased with the SiC percent increasing). These two opposite effects resulted in a maximum strength observed when the SiC content in the composite is around 20vol%.

Bending strength values ranging between 250 MPa and 519 MPa have been reported for 80%ZrB_2-20%SiC composite obtained by pressureless sintering, depending on the presence of different sintering additives (38; 89; 90).

Nevertheless it was very difficult comparing mechanical features of ceramic materials with so many different characteristics: for example the bending strength of sintered SiC, ZrB_2 and their composites greatly depends on the processing method, the material microstructure, the configuration used for the test and the size of the samples.

On the other hand the materials to be used as the component of the TPS facing the atmosphere were not required to display very high strength, being their oxidation resistance the main concern.

Literature data dealing with the hardness of fully dense SiC and ZrB_2 were widely scattered: hardness values between 27 and 32 GPa and between 25 GPa and 29 GPa have been reported for SiC and ZrB_2 respectively (59; 94; 95).

The hardness values measured in this work for SiC and its ZrB_2/SiC composites ranged between 16.9 GPa and 25.5 GPa. They were lower respect the value reported in literature for hot pressed materials: reasonably the residual porosity and the presence of graphite lowered the hardness of laminates.

On the other hand for composite with composition 80%ZrB_2-20%SiC the hardness was 17.5 GPa, that is slightly higher than those reported in the literature for ceramics with the same composition and densification method (89; 90).

5.2.5 SPS densification process for ZrB_2 and SiC laminates

In addition to the pressureless sintering, Spark Plasma Sintering is an alternative method to densify ZrB_2 based ceramics as previously discussed in Section 3.3.6; Tecnalia was able to perform this kind of process on the SiC and ZrB_2 multilayer prepared by tape casting technique in Politecnico of Turin.

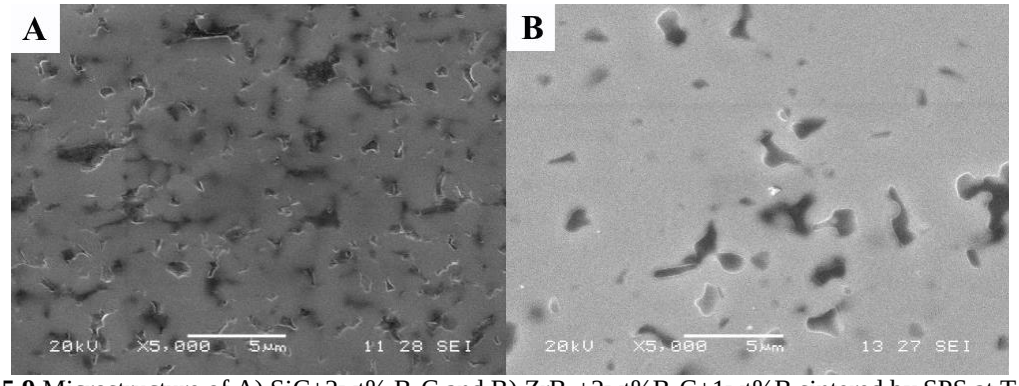

Figure 5.9 Microstructure of A) SiC+2wt% B_4C and B) ZrB_2+2wt%B_4C+1wt%B sintered by SPS at Tecnalia

The microstructure in Figure 5.9 shows the presence of higher porosity in case of SPS sintered Silicon Carbide respect to the ZrB_2 based material; probably the addition of Boron Carbide was more effective in former case respect to the second one (take into account that for ZrB_2 a combination of B_4C and C were used).

Material	Sintering Process	Sintering Temperature [°C]	Relative Geometrical Density [% of the theoretical]
SiC +2wt%B_4C	SPS	1850	91
SiC +1wt%B +3wt%C	PS	2200	92
ZrB_2	PS	2200	82
ZrB_2 +5wt%TiC	PS	2200	92
ZrB_2 +2wt%B_4C +1wt%B	SPS	1900	94

Table 5.II Comparison between SiC and ZrB*2* based multilayer sintered by SPS

In SPS process of both SiC and ZrB_2 the temperature used to obtain the maximum densification degree mainly depended on the composition: for SiC the maximum densification was obtaining using a sintering temperature of around 1850ºC, while for pure ZrB_2 was necessary to reach 1900ºC. B_4C, TiC, C and B were used as sintering additives, but any significant difference in term of densification degree was observed (Table 5.II). In all cases the geometrical density of materials densified by SPS or PS was higher than 91% respect to the theoretical one; the lowest value resulted for pure ZrB_2 sintered by PS.

5.3 Laminates with alternate ZrB_2/SiC and SiC layers

The concept of multilayer integrating ZrB_2/SiC composite layers in between SiC ones was born from the crescent interest in developing reusable thermal protection system which is able to withstand critical conditions for repeated aerospace missions. Silicon Carbide was one of the most used material for this kind of applications; unfortunately its limit was the temperature range of use. The oxidation of SiC involved the production of a SiO_2 layer which protected the underlying components from further Oxygen penetration. For very high temperature (above 1600°C) this passive layers melted and could be easily consumed and carried away due to the air friction during the vehicle re-entry in the Earth atmosphere. Moreover, in particular conditions of high temperature and low Oxygen partial pressure, SiC undergoes active oxidation. A TPS with an external layer made of only Silicon Carbide can't guarantee good performance at very high temperature (up to 2000°C).

When the SiC layers are damaged the underlying ZrB_2/SiC layer can protect the vehicle structure slowing down the diffusion of Oxygen and so improving the oxidation resistance of the laminates.

The aim was to verify the feasibility of a laminates with this particular configuration and then characterize the sintered material from physical and mechanical point of view.

The most important design parameters for this kind of laminates were chemical composition, thickness, number and position of the interlayers: tape casting is the processing technique able to control and regulate all the mentioned parameters.

The choice was to use a composite with composition 80vol%ZrB_2-20vol%SiC on the base of previous results which showed that this material represented one of the best compromise in term of density and mechanical properties; moreover this composition was the most studied in literature for aerospace applications (85; 87; 22).

The multilayer were prepared stacking 10 layers with a doctor blade height set on 1 mm (the same parameters respects to the specimens previously sintered and characterized, in order to compare similar materials with a thickness of about 1-1,5 mm): 8 layers were made of SiC and 2 were constituted of composite (Figure 5.10). The introduction of only two ZrB_2/SiC layers was justified considering that no previous studies were made on a so assembly samples so it could be not cautious introducing an high number of interfaces SiC/composite into the material without knowing the effects of these on the material properties. Moreover a symmetrical structure can balance the opposite tensional states present in layers with different properties.

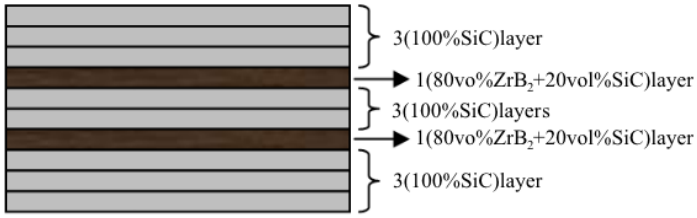

Figure 5.10 Configuration of multilayer integrating SiC and ZrB_2/SiC composite layers

The specimens were submitted to two heat treatments: the first one up to 800°C in order to remove the organic components from the slurry and a second pressureless sintering at 2200°C for 30 minutes. The microstructure of *Serie 1* sintered samples are shown in Figure 5.11, while the density values and mechanical properties are summarized in Table 5.III.

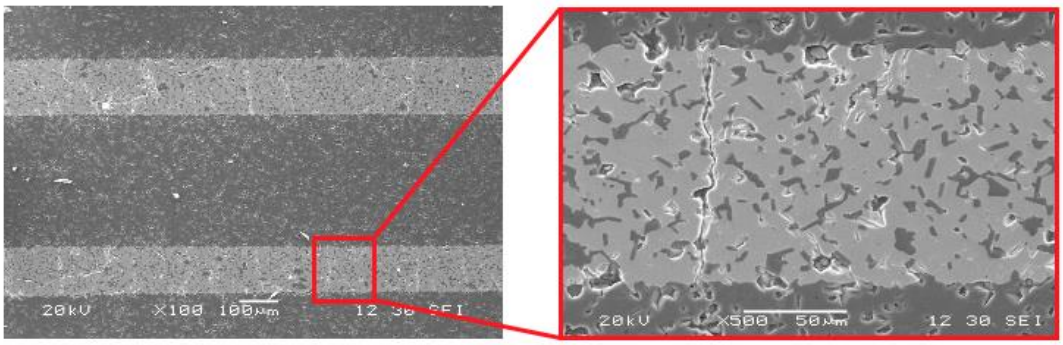

Fig 5.11 SEM images of polished sections of multilayer belonging Serie 1.

	Geometrical density [% of theoretical]	**Apparent density** [% of theoretical]	**Elastic modulus** [GPa]	**Bending strength** [MPa]
Serie 1	72.3±5.6	88.7±2.4	209.4±27.3	106.8±14.3
Serie 2	75.3±8.3	90.2±3.3	310.1±27.6	263.3±56.6

Table 5.III Physical and mechanical properties of multilayer belonging Serie 1.

From the micrographs it was evident the presence of many cracks with not negligible thickness: they cross the composite layers in all their depth, however they do not propagate in SiC layers. The geometrical, bulk and apparent densities had comparable values respect to those experimentally measured for multilayer made of only SiC and composite layers (Fig. 5.7).

Similar considerations can be done for mechanical properties: the elastic modulus and the bending strength resulted lower than the respective values calculated by the mixture rules. The cause of these low properties can be probably found in the evident cracks formed in the composite layers and so in the residual porosity higher than 10vol%.

The presence of cracks is caused by residual stresses which were developed during sintering process. Actually there was a difference in sintering rates between the ZrB_2/SiC composite and SiC layers, and equiaxial stress was developed in both laminae being compressive in the layer which densified more slowly and tensile in the layer that is shrinking faster. For a sinterable ceramic powder the magnitude of sintering stress was of the order of 10 MPa and consequently also the tensile stress should be of the same order (96). Even if present, these kind of stresses should not cause failure of the laminate (97).

On the other hand more relevant were the effect of stresses developed on cooling from the sintering temperature: the dimensional shrinkage of composite layer resulted higher respect to the SiC one.

Moreover the mismatch between the SiC and composite thermal expansion coefficient caused thermal stresses at the interface between layers with two different chemical composition.

The result was the formation of compressive stresses in layers with lower CTE, in our case Silicon Carbide, while tensile stresses were developed in composite layers showing higher CTE.

The contribution of CTE difference between the two materials was greater during sintering respect to the debinding process: CTE of SiC was $5{,}1\cdot10^{-6}$ °C^{-1} (25°-1000°C) and $5{,}8\cdot10^{-6}$ °C^{-1} (25-2500°C) (98), while the composite with 80vol%ZrB_2-20vol%SiC had CTE values, calculated by the mixture rule, of $5{,}7\cdot10^{-6}$ °C^{-1} (25°-1000°C) and $7{,}8\cdot10^{-6}$ °C^{-1} (25-2500°C).

In order to estimate the magnitude of the elastic strains based on the difference in thermal expansion coefficients, we can take as reference the "cut and weld technique" (99; 96):

$$\varepsilon_t = -\frac{E_t}{E_t \cdot f_t + E_c \cdot f_c} \cdot f_t \cdot (\alpha_c - \alpha_t) \cdot \Delta T \qquad \text{(Eq. 5.2)}$$

Where ε_t is the residual strain in tension layer (composite one), E is the elastic modulus, α is the thermal expansion coefficient, f_t is the thickness fraction of composite and ΔT is the temperature change the sample undergoes the cooling.

The same equation can be written also for estimate ε_c that is the residual strain in SiC layers placed in compressive strains.

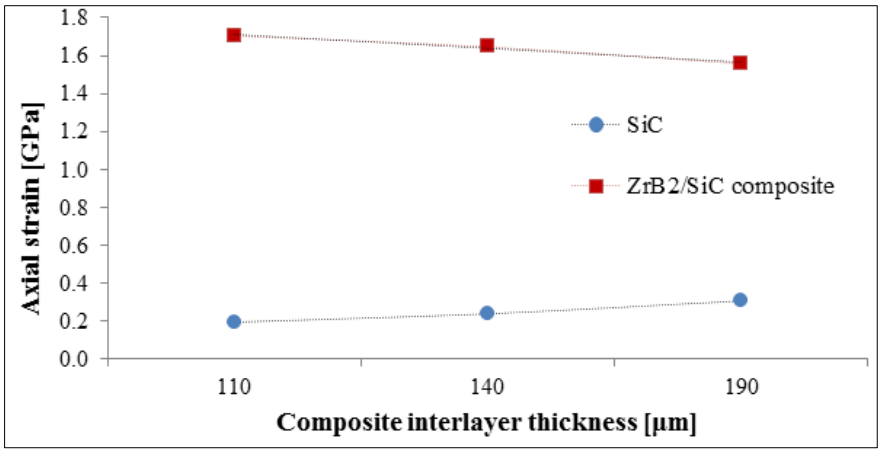

Figure 5.12 Estimation of residual stresses in SiC and ZrB_2/SiC layers using "cut and weld technique".

The high value of strain found in the ZrB_2/SiC composite (Figure 5.12) justified the presence of stresses in these layers; these tensile stresses caused the formation of cracks along the layer thickness.

In order to reduce the residual stresses at the interface SiC/composite layers two strategies have been adopted:

(A) To vary the grain size of the starting powder.

(B) To modify the thickness ratio of layers with different composition.

5.3.1 The effect of starting powder milling

The use of milled ZrB_2 powder has been successfully adopted in order to improve the densification: *Chamberlain et al.* (60) reported that submicron particles (obtained after ZrB_2 milling in hexane at 600 rpm for 2 hours with tungsten carbide media) provided high surface area which increased the driving force for sintering. Previously studies on ZrB_2 particle size (100) justified this effect supposing an increasing in concentration of point defects and dislocation which promoted the densification process.

SiC and ZrB_2 used in this work showed particles with very different size respectively 0,55µm and 2,25 µm: the problem of the different shrinkage during the cooling from 2200°C (sintering temperature) could be overcome by reducing the size of ZrB_2 particle size.

With this aim milling tests have been done in order to find the necessary conditions to make the two powders grain size comparable. As shown in Figure 5.13 and Table 5.IV, after 3hours milling with Tungsten Carbide media the grain size of ZrB_2 was 0,568µm (D90%) so resulting very similar to the SiC one.

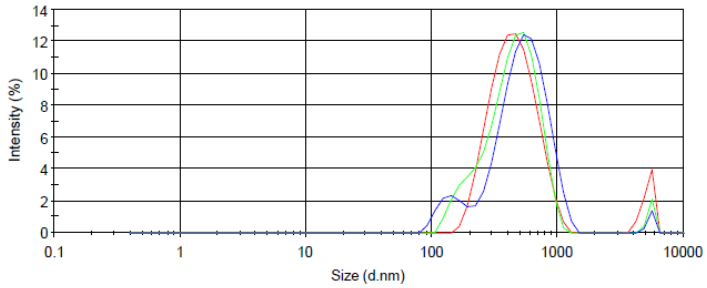

Figure 5.13 ZrB_2 size distribution by intensity (after 3 hours milling).

Milling Time (hours)	Particle size D90% (µm)
2	0.667
3	0.568
4	0.463

Table 5.IV ZrB_2 particle size after 2, 3 or 4 hours milling

This milled powder was used to prepare *Serie 2* samples: two layers with composition 80vol%milled ZrB_2+20vol%SiC were integrated into the multilayer (Configuration from Fig.5.10); the green specimens were then submitted to the same debinding and sintering cycles than the previous ones.

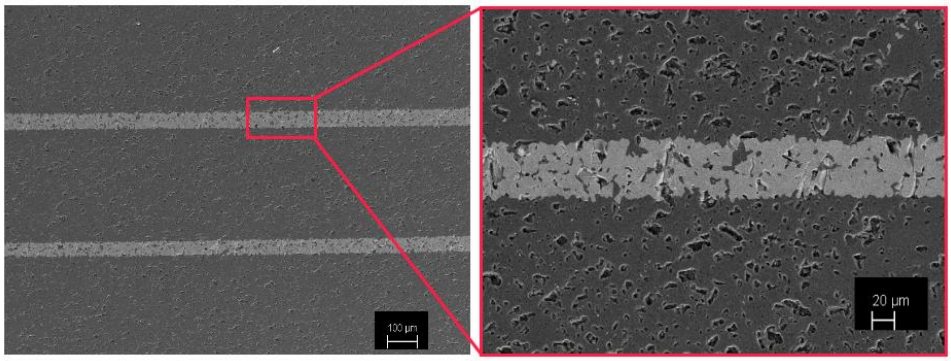

Fig 5.14 SEM images of polished sections of multilayer belonging to Serie 2.

The micrographs in Figure 5.14 showed the presence of cracks which were thinner and in lower number respect to those observed in sample integrating composite layers with not milled ZrB_2 starting powders.

The effects of ZrB_2 powder milling were evident on the mechanical properties (Table 5.III): the densification degree improved, the elastic modulus increased of 30% respect to the Serie 1 and also the bending strength considerably increased (more the double than the Serie 1 value).

The reduction in size of ZrB_2 starting powder led to a reduction of the stresses developed at the SiC/composite interface; it improved the densification process allowing to obtain multilayer with a density around 90% and enhanced mechanical properties.

5.3.2 The effect of the thickness ratio of layers with different composition

A second factor which can influence the properties of laminate integrating SiC and composite layers and moreover decrease the entity of developed stresses (leading to the formation of less cracks in composite layers (Fig 5.11 and Fig 5.14)) was the variation of the thickness of layers with different chemical composition.

Considering the beneficial effects observed after ZrB_2 powder milling, for all samples belonging *Serie 3* the composite layers were prepared using milling ZrB_2 powder.

A systematic investigation on the effects of thickness ratio between SiC and composite layers on the multilayer properties has been done: the SiC layers thickness was maintained at a fixed value (the blade height was set at 1 mm which corresponded to a green tape thickness of 240 µm) while the thickness of composite layers was varied between 100 and 550 µm (in term of green tapes thickness) as shown in Table 5.V.

Serie 3	
Blade height [mm]	**Tape thickness [µm]**
2*	110
0,7	140
1	190
2	330
2,4	550

Table 5.V Samples belonging to Serie 3: correspondence between set blade height and green tape thickness.

A blade height of 2 mm was repeated two times in Table 5.V and they corresponded to two very different tape thickness: in the first case the slurry preparation resulted not good and a lump was found in the slurry. It was probably caused by an inhomogeneous mixing of binder with the other components after the second mixing step; for this reason the slurry was less viscous than the standard one and the tape thickness was only 110 µm (obtained after the lump removal).

On the base of this consideration a second attempt was done in order to obtain a so thin green film again: the choice was to decrease the plasticizer amount estimated to 30w% on the base of the lump size. The thickness of the tape was found 330 µm, so the reduction in plasticizer amount was not enough to repeat the condition which had allowed to obtain a thin composite layer. However this result was taken into account in characterization of specimens.

After the debinding process the samples integrating “very thick” composite layers (550 µm) resulted delaminated in correspondence of both the interface SiC/composite layers.

On the other hand the sample with composite layer 330 µm thick in between SiC ones presented problems after the sintering process at 2200°C: half of samples were delaminated and the rest had a very poor structural integrity; in fact they broke after a short handling.

According with *Clegg et al*. (96) the main factors which influence the delamination were: the misfit strain which depended on the difference in the thermal expansion coefficient and the sintering temperature, the elastic modulus, the layer thickness and the relative volume fraction of the two sets of layers.

For a laminate where the two materials had different elastic modulus, in particular if the interlayer in which the delamination cracks grew had an higher Young modulus, the driving force for delamination resulted increased. In our case the composite elastic modulus was measured higher than that of the SiC one (444 GPa and 339 GPa respectively).

In addition it has been found that the driving force for delamination reached the maximum for increasing thickness of interlayers showing high elastic modulus. For example *Howard et al*. (99) reported good structural integrity in processing of SiC/graphite system where the carbide laminae were 10 times stiffer than the graphite interlayer and moreover these last had thickness fraction in the laminate correspondent to only 0.03.

Integrating in the laminate composite layers with higher elastic modulus than SiC one and increasing its thickness more than 330 µm, we were in the optimal conditions for promoting the delamination.

An additional factor which can contribute to the formation of cracks in the composite layer is the different behaviour in term of dimensional shrinkage of layers with different chemical composition during the debinding cycle.

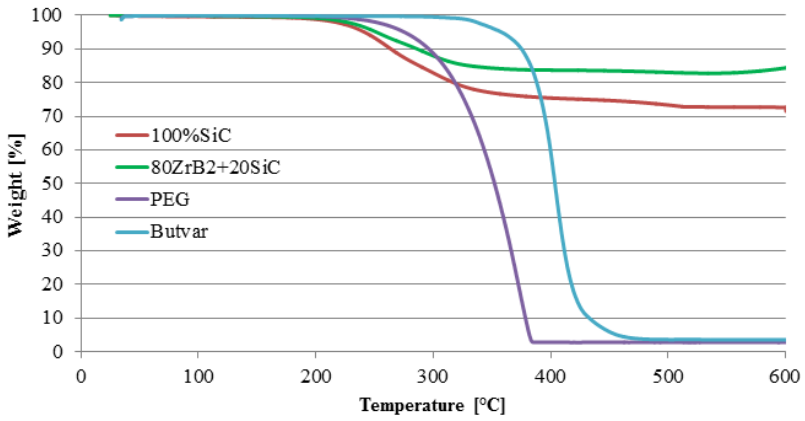

Figure 5.15 Thermogravimetric analysis of Butvar, PEG, green tape made of 100%SiC and green tape with composition 80%ZrB_2+20%SiC.

For this reason thermogravimetric analysis (Figure 5.15) have been performed on the two main organic compounds in the slurry (Butvar and Polyethylenglycol) and on green tapes with composition respectively 100%SiC and 80%ZrB_2-20%SiC. The decomposition of organics species occurred mainly between 250°C and 500 °C. In this temperature range a weight loss was observed for both the tapes: in SiC sample the decomposition process started at lower temperature, it progressed more quickly and involved higher weight losses respect to the composite ones. This difference in debinding behaviour caused stresses which were probably marked in the case of tapes with different thickness causing the failure of the multilayer just during this phase.

Serie 3 -Density-	Relative Geometric Density (%)	Relative Bulk Density (%)	Apparent Relative Density (%) (Helium picnometer)
Serie 110	90.01 ± 0.08	90.80 ± 1.80	94.830 ± 0.003
Serie 140	87.24 ± 0.07	92.87 ± 1.77	96.448 ± 0.004
Serie 190	88.64 ± 0.09	93.07 ± 0.98	95.735 ± 0.004

Table 5.VI part A-density- of sample integrating composite layers with different thickness

Serie 3 -Mechanical properties-	Elastic Modulus [GPa]	Bending Strenght [MPa]	Vickers Microhardness for SiC [GPa]	Vickers Microhardness for Composite [GPa]
Serie 110	348 ± 20	510 ± 39	37.32 ± 3.33	22.17 ± 1.73
Serie 140	297 ± 14	313 ± 10	32.49 ± 5.88	22.08 ± 2.01
Serie 190	319 ± 22	289 ± 56	33.69 ± 5.01	21.07 ± 1.96

Table VI part B-mechanical properties- of sample integrating composite layers with different thickness.

Table VI summarized the mechanical properties of samples integrating composite layers with thickness respectively 110 µm, 140 µm and 190 µm.

The differences in apparent and bulk density were due to the different fluids used for measuring them: Archimedes' value were obtain using deionized water, while pycnometer measurement were done using Helium. He molecules were smaller than water ones so they can fill better the open porosity.

However apparent density for all three series of samples were in the range 94% - 96.5%, these values resulted slightly lower than the laminate constituted by layers with all the same composition, but substantially higher than the laminated belonging to Serie 1 and 2. Using ZrB_2 starting powder with reduced grain size and integrating composite layers with thickness lower than 200 µm, it was possible to obtain laminates with improved densification degree.

The micrographs of cross section in Figure 5.16A and 5.16B shows the microstructure of the three series of samples different in term of composite layer thickness: in the second line (Fig5.16 110-B, 140-B and 190-B) a zoom of the composite interlayer put in evidence the presence of cracks propagating only in the composite without affecting the underlying and over SiC layers. Figure 5.16C shows the fracture surface of the laminated belonging to Serie 3, indicating a mixed of trans/intergranular fracture mode: in SiC layers there were cleavage planes characteristic of transgranular fracture, while in the composite interlayer an intergranular fracture mode was observed.

Moreover from Figure 5.16-190C it was evident that crack did not travel right across the specimen, but it was deflected at the interface between SiC and composite layer.

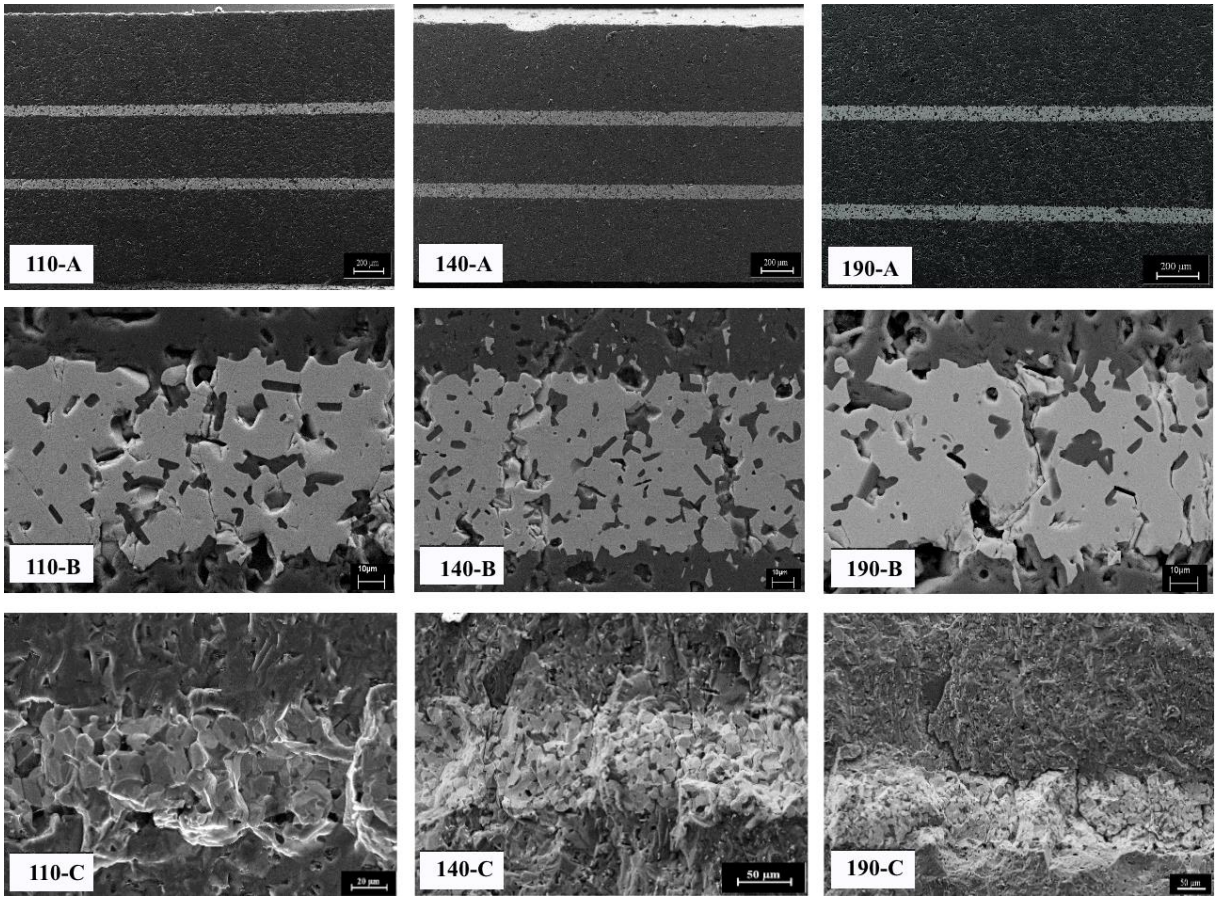

Figure 5.16 Microstructure of laminate belonging to Serie 3 with composite layer thickness 110µm, 140µm and 190µm: A-Overview of the polished cross section, B-Zoom on composite interlayer and C-fracture surface.

The mechanical properties such as elastic modulus and bending strength (Fig 5.12) showed a similar trend: their values increased in function of the decreasing of composite interlayer thickness.

According to *Sanchez-Herencia et al.* (101) large improvement in strength can be achieved when the external layers of a laminate were in compression; this was the so called "strengthening

approach" because of the laminate showed increased strength compared to the monoliths with the same composition of the external layers composition. This effect could be significant for the laminates integrating 110µm thick composite layers: their flexural strength were much higher than those of monolithic ceramics with composition 100%SiC (their strength was 359MPa (102)) as well as the multilayer with this composition (Fig. 5.7). Moreover this value was higher than the multilayer with composition 80vol%ZrB_2-20vol%SiC too. For future activities it would be interesting trying to increase the magnitude of compression state in Silicon Carbide layers with the aim to study the effect on flexural strength.

The microhardness test were performed on both SiC layers and the composites ones; the scattering of results for SiC material was the double than those for composite layers: this implied a higher homogeneity in the ZrB_2/SiC based layers. In fact in Silicon Carbide the presence of an higher residual microporosity and Carbon inclusions have made the measure of the imprint more difficult. Also in this case enhanced microhardness was observed respect to the single-composition multilayer values (Fig.5.7). The improvement in mechanical properties was attributed to the presence of residual stress in the ZrB_2/SiC based composite interlayers.

5.3.3 Alternative SPS sintered laminates

In addition to the pressureless sintering, another alternative process for the sintering of multilayers integrating ZrB_2/SiC composite layers in between SiC ones was the Spark Plasma Sintering (the principle of this technique is reported in Section 3.3.5 and the application in ZrB_2 base material in Section 3.3.1.1) ; the consolidation experiments were performed at Tecnalia.

Different configurations of multilayers were successfully obtained and reported in Figure 5.17.

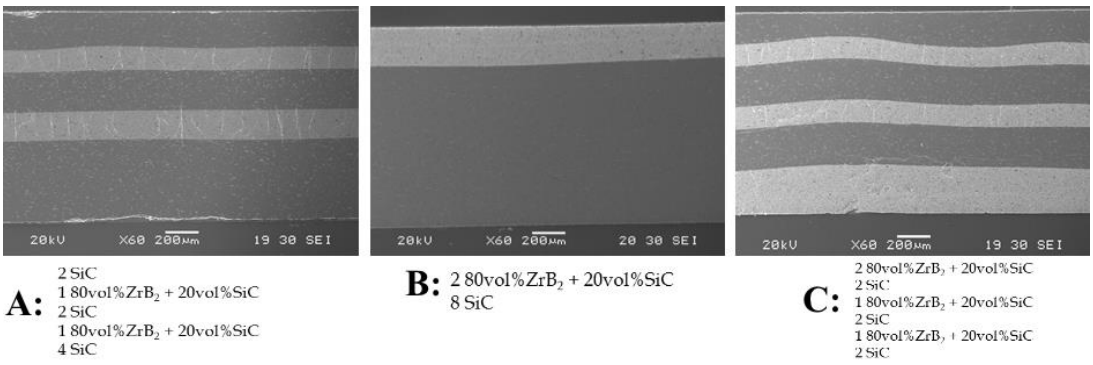

Figure 5.17 SEM microstructure of laminates integrating composite layers in between SiC ones sintered by SPS at Tecnalia.

The most evident defect was the presence of cracks after the sintering which were perpendicular to the load application; the same problem was identified in pressureless sintered laminate integrating composite layers in between SiC ones. In addition to the consideration previously

done, a reason of these cracks were the stresses probably produced by the difference in CTE during the fast cooling. A possible solution to avoid or at least limits their formation was the change of the load cycle: it was necessary to release the pressure at high temperature in order to decrease the stresses produced by the difference in CTE.

The architecture shown in Figure 5.17B was also prepared and sintered without pressure assistance, but it failed just after the debinding cycle.

Chapter 6
Oxidation behaviour of ZrB_2/SiC based multilayer

Besides mechanical properties, the oxidation resistance is also very important property for materials to be used as external part of a thermal protection system, especially because the goal was the development of reusable TPS which should be submitted to high temperature, oxidant environment and high thermal flux for repeated times. In this chapter the oxidation behaviour of laminates with different ZrB_2:SiC ratio will be examined.

6.1 TGA oxidation tests

The TGA results are summarized in Figure 6.1A and 6.1B:

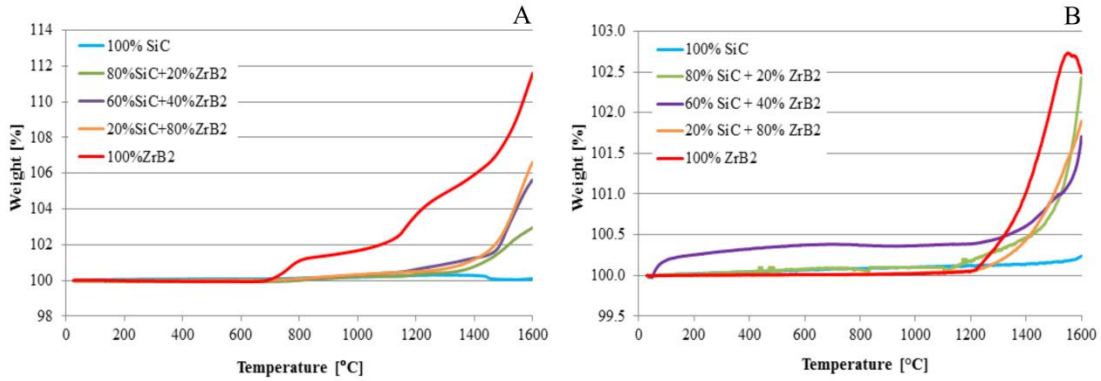

Figure 6.1: Comparison of TGA fist runs (5.1A) and second runs (5.21B) in air up to 1600°C: pure ZrB_2; 80 ZrB_2-20 SiC; 60 ZrB_2-40 SiC; 20 ZrB_2-80 SiC and pure SiC.

In order to explain the oxidation mechanism of ZrB_2/SiC based composites it is interesting to analyze the oxidation behaviour of the two components SiC and ZrB_2 separately.

It is well-known from the literature that SiC can oxidize in two different ways in function of the temperature and the Oxygen potential.

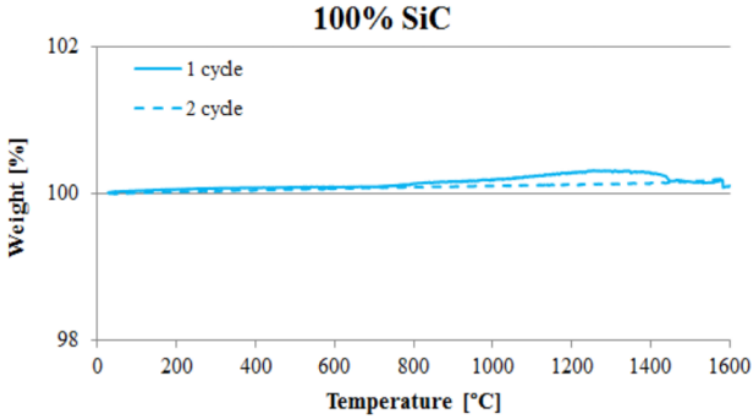

Figure 6.2: TGA curves obtained during the first and second run for multilayer with composition 100%SiC.

The TGA curve of SiC (Figure 6.2) shows a very small weight gain starting from 1000°C (it corresponded to less 0,3w%) caused by the oxidation of SiC and the formation of a silica layer on the surface. Only little SiC oxidized and consequently a very thin oxide layer was formed.
For temperature above 1500°C the mass gain resulted well counterbalanced by the formation of $CO_{(g)}$ coming from the oxidation of Carbon.
For temperature up to 1600°C and at Oxygen pressure close to one bar SiC oxidized according to the reaction (6.1):

$$SiC_{(s)} + {}_{3/2}\, O_{2(g)} \leftrightarrow SiO_{2(s)} + CO_{(g)} \qquad \text{(Eq. 6.1)}$$

This "passive oxidation" involved the formation of a thin and continuous layer of crystalline silica on the surface; it greatly slows down a further Oxygen diffusion. This was confirmed by the second oxidative cycle: repeating on the same sample an equal heat treatment in flowing air up to 1600°C the resultant TGA curve appears flat so no weight gain was more observed.
The limitation in using Silicon Carbide in aerospace application up to 2000°C is linked to two factors: the thin silica layer, during reentry trajectories and at high velocities, melts and can be consumed and easily carry away due to the air friction.
Moreover in particular at this pressure and temperature conditions the mechanism of passive oxidation could not be the most favorable one. In fact according to Schneider (103) for temperature higher than 1400°C and if contemporaneously the Oxygen partial pressure greatly decreases below 10^{-2} atm (104; 105; 106) the "active oxidation" of SiC can occur according to the equations (6.2), (6.3) and (6.4) :

$T \geq 1400°C$ $\quad SiC_{(s)} + ½\, O_{2(g)} \leftrightarrow SiO_{(g)} + C_{(s)}$ (Eq. 6.2)

$$SiC_{(s)} + O_{2(g)} \leftrightarrow SiO_{(g)} + CO_{(g)} \qquad \text{(Eq. 6.3)}$$

$1500° \leq T \leq 1900°C$ $\quad SiC_{(s)} + ½\, O_{2(g)} \leftrightarrow Si_{(g)} + CO_{(g)}$ (Eq. 6.4)

The passive-to-active transition is very important in some applications such as SiC-based spacecraft reentry shield: during the crossing of earth's atmosphere the surface of hypersonic vehicle could be in the ideal conditions for active oxidation.
The mechanism of passive-to-active oxidation involves the breakdown of the SiO_2 film and it can happen through different reactions (107; 104):

$$SiC_{(s)} + SiO_{2(s)} \leftrightarrow 2\, SiO_{(g)} + C_{(s)} \qquad \text{(Eq. 6.5)}$$

$$SiC_{(s)} + 2\, SiO_{2(s)} \leftrightarrow 3\, SiO_{(g)} + CO_{(g)} \qquad \text{(Eq. 6.6)}$$

$$2\, SiC_{(s)} + SiO_{2(s)} \leftrightarrow 3\, Si_{(s,l)} + 2\, CO_{(g)} \qquad \text{(Eq. 6.7)}$$

$$SiO_{2(s)} \leftrightarrow SiO_{(g)} + ½ O_{2(g)} \qquad \text{(Eq.6.8)}$$

Equation (6.5), (6.6) and (6.7) are three different reactions which may occur at $SiC_{(s)}$-$SiO_{2(s)}$ interface and lead the consumption of silica layer; moreover the formation of volatile species such as $SiO_{(g)}$ and $CO_{(g)}$ can lift the SiO_2 film interrupting the continuity of the scale.

Equation (6.8) represents the decomposition of SiO_2 film; this process is effective at temperature higher respect to interfacial reactions (6.5), (6.6) and (6.7). (106; 108)

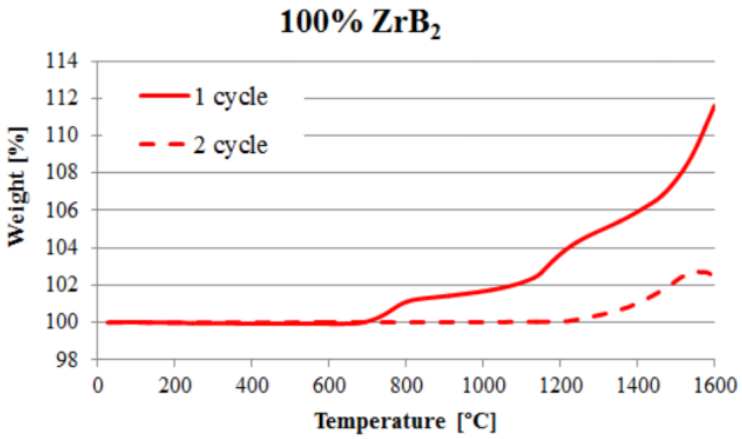

Figure 6.3: TGA curves obtained during the first and second run for multilayer with composition 100%ZrB_2.

TGA curve reported in Figure 6.3 shows a mass gain from 800°C and correspondent to about 12% at the end of the first cycle : pure ZrB_2 undergoes stoichiometric oxidation (Eq. 6.9) producing a scale composed of ZrO_2 and B_2O_3 (109; 22; 110):

$$ZrB_{2(s)} + 5/2\ O_{2(g)} \leftrightarrow ZrO_{2(s)} + B_2O_{3(s,l)} \qquad \text{(Eq. 6.9)}$$

For temperature below 1100°C the B_2O_3 forms a liquid continuous layer which grants protection from further Oxygen penetration.

As *Kuriakose et al.* (109) reported, in this temperature range the oxidation rate of zirconium diboride appeared to be controlled by the transport of Oxygen through $B_2O_{3(l)}$.

On the other hand ZrO_2 scale seemed not to give an evident contribute in protection against oxidation, but it may enhance the mechanical stability and integrity of the over liquid layer (110; 111; 112).

If below 1100°C the oxidation can be described with a parabolic kinetics controlled by the Oxygen diffusion through boria, between 1100° and 1400°C the kinetics of reaction changes in a so-called *para-linear kinetics* (109; 113) because of the process of B_2O_3 formation and its volatilization have similar rates. The total mass changes are in fact the results of two contributions: a weight gain comes from the formation of $B_2O_{3(l)}$ and $ZrO_{2(s)}$ and contemporaneously a weight loss is caused by the volatilization of $B_2O_{3(l)}$.

For temperature higher than 1400°C ZrB_2 oxidation can be described with a fast linear kinetics (the slope of TGA curve significantly increased): the evaporation rate of $B_2O_{3(l)}$ was similar to

the rate of its production. In this condition the underlying porous ZrO_2 scale would be directly exposed to Oxygen contact with a resultant dramatic worsens of ZrB_2 oxidation resistance. Oxidation behaviour of ZrB_2/SiC composites containing from 20 to 80vol% of SiC has been investigated (Figure 6.4).

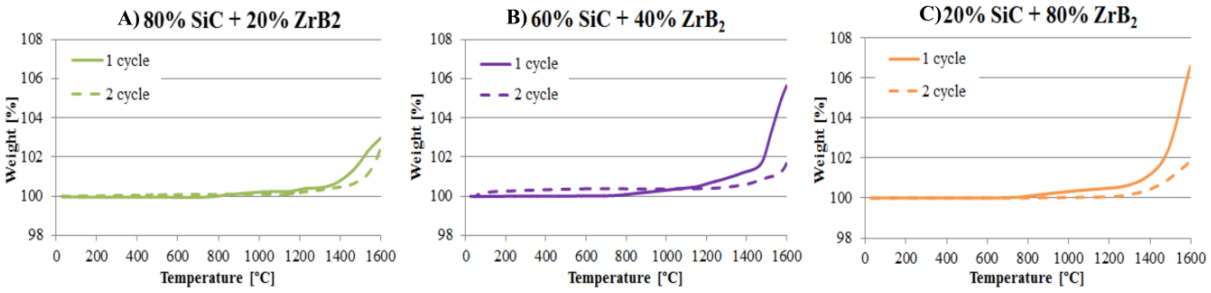

Figure 6.4: TGA curves obtained during the first and second run for multilayer with composition A) 80%SiC-20%ZrB_2; B) 60%SiC-40%ZrB_2; C) 20%SiC-80%ZrB_2.

The mass gain was proportional to the increasing amount of ZrB_2 in the composite: for laminates containing 20%, 40% and 80% ZrB_2 the observed mass gain were respectively 3%, 5%, 6% and 6,6% during the first cycle in flowing air.

The oxide scales produced on the surface of laminates after the first heating were able to reduce the Oxygen penetration during the second cycle in all the three cases.

Considering the starting oxidation temperature and the trend of TGA curves we can conclude that below 1200°C composites behaved like pure ZrB_2: in fact they start undergoing oxidation just from 800°C, temperature at which SiC not oxidises. Above 1200°C also SiC quickly oxidized contributing to the composites oxidation process.

The oxidation of all laminates resulted in the formation of a passive layer which was more effective with increasing amount of SiC.

6.2 Long term oxidation tests

Ceramic laminates were submitted to 24 hours isothermal oxidation at 1600°C under static air with the aim to study the morphology of the produced oxide layers; the microstructure of oxidized multilayer are compared in Figure 6.5.

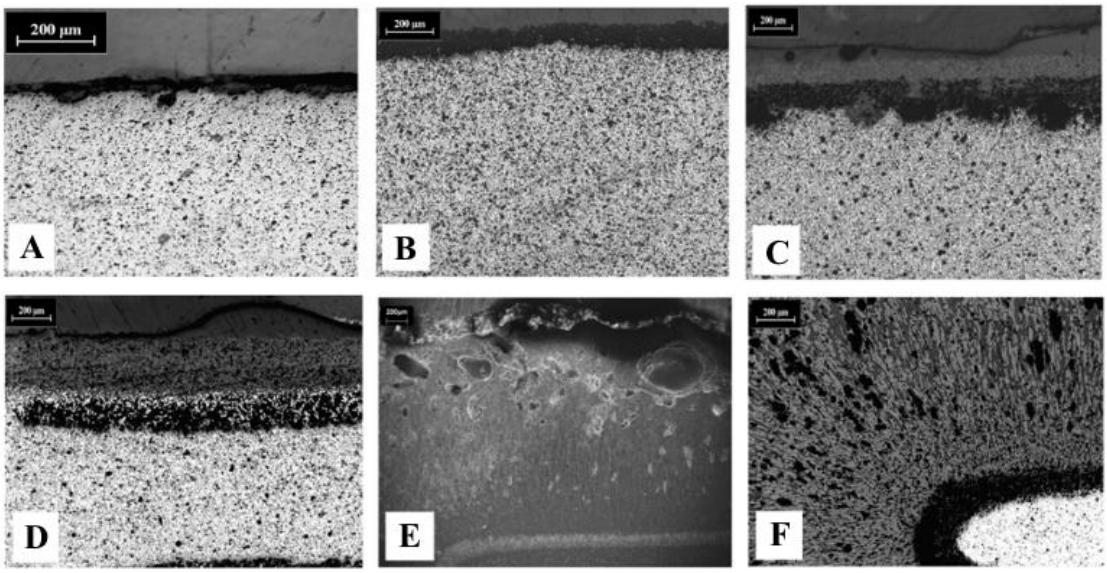

Figure 6.5: Microstructure of ceramic laminates (consisting of layers with the same composition): A) SiC laminate; B) 80%SiC-20%ZrB_2 laminate; C) 60%SiC-40%ZrB_2 laminate; D) 40%SiC-60%ZrB_2 laminate and E) plus F) 20%SiC-80%ZrB_2 laminate.

Laminates with high amount of SiC (Fig.6.5A-100%SiC and Fig.6.5B-80%SiC+20%ZrB_2) showed a thin and continuous oxide layer made of SiO_2, while laminates containing equal or higher than 40vol% amount of ZrB_2 (Fig.6.5C, 6.5D and 6.5E) displayed an oxide layer with a more complex structure on their surface. It was possible to identify three layers: an external glassy layer, an intermediate and a porous ones.

Moreover the samples from 40vol% to 80vol% ZrB_2 blistered during the isothermal treatment: as results their surface presented an inhomogeneous thickness and many small bubbles inside. This surface morphology indicates the formation of gaseous phases: in addition to Carbon oxides coming from the oxidation of SiC we have to take into account the Boron oxide produced by the oxidation of ZrB_2: this compound melts at temperature higher than 800°C and then volatilizes.

Moreover putting in comparison the different microstructures in Figure 6.5 some differences in the morphology of layers in function of the composition were evident.

The intermediate oxide layer was constituted by gray crystals embedded in a dark matrix. While for sample containing up to 60vol% ZrB_2 (Fig.6.5C and 6.5D) the light phase appeared like small spots homogeneously distributed in the darker one, for laminates containing 80vol% ZrB_2 (Fig 6.5E and 6.5F) these two phases gave rise to a columnar structure with a preferential orientation that is perpendicular to the sample surface.

Regarding the porous layer there was a difference in porosity degree among laminates.

The oxidation of multilayer containing high amount of ZrB_2, especially in the case of 20%SiC-80%ZrB_2, led to a great increase of the overall sample thickness which correspond to the formed oxide layers.

In Table 6.I the thickness of the oxide layers are reported in function of laminates composition: multilayer containing 100% and 80% SiC which showed only a thin silica layer on their surface (up to around 100μm thick); in spite of the small thickness it acted as a barrier to Oxygen diffusion through the bulk of the sample.

Material composition	Layer thickness (μm)			
	External glassy layer	Oxide intermediate layer	Porous layer	Sample core
100%SiC	-	21-36*	-	1750
80%SiC-20%ZrB_2	-	97-115*	-	1700
60%SiC-40%ZrB_2	30-164	192-256	95-170	750-1200
40%SiC-60%ZrB_2	83-128	105-180	120-230	1600-1300
20%SiC-80%ZrB_2	600-700	1200-1300	140-200	640

Table 6.I Thickness of oxide layers grown on the surface of laminates with different composition after oxidation treatment under calm air for 14 hours at 1600°C.

The thickness of external glassy layer and intermediate one was strongly dependent on the ZrB_2 content: both the layers increased their thickness with the growing amount of ZrB_2. The most evident case was the laminate with 20%SiC-80%ZrB_2 where the external layer had a similar thickness respect to the sample core; moreover this last one resulted to be the half in thickness compared to the intermediate layer. On the contrary the thickness of porous layer seemed not to be dependent on ZrB_2 content.

Various techniques such as standard and micro-XRD, SEM-EDS and XPS have been used in order to investigate more in details not only each layer microstructure, but also their chemical composition.

XRD spectra of SiC before and after long term oxidation at 1600°C are compared in Figure 6.6: before oxidation SiC was the main phase, a little amount of graphite was present too. The graphite came from the Carbon added to the slurry as SiC sintering aid and moreover it could be a residual from the debinding heat treatment. After oxidation the intensity of both the SiC and the graphite peaks decreased and SiO_2 became the main component.

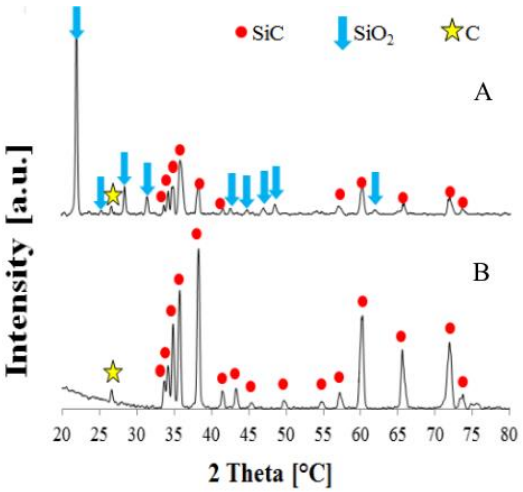

Figure 6.6: XRD spectra of laminate with composition 100%SiC A)before and B) after oxidation at 1600°C.

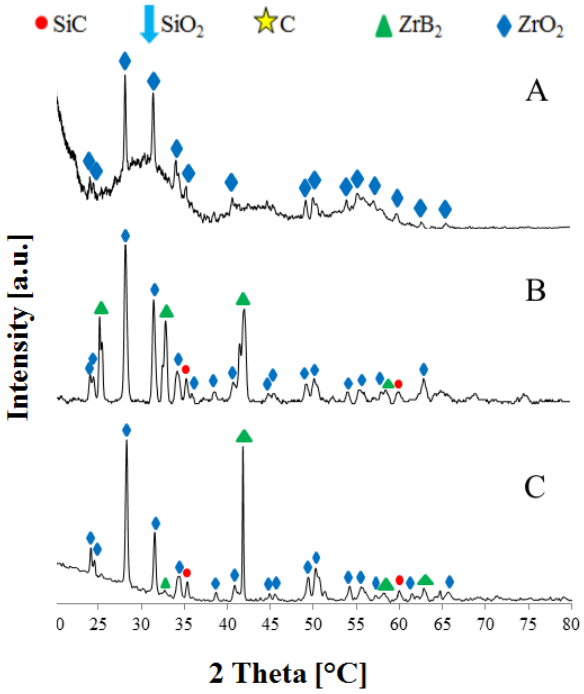

Figure 6.7: XRD spectra of laminate with composition 60%SiC-40%ZrB_2 after oxidation A)external glassy layer B) intermediate layer and C) porous layer after oxidation at 1600°C.

The XRD spectra of laminate with composition 80%SiC-20%ZrB_2 are very similar to those reported in Figure 6.6: before oxidation ZrB_2 peaks were present too, but silica was the only additional phase present on the surface.

Multilayer with ZrB_2 amount higher than 40vol%, as earlier specified, were characterized by a three sub-layers with very different composition.

The glassy external layer was mainly constituted by Oxygen, Silicon and Boron; moreover some traces of Carbon and Zirconium were present. The semi-quantitative EDS analyses showed a ratio between the different component compatible with silica plus boria formation that meant the presence of borosilicate glass. In sample with composition 60vol%SiC-40vol%ZrB_2 the content of Si and consequently O was higher than in laminate containing 20vol%SiC; so the glassy phase resulted more Si-rich with increasing amount of SiC.

XRD micro-diffraction on this area (Fig 6.7A) showed peaks belonging to ZrO_2 superimposed to a broad signal that was characteristic of the presence of an amorphous phase such as a glassy one.

Also XPS analyses allowed to confirm the presence of silica: the Si 2p peak at 103.3 eV correspond to Si-O bonds while the O 1s at 533.1eV is O-Si bonds (Fig 6.8A). Moreover we can suppose the formation of some graphite, probably partially oxidized, inclusions: C1s spectrum showed mainly C-C bonds while only little Carbon was bonded to Si or O. Unfortunately XPS

technique shows a low sensitivity with respect to Boron, so it was not possible obtain information about the bonds formed by this element.

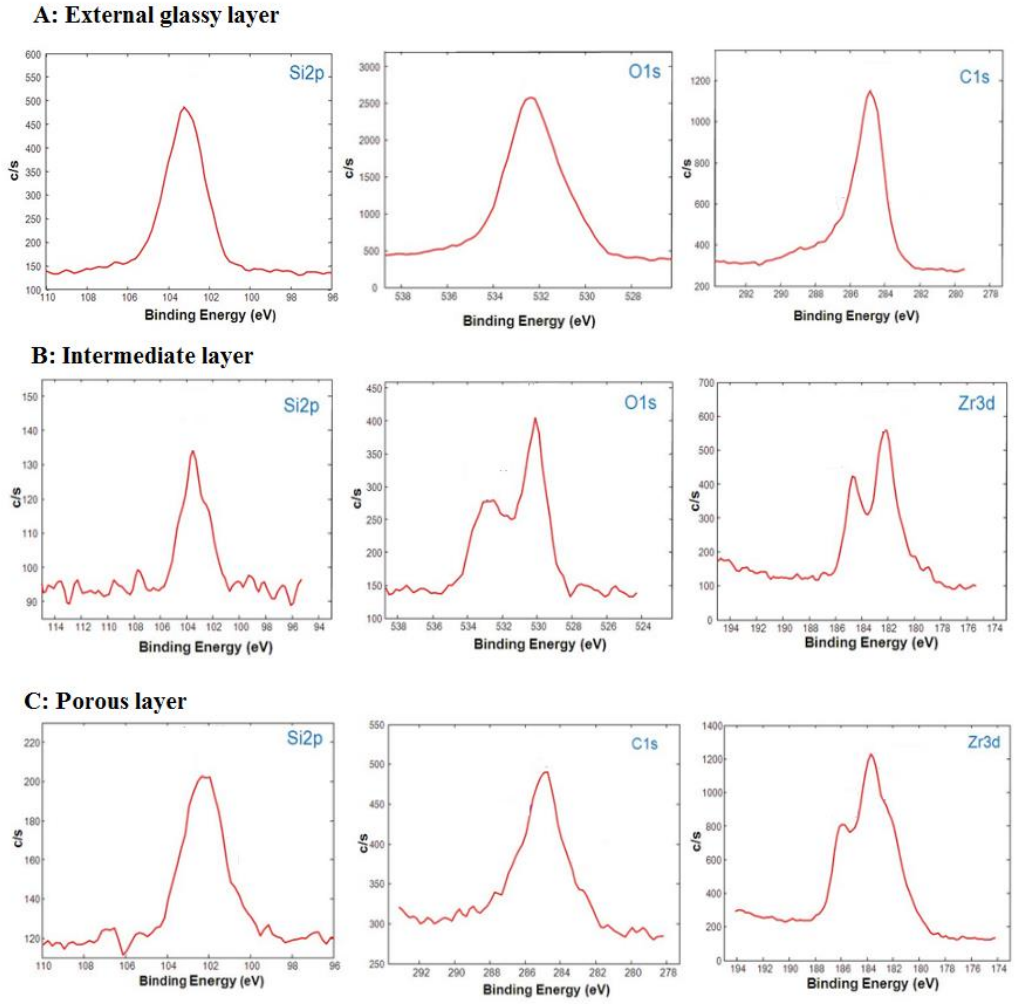

Figure 6.8: XPS analyses performed on three oxide layer on a 80%ZrB_2-20%SiC laminate: A: External glassy oxide layer (Si2p, O1s, C1s spectra); B: Intermediate oxide layer (Si2p, O1s, Zr3d spectra); C: Porous layer (Si2p, C1s, Zr3d spectra).

In fact XPS sensitivity factor of Boron is only 0.15, much lower than those of Carbon -0.29- and Oxygen -0.71-.

Bubbles of different size were detected in the outermost layer as shown in in Figure 6.9; they were likely due to the coalescence of gaseous species inside the forming glass. The bubbles tend to burst when the vapor pressure is higher than the ambient pressure.

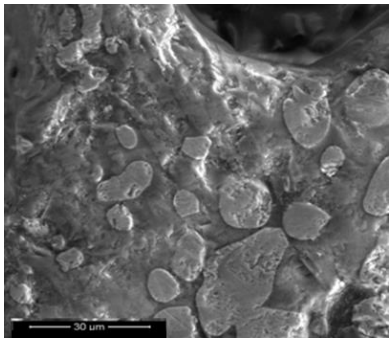

Figure 6.9 SEM image of external glassy layer.

Considering all these results the conclusion was that the external layer consisted of borosilica glass with graphite and ZrO_2 inclusions and large pores.

The intermediate layer consisted into two different phases appearing in the SEM microstructure (Figure 6.10) with different colors. It was not so easy to obtain information about the composition of these two-phases oxide: in fact the spatial resolution of the used techniques resulted limited respect to the extension of a single phase. Consequently we cannot be sure to analyze exclusively one area without including the next one.

EDS punctual analyses on the intermediate layers observed on laminates with composition 60%SiC-40%ZrB_2 and 20%SiC-80%ZrB_2 gave the results summarized in Table 6.II.

Sample	Zone under investigation	Atomic percentage of elements				
		Si	O	C	Zr	B
60%SiC+40%ZrB_2	Dark area	22,6	64,4	0,4	--	12,6
	Light gray area	--	*57*	*9,6*	*30,5*	*2,9*
20%SiC+80%ZrB_2	Dark area	20,1	69,7	2,1	0,2	7,9
	Light gray area	--	*60,1*	*8,7*	*27*	*4,2*

Table 6.II: EDS analyses of intermediate layers for laminates with different composition.

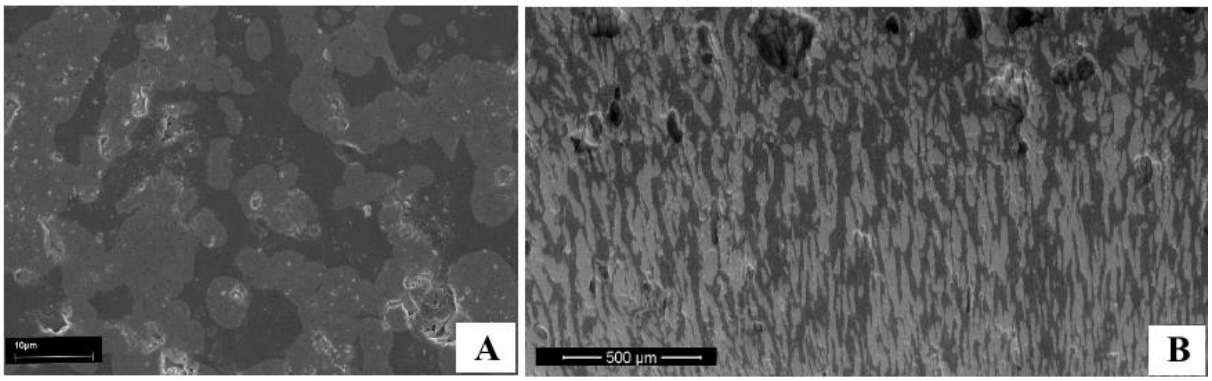

Figure 6.10: SEM microstructure of the intermediate layer for laminates with different composition: A) 40%SiC+60%ZrB_2 and B) 20%SiC+80%ZrB_2

The darker phase mainly consisted in O, Si and B with very small amount of Carbon; the atomic ratio among these elements suggested the presence of SiO_2 and B_2O_3 in both the cases (an excess

in Oxygen is observed in laminate with higher amount of ZrB_2). The dark area should be made of borosilicate glass.

In the light gray phase was evident the prevalence of O and Zr without Si and with not negligible amount of Carbon and Boron (about 9%at C and 3-4%at B).

Moreover the micro-XRD spectrum on this area (Fig 6.7B) showed the presence of ZrO_2 as the only crystalline phase in addition to few and low intensity peaks belonging to ZrB_2 and SiC (this means that the oxidation did not occur completely in the intermediate layer).

The XPS spectra (Fig 6.8B) of Si2p, O1s and Zr3d showed that both Zr and Si were mainly linked to the Oxygen. The Zr 3d peaks could be identified as a spin-orbit coupling of Zr-O bonds corresponded to ZrO_2: the first was at 182.4 eV ($Zr_{5/2}$) and the second one was at 184.9 eV ($Zr_{3/2}$). Moreover O 1s peak at 530.6 eV corresponds to Zr-O bonds for ZrO_2. The Si 2p peak at 103.3 eV corresponds to Si-O bonds and the peak at 533.1 eV was linked to O-Si bonds; so silica was present.

All these considerations let to conclude that the dark phase is made of a borosilicate glass and the light grey phase consisted mainly of ZrO_2.

The morphology of the two-phases oxide layer was different and depended on the chemical composition (Fig 6.10) : for laminates containing from 40% to 60% ZrB_2 (Fig 6.10A) there was not a preferential orientation of the two phases which resulted interpenetrated. When amount of ZrB_2 increase up to 80vol% (Fig 6.10B) it was possible to observe columnar glassy phase which resulted parallel to the direction of the Oxygen penetration.

In literature has been reported this oriented growth of the scale in the case of oxidized laminate with very high (80vol%) amount of ZrB_2 (114; 115).

This configuration of ZrO_2 skeleton was compatible with the model which involved liquid glassy phase convection during high temperature oxidation of refractory diborides, especially in presence of SiC (116; 115; 117; 118; 119).

The oxidation of ZrB_2 resulted in the formation of crystalline ZrO_2 and B_2O_3 which behaves as a quite liquid phase (B_2O_3 viscosity at 1550°C: 40 Pa·s); the oxidation of SiC produced SiO_2 which was a viscous fluid (SiO_2 viscosity at 1550°C: 100 GPa·s) (116). A two-layer oxide film forms with the porous zirconia skeleton filled with SiO_2 phase; it can dissolve B_2O_3 with the resultant formation of B_2O_3-SiO_2 liquid phase.

The instability of moving interface between liquid with very different viscosities originated vertical convection patterns where fluid Boron oxide-rich borosilicate flowed through a more viscous silica-rich outer layer. These convection movements were probably the cause of oriented

grow of the scale; moreover they creates localized path for Oxygen toward the core of the sample.

When the ZrB_2 content decreased (specimens containing 40% and 60% ZrB_2) the convection pattern were very limited because of the ZrO_2 skeleton was less compact and structured; the two oxides layer has consequently a not elongated shape; in this condition also the channel for Oxygen diffusion were lost.

On the other hand Han and others (114; 119) hypothesized the formation of gaseous by-product (so no liquid mass convection) that promoted the growth of zirconia in a parallel direction respect to the discharge of the gas.

A third porous oxide layer was observed (120) (121) (122) (115) (116) (123) at the interface between intermediate layer and the not oxidized laminate with ZrB_2 amount equal or higher than 40vol%.

The micro-XRD spectra of this area (Fig 6.7C) for laminate with composition 60%SiC+40%ZrB_2 showed the presence of few and low intensity peaks belonging to the original components ZrB_2 and SiC; moreover crystalline ZrO_2 was also present.

The EDS analysis put in evidence a very interesting result: in this area the Silicon content was very low (less than 2% at) while the Carbon was present in amount between 16% and 40% on depending on the composition of ZrB_2/SiC laminate. The elemental EDS maps taken at the interface between the porous layer and the not oxidized core (Fig. 6.11) confirmed that the porous layer is characterized by a Silicon depletion but not a depletion of Carbon, Zirconium and Oxygen depletion.

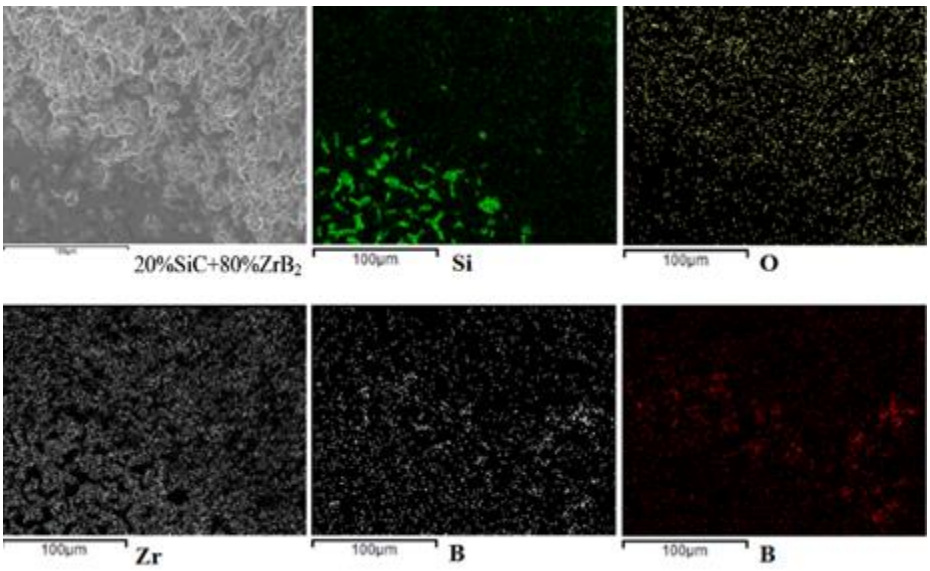

Figure 6.11 Element distribution at the interface between porous layer and sample core after long-term oxidation up to 1600°C for laminate with composition 20%SiC-80%ZrB_2 laminate (porous layer in the right and upper part of the maps; elemental maps of Zr, B, C, Si, O).

XPS spectrum for C1s showed that the C was mainly linked through C-C bonds, while only few bonds existed between C-O and C-Si (Fig. 6.8C).

These results let to conclude that:

- The low amount of the observed Si was bonded with C; in fact traces of not oxidized SiC were present in micro-XRD spectra);
- There was an excess of Carbon not found before in the other two oxide layers;
- The Zirconium was present in ZrO_2 oxidized form.

Conclusively SiC could be consumed by active oxidation mechanism: this would justify both the lack of Silicon and the formation of amorphous Carbon (Eq.6.2).

The Oxygen can diffuse trough the scale and reach the core of the sample, reasonably its activity decrease in function of the distance from the surface of the sample and this justify the favorable conditions for SiC active oxidation, according to reactions (6.2) and (6.3) in addition to the main oxidation process (Eq. 6.1) :

$$SiC_{(s)} + ½\ O_{2(g)} \leftrightarrow SiO_{(g)} + C_{(s)} \qquad \text{(Eq. 6.2)}$$

$$SiC_{(s)} + O_{2(g)} \leftrightarrow SiO_{(g)} + CO_{(g)} \qquad \text{(Eq. 6.3)}$$

$$SiC_{(s)} + {}_{3/2}\ O_{2(g)} \leftrightarrow SiO_{2(l)} + CO_{(g)} \qquad \text{(Eq. 6.1)}$$

Our investigations showed that the occurred reaction was the first one (Eq. 6.2).

According to *Han et al.* (119), the formation of a SiC-depletion region depended both from the surrounding pressure and temperature conditions and on the structure distribution of SiC particles in ZrB_2 matrix.

In presence of 20vol% or higher amount of SiC in ZrB_2 matrix, SiC particles formed a network. ZrB_2 in contact with depleted SiC grains was directly exposed to Oxygen and it oxidized according the reaction (6.9) producing an oxide layer that mainly consisted in ZrO_2.

The long-term oxidation tests confirmed the above mentioned TGA results: exposing ZrB_2/SiC laminates in air up to 1600°C their oxidation resistance progressively got worse increasing the amount of ZrB_2 in the material. Nevertheless after a first oxidation treatment a glassy external layer formed on the surface of laminates which acted as barrier against further Oxygen penetration. This is important in the context of reusable-thermal protection system.

Because of the formation of a oxide scale with a complex structure in the case of laminates with amount of ZrB_2 higher than 40vol% it is important optimize the SiC/ZrB_2 ration in laminates.

Nevertheless we can expect that the oxidation resistance of ZrB_2/SiC composites is better than that of both pure ZrB_2 and pure SiC at temperature higher than 1700°C: *Han et al*. (124) reported that ZrB_2–20 vol% SiC composites exhibited excellent oxidation resistance at 2200 °C: any macro-cracks or spallation were detected after oxidation.

In the first case the explanation is easily understood: the oxidation of ZrB_2 leads to the formation of B_2O_3 that melts at 450°C and evaporates quickly above 1100°C. On the other hand SiO_2 formed from the oxidation of SiC has a higher viscosity, higher melting temperature and lower vapor pressure: the Oxygen diffusion should consequently be slower in silica-rich liquid respect to the boria layer which, in addition, evaporate just above 1100°C.

The superiority of ZrB_2/SiC oxidation resistance respect to pure SiC is more complex: the porous ZrO_2 coming from the oxidation of ZrB_2 forms a skeleton which acts as a condensing substrate and mechanical support to the borosilicate liquid.

Obviously this porous ZrO_2 structure, in order to form a mechanical support, has to be enough strong; this condition is realized for laminate with high amount of ZrB_2.

In the case of monolithic SiC or laminates with all SiC layers, even if the oxidized SiO_2 layer is thermochemically and diffusion-kinetically stable after melting, it results unstable for mechanically point of view because of the formation of bubbles.

6.3 Multilayer mechanical properties after oxidations at 1500°C

In case of composites with a content of ZrB_2 exceeding 40vol% the growth of the scale outwards and the emission of gaseous species caused the loss of the original size and shape of specimens.

For this reason, in order to investigate the effect of the oxidation process on the mechanical characteristics, only few ceramic laminates containing less than 50vol% of ZrB_2 were mechanically tested before and after oxidation in calm air at 1500°C for 24 hours. The results are summarized in Table 6.III.

The decreasing of geometric density in oxidized samples with progressive increase in ZrB_2 amount can be justified as consequence of the shape deformation of the sample which makes difficult their dimensions measurements. Also the apparent density decreased particularly in the case of the laminate containing 40vol% of ZrB_2; this was consistent with the formation of a porous layer within the scale.

The oxidation treatment at 1500°C only slowly decreased both elastic modulus and strength of SiC laminates, while it heavily worsened the mechanical behaviour of composite laminates containing ZrB_2: in fact both elastic modulus and strength were appreciably lowered after this prolonged oxidation.

Sample composition	Geometrical density [% of theoretical]	Apparent density [% of theoretical]	Elastic modulus [GPa]	Bending strength [MPa]	Microhardness [GPa]
100% SiC	89.0 ± 2.6	94.8 ± 0.2	339 ± 19	324 ± 24	21.2 ± 0.6
100% SiC after oxidation at 1500°C	89.7 ± 1.0	95.9 ± 0.2	336 ± 15	274 ± 17	20.7 ± 2.1
80%SiC-20%ZrB_2	90.2 ± 2.9	95.6 ± 0.2	364 ± 19	361 ± 34	25.5 ± 0.8
80%SiC-20%ZrB_2 after oxidation at 1500°C	81.1 ± 2.5	94.1 ± 0.2	127 ± 11	196 ± 5	22.4 ± 2.4
60%SiC-40%ZrB_2	92.3 ± 0.9	99.0 ± 0.2	389 ± 11	325 ± 41	24.4 ± 1.0
60%SiC-40%ZrB_2 after oxidation at 1500°C	61.1 ± 3.7	88.6 ± 0.1	164 ± 29	176 ± 28	20.8 ± 2.2

Table 6.III Physical properties of laminates before and after long-term oxidation treatment.

Anyway the final stiffness and strength of the oxidized laminates still seem sufficient for application in TPS, since for this application high mechanical performance is not required while oxidation resistance is the main material requirement.

Chapter 7
Results from SMARTEES

Great part of this research work was carried out in the context of an European integrated project SMARTEES - Multifunctional components for aggressive environments in space applications (125). SMARTEES targeted on the creation of new multifunctional materials to be used as thermal protection system.

Some general requirements have to be taken into account in order to develop a TPS structure: first of all the design of space vehicle was very important in order to make a systematic investigation on all the system properties specifications.

For this project, among the possible different shapes, a conservative APOLLO-type has been selected by Airbus Group Innovations (partner of the project). One of the main advantage of using a blunt vehicle respect to a more streamlined one is linked to the maximum heating rate which depends on the shape of the shock wave surrounding each vehicle. Blunt vehicles have detached shock waves that spread the re-entry heat over a relatively large volume. Moreover the air flowing near its surface tends to inhibit convective heat transfer. Consequently the heating rate for blunt vehicles results relatively low. On the other hand the streamlined vehicles concentrates a large amount of heat near the sharp tip causing it to reach higher temperatures respect to those expected for a blunt body. In this case the air flowing near the surface cannot inhibit the heat transfer; as a result, the overall heating rate is higher. For this reason "needle-nosed" vehicles are not very practical and usually has slightly rounded noses to keep the tips from burning off.

The heat shield for such vehicle shape has been divided in two parts: the front shield with

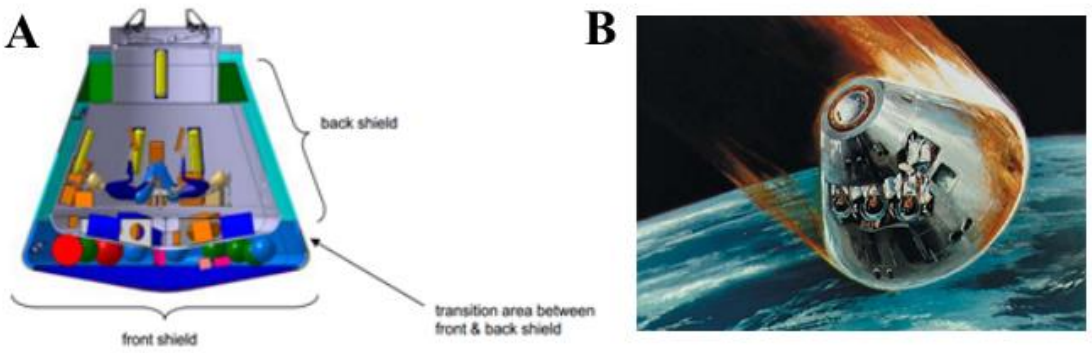

thermally high loaded areas and the back shield which was moderately loaded (Figure 7.1).

Figure 7.1 Apollo-type vehicle shape A) with heat shield locations and B) shows that air friction causes the capsule to glow red hot (Courtesy of NASA/Johnson Space Center)

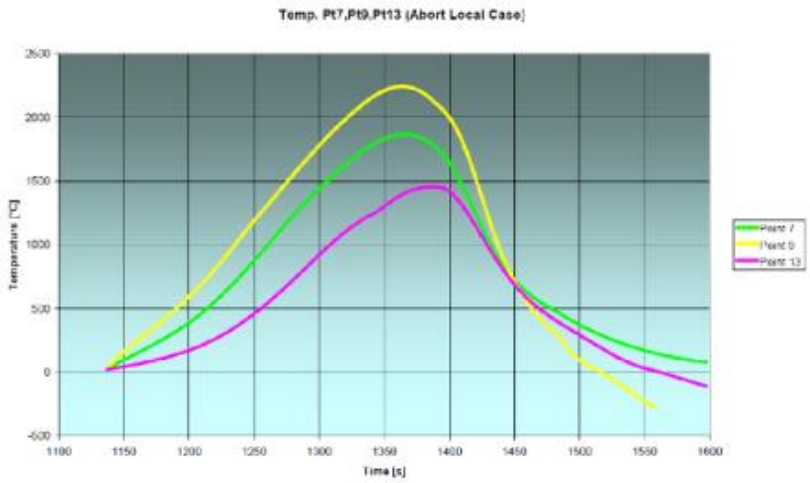

Figure 7.2 Heat flux timelines for the sizing trajectories (Courtesy of "Airbus DS GmbH")

Thermal loads have been calculated by Airbus Defence and Space for different so-called "control points" on the outer surface of both the front and back heat shields; they ranged from high to moderate and the SMARTEES materials have to be designed to cover them with a certain margin of safety. Figure 7.2 shows the heat fluxes distributions under the assumption of fully catalytic wall.

For the development of the SMARTEES TPS the attention was focused on few specific control points which needed different materials for the two shield regions (Figure 7.3); specifically two classes of materials were foreseen, one suited for the ARV back shield area whereas the second ones could be applied in certain areas of the front heat shield.

It has to be mentioned that in the foregoing studied the calculated heat fluxes for the thermal loads were based on the fully catalytic wall assumption. Experience from tests performed in the past years on C/SiC materials showed that the recombination velocity for Oxygen and Nitrogen was quiet low (below 5 m/s) resulting in loads which resulted more than 30% lower than those calculated for the fully catalytic wall.

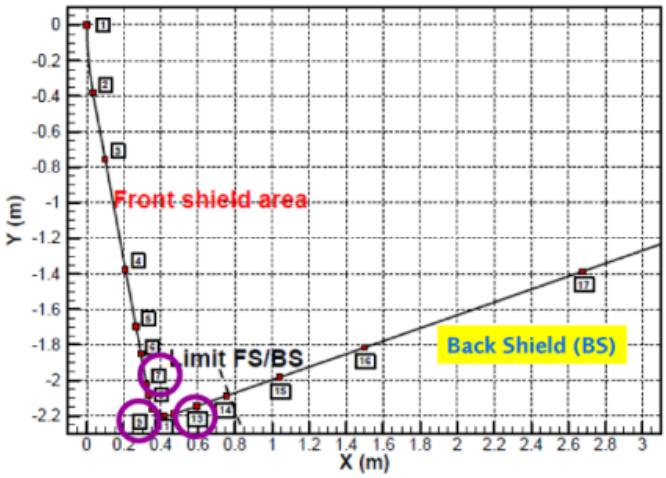

Figure 7.3 Locations of control points on the outer vehicle surface (Courtesy of "Airbus DS GmbH")

For SMARTEES two control points have been selected for the different material classes; the corresponding load class scenarios were :

- *Load class I*: back shield with corresponding control points #13. For this area the heat fluxes and thermal loads (sizing trajectory) were moderate and therefore offered an interest for the SiC based materials. This selected point led to a maximum temperature of approx. 1300 ºC and heat fluxes around 0.3 MW/m^2 .
- *Load class II*: front shield with corresponding control points #7. For this area the heat fluxes and thermal loads (size trajectories) were realistic for integrate ZrB_2/SiC based materials. This selected point involved a maximum temperature of about 1800°C and heat fluxes around 0.8 MW/m^2.

7.1 Determination of Multilayer Total Emissivity of multilayer

Since the main function of the TPS is the thermal protection of the vehicle during the occurrence of severe loads, the designer of the TPS must guarantee that most of the incident heat flux is transferred to environment and only a smaller amount is penetrating the structure itself.

Especially during re-entry phase into the Earth's atmosphere, reusable launch vehicles (RLVs) encounter high gas rates and thermal heat loads; gaseous molecules of Oxygen and Nitrogen passing through the bow shock become dissociated. Then the atoms can recombine again to form molecules in gas phase or directly on the TPS surface; it can happen with different rates in function of the thermal protection system catalytic efficiency. The heat flux on the re-entry vehicle depends on catalytic efficiency of the TPS materials. Because of the catalytic properties of these materials depend on temperature, the heat flux results indirectly dependent on the

vehicle surface temperature and, consequently, on the thermal emissivity of the TPS materials (126).

In order to develop and optimize a TPS structure, it was necessary to determine the thermal material properties and closely investigate these surface phenomena and their interaction in ground tests and flight experiments. In this context the measurement of the emissivity of the two materials chosen as main constituents for the external part of the TPS (SiC for Load Case 1 and ZrB_2/SiC for Load Case 2) resulted very important.

In literature different facilities have been described to determine the emissivity of a solid material at high temperature; two were the most used approaches (127):

- *A combined transient and brief steady state technique*: the specimen is quickly heated from room temperature (T_{amb}) to a high temperature (T_h) and then it remains at T_h for a brief steady-state period, before beginning to be cooled down by thermal radiation. This technique is based on the heat balance on the specimen held at a present high temperature T_h: under steady-state conditions, the electrical power imparted to the specimen is equal to the power loss from the specimen itself. Based on the Stefan-Boltzmann law, the power balance on the effective specimen let to calculate the hemispherical total emissivity (128).

The main disadvantage of this technique is the limitation in investigating electric conductor that means metals, while modern thermal protection system are mainly constituted by a mixture of metals and ceramics.

- Emissivity measurement facility (EFM) worked on similar principle respect to *Variable Black body source* (129; 130).

IRS (Institut fur Raumfahrtsysteme) has been qualified for total emissivity test on SiC and 80vol%ZrB_2-20vol%SiC multilayer as external part of thermal protection system.

The quite complex apparatus used for the tests was showed in Section 4.2.14: it mainly consisted of a moveable sample support system within the blackbody cavity. It was made of a graphite rod with high length respect to the diameter; this configuration had an apparent emissivity $\varepsilon > 0.999$ so it can be assimilated to a blackbody.

Inside the rod there was the graphite sample holder; it was fixed on a Molybdenum stick linked to a special flange which allowed an axial shift of the stick also in vacuum environment. During the measurement it was very important reduce as much as possible the sample shift time in order to minimize the drop in it; for this reason a special pneumatic piston it was used.

The measurements procedure has been explained in Chapter 4; all the samples have been polished by ERBICOL in order to achieve a thickness of 2 mm; the surface roughness was 0.20-0.25 μm.

Total emissivity have been tested on laminates with composition 100% SiC and 80vol%ZrB_2+ 20vol%SiC; a set of three different specimens for both the compositions have been tested in order to get a good reproducibility and obtain a statistical trust value.

Figure 7.4 shows the measured total emissivity of Silicon Carbide multilayer in comparison to values from other literature sources: our results had an average value respect to those measured by *Brandt et al.* (131) and *Pidan et al.* (126). This underlined the dependence of experimental emissivity values from the different method used to measure it: *Pidan et al.* have been performed the test using plasma wind tunnel with a magnetoplasmadynamic generator, while *Brandt et al.* used the "*radiation comparison technique*" (a round sample is heated by an electron beam in vacuum; the temperature is measured in a radial hole while a thermoelectric microsensor is used to measure the total emissivity).

Overall the average value is around 0.85 in the 700-1700K range.

The picture in Figure 7.5 showed the sample surface before and after testing: in all cases the

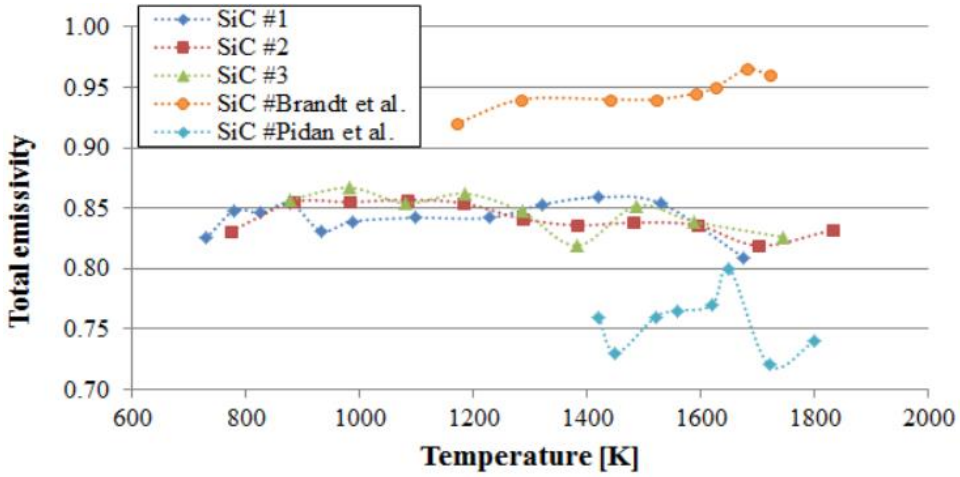

surface was not damaged; moreover any weight variation was observed.

Figure 7.4 Measurement of total emissivity for three SiC laminates: comparison between experimental and literature data.

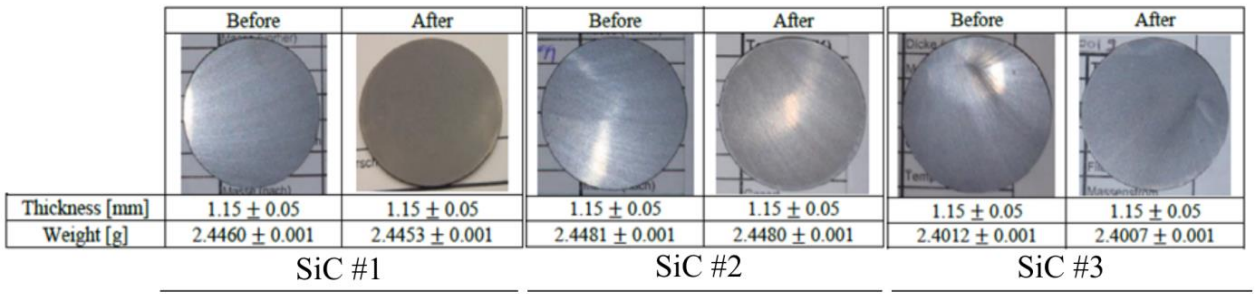

Figure 7.5 Photographs of SiC samples before and after emissivity test.

In literature only very little data can be found on the radiative properties of ZrB_2/SiC based ceramics at high temperature. *Meng et al.* (132) reported the spectral and normal total emissivity

values (in the range from 3µm to 18µm) measured for pre-oxidized ZrB_2/SiC composite containing 15vol% C: the results showed that the total normal emissivity decreased when the testing temperature increased from 1373 to 2073K.

J.F. Justin et al. (133) reported the total hemispherical emissivity of ZrB_2/SiC/$TaSi_2$ ceramic composite before and after an oxidation treatment at 1273K showing values in the range from 0.8 to 0.95.

In our investigation the total emissivity of laminates with composition 80vol%ZrB_2-20vol%SiC (Figure 7.6) was found increasing in the range of temperature from 900K to 1300K and then reached a plateau up to 1800K.

The Figure 7.7 shows the samples surface before and after testing: also in this case any of them appeared damaged; however a change in color was evident.

Usually the TPS should have a degree of emissivity above 0.8: a high degree of outer surface emittance causes rejection of the major part of the incident heat flux to the environment (134). Both for SiC and composite made of 80vol% ZrB_2+20vol% SiC the emissivity resulted higher

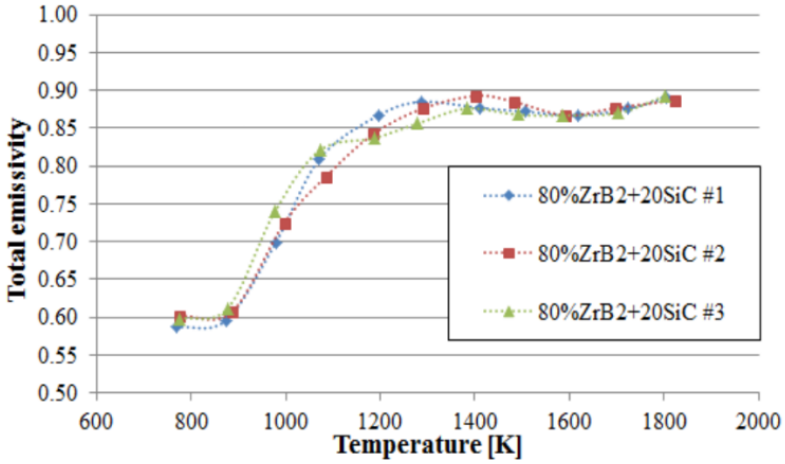

than the suggested value.

Figure 7.6 Measurement of total emissivity for three laminates with composition 80%ZrB_2+20%SiC.

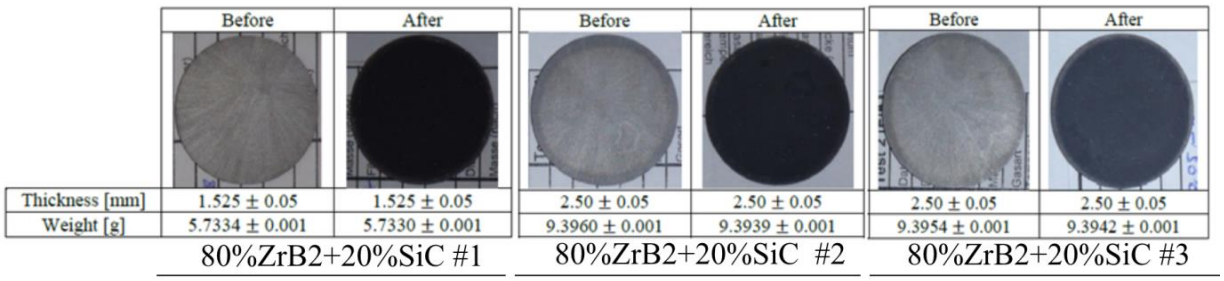

Figure 7.7 Photographs of 80%ZrB_2-20%SiC samples before and after emissivity test.

7.2 Thermal conductivity of SiC laminates

Among the thermal properties which have a significant impact on the space vehicle surface temperatures there is the thermal conductivity: it must be low especially in the Z direction in order to protect the capsule inner shell as effective as possible. This property significantly influences the thickness of the TPS as well as the mass figures.

Figure7.8 shows the thermal conductivities-temperature relationship of SiC multilayer in X, Y and Z directions before (Fig. 7.8A) and after (Fig. 7.8B) oxidation treatment.

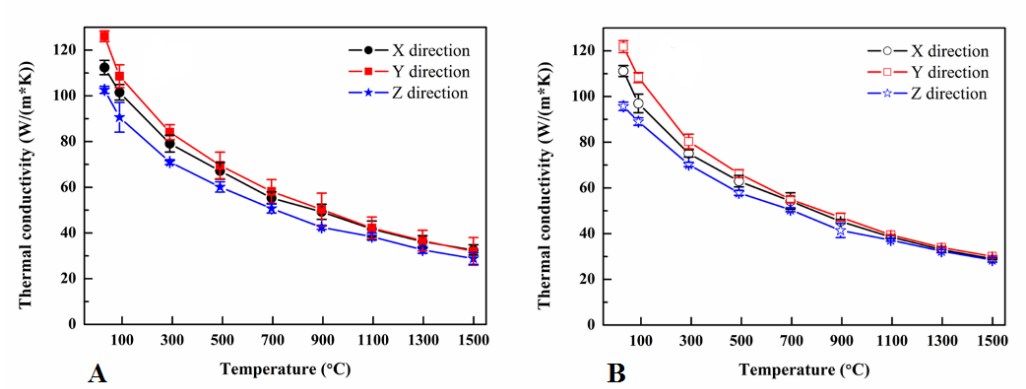

Figure 7.8 Thermal conductivities-temperature relationship of SiC multilayer A) before and B) after oxidation treatments.

The thermal conductivities (κ) of SiC multilayer in three directions were calculated by Equation 7.1:

$$\kappa = \rho \cdot C_p \cdot D \qquad \text{(Eq. 7.1)}$$

where κ is the thermal conductivity [W/(m·K)], ρ is the density [Kg/m^3], C_p is the specific heat [J/Kg·K] and D the thermal diffusivity [m^2/sec]. *Yang et al.* reported the values of thermal diffusivity and heat capacity for pressureless sintered SiC multilayer (135).

The thermal conductivities decreased when temperature increased from 30 to 1500 ºC.

From the comparison between Figure 7.8A and Figure7.8B it is possible to observe that the thermal conductivities in all directions slightly decreased after oxidation treatment because of the formation of a thin layer of silica which surround the samples. The formed silica layer presents very low thermal conductivity (less than 2 W/(m·K)) (136), which results to the slight decrease of thermal conductivity in SiC multilayer in all directions.

7.3 Tests under Re-entry conditions

The thermal tests were not only performed on the single components of the TPS, but also on the full assembly; we will report the characterization on technological samples (size the 50×50 mm^2) with external part made of SiC multilayer (137).

Tests of subscale full assemblies components (Figure 7.9) consisting of:

- SiC Multilayer
- Brazing interlayer (using $Ti_3Si_{1.5}C_2$ powder)
- CMC
- Pore filled SiC foam
- CMC
- Brazing interlayer (using TiCuAg filler metal)
- Titanium plate

Figure 7.9 150x150 mm^2 technology sample

Four samples with the same configuration underwent thermal cycles under three re-entry conditions: sample #6 has been submitted to 10 cycles under vacuum at maximum temperature of 1612°C and moreover 40 cycles under vacuum too using profile reaching the temperature of 1392°C. Sample #7 had been slightly over-tested: 50 cycles to 1392°C as maximum temperature plus other 50 cycles up to 1612°C and in the end to other 50 cycles at 1794°C; all cycles were performed in vacuum.

On samples #8 and #9 had been performed 100 times each under vacuum (sample #9) or 40 mbar air pressure (sample #8) reaching a temperature of 1392°C.

The characterization of the sample surface had involved the Institute of Nuclear & Radiological Science, Energy, Technology & SafetyN.C.S.R. "Demokritos" in Athens in addition to Politecnico of Turin.

SEM and Micro-XRD analyses have been performed on samples with reference number 6, 7, 8 and 9 (Figure 7.10); the choice of using this last equipment instead of a standard XRD instrument depends on the opportunity to perform analysis on specific and little areas, selected on the base of a variation in colour and shape respect to the multilayer original surface. All the measurements were done using 300 µm diameter collimator.

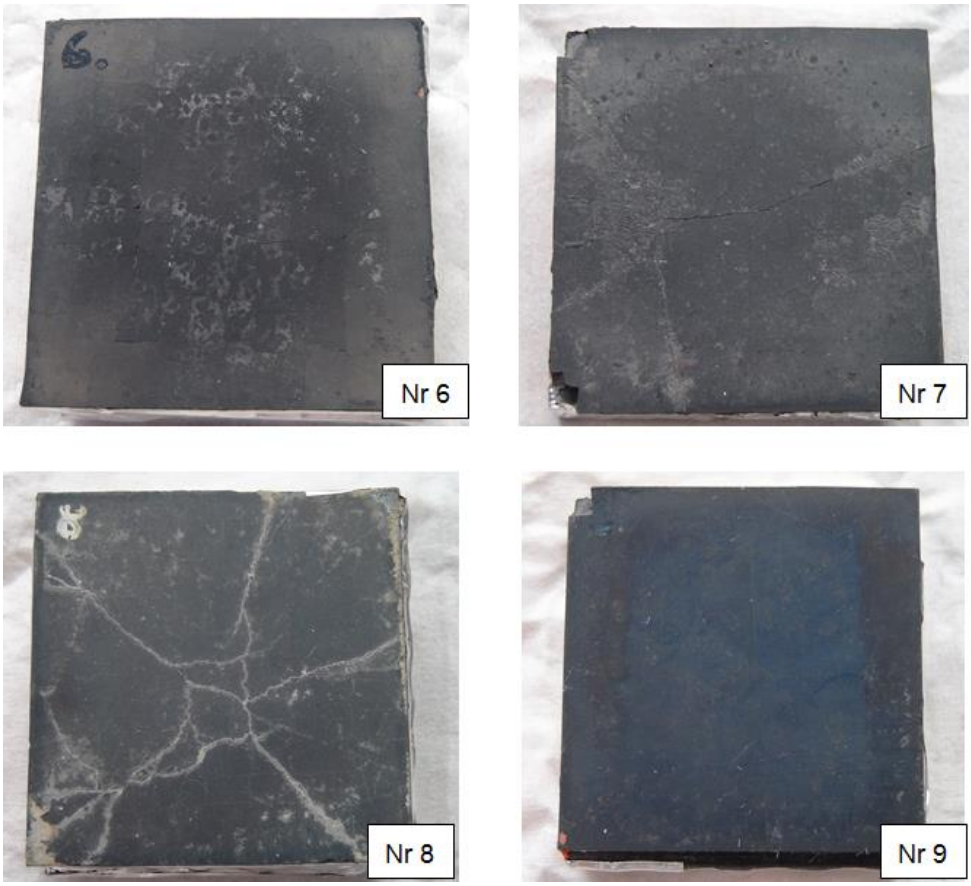

Figure 7.10 Photographs of samples surfaces after testing in AAC facility.

7.3.1 Sample reference 6

A visual inspection of the sample has been performed before analysing it with SEM equipment; the sample surface showed very thin cracks (Figure 7.11D): the longest ones were parallel to one side of the multilayer and among them while shorter cracks propagated in the transversal direction.

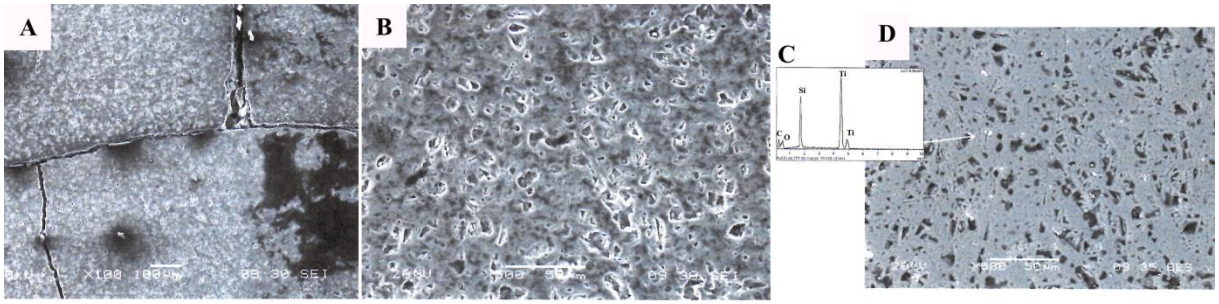

Figure 7.11 SEM surface analysis of sample #6: A)detail of surface cracks B) image obtained using SE detector C)EDS analysis on white spots D) image obtained with BSE detector

The SEM analysis (Figure 7.11B) showed a roughness surface and moreover some voids left after the thermal treatment; the image obtained using backscattering electrons detector (Figure 7.11D obtained by Demokritos) puts in evidence some white spots whose composition was mainly Titanium coming from the underlying brazing agent (Figure 7.11C) which was used to join the multilayer and the CMC.

Three areas were selected and on each of them micro-XRD analysis has been done (Figure 7.12):

Area 2A looked in “silver colour” and was in the shape of pulled over ellipses; such areas were found especially in the central part of the sample.

Area 2B was “black” and should correspond to the not damaged multilayer surface.

Area 2C looks like grey spot; there were few of this spots on the samples.

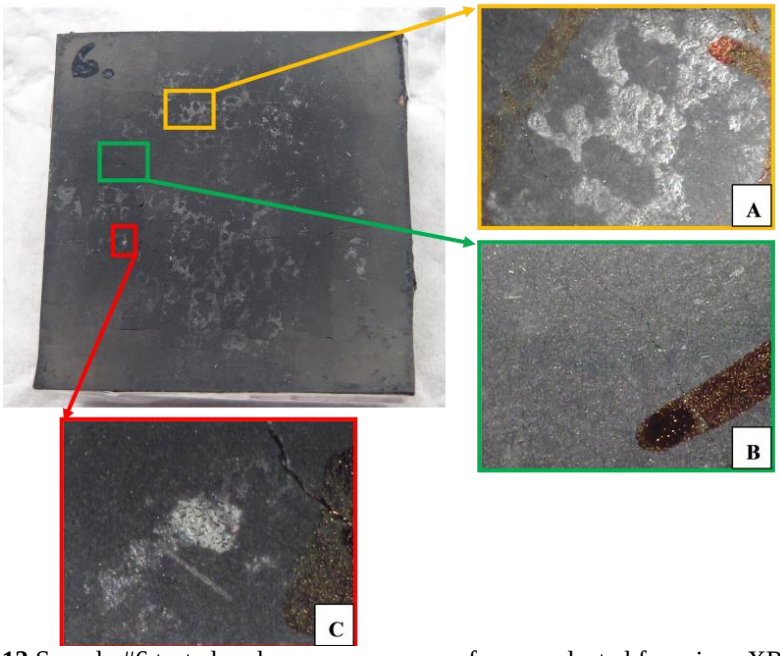

Figure 7.12 Sample #6 tested under vacuum, zoom of areas selected for micro-XRD analysis.

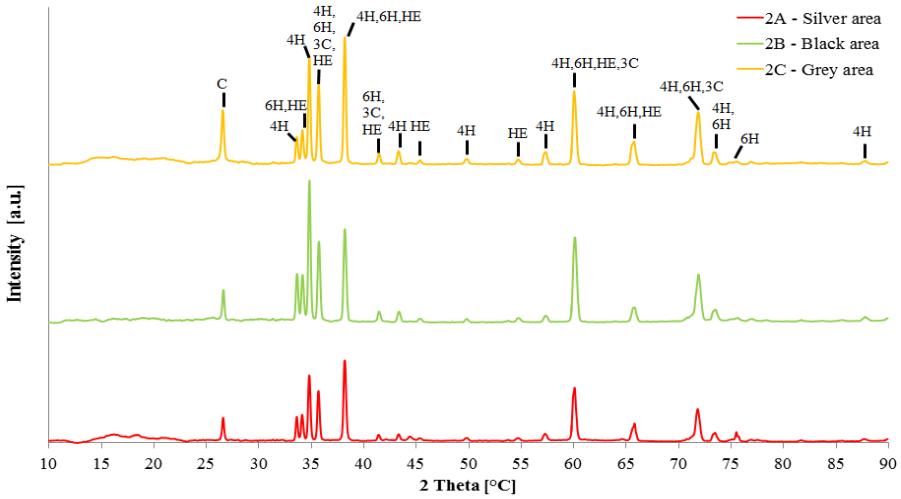

Figure 7.13 XRD spectra of the different areas selected for sample Number 6.

X-Ray spectra (Figure 7.13) were very similar for the three areas and put in evidence the presence of mainly the original matrix that is Silicon Carbide in different polytypes; the relative amount of them changed in the three cases. A little amount of graphite is always present; it is probably a residual coming from the original multilayer compositions.

7.3.2 Sample reference 7

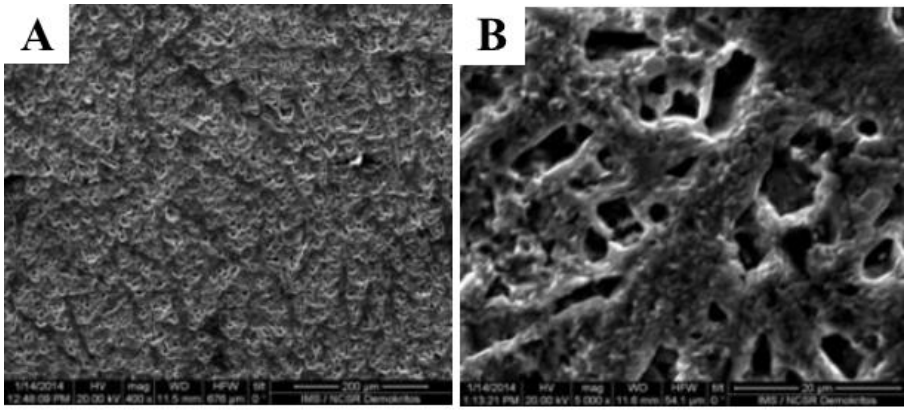

Figure 7.14 SEM surface of SiC multilayer after thermal exposure A) Dendritic area were observed B) details of a dendritic area.

The sample 7 morphology was drastically different from sample #6: a surface with a dendritic structure can be observed (Figure 7.14): SiC resulted not as dense as at the lower tested temperatures and was depleted from Si. EDX analysis showed a higher Carbon content (61 at% on average) with respect to the Si content (39 at% on average).

The sample surface showed some cracks without a preferential direction; some of these cracks were filled with material probably coming from the underlying joining. Moreover there was an orientation of the holes along the entire SiC multilayer.

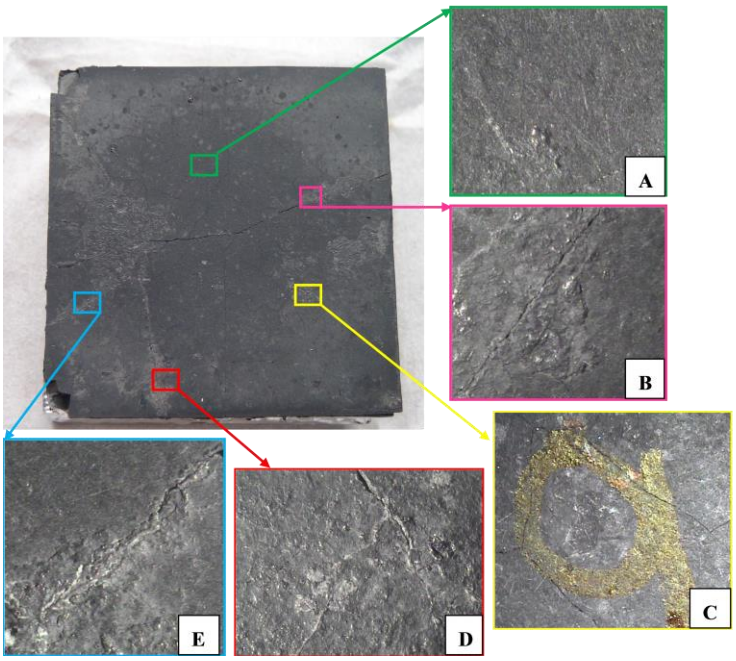

Figure 7.15 Sample #7 tested under vacuum, zoom of areas selected for micro-XRD analysis.

XRD analysis on the cracks resulted very similar and they were reported in Figure 7.16: the Graphite peak was very high respect to the intensity of the other peaks which belong to Silicon Carbide. This means that the cracks were mainly filled with carbonaceous residuals.

The area C was selected because of it looked in a different greyscale with some needle-shape light grey spots. This difference in colour gradient didn't mean a change in composition: in fact XRD pattern of area A and area C were very similar and correspond mainly to Silicon Carbide. Also in this case graphite was present.

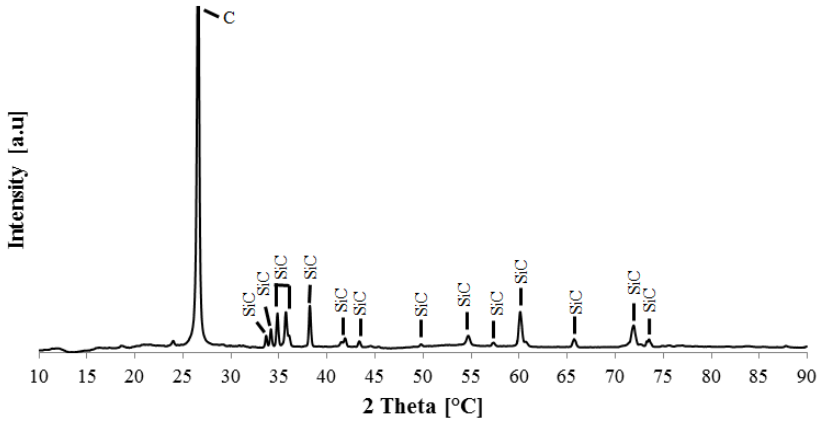

Figure 7.16 XRD pattern for areas B, D and E

7.3.3 Samples reference 8 and 9

Both of samples underwent 100 cycles under vacuum (sample #9) and 40 mbar air pressure (sample #8).

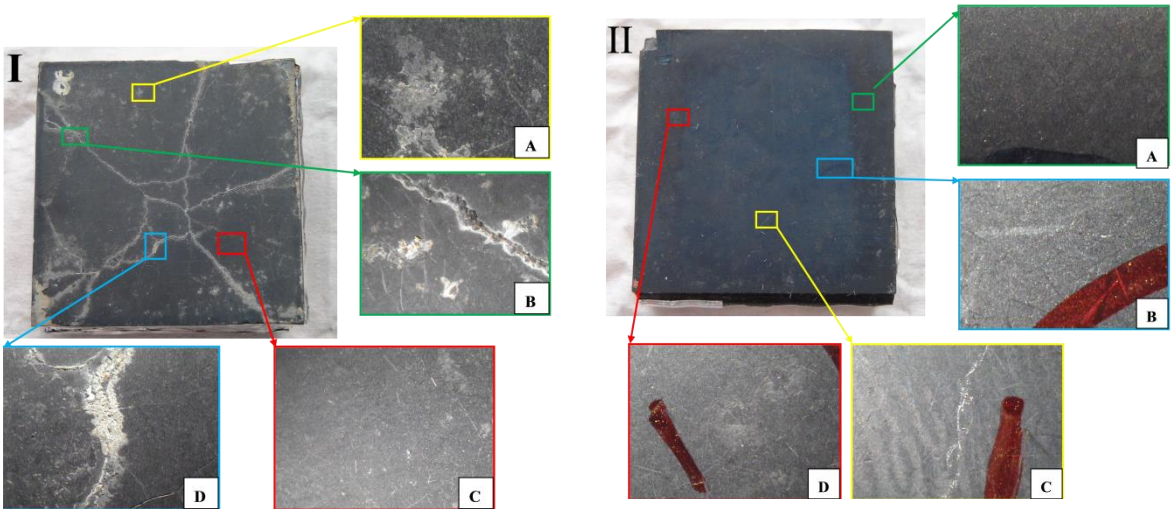

Figure 7.17 I)Sample #8 and II)Sample #9: zoom of areas selected for micro-XRD analysis.

From Figure 7.17-I cracks were clearly visible thanks to the light grey filler: they are attributed to the CTE difference between the base materials and the filler. These cracks are vertical to the SiC/CMC interface and they do not propagate inside the CMC.

They have been reduced in their width with the improvement of the flatness of the SiC multilayer.

XRD analysis in Figure 7.18 pointed out the presence of Titanium oxide in both the examined cracks (reference to areas B and D). It probably came to the underlying joining. A little amount of graphite was present too.

No evident changes in the surface morphology were observed after the thermal tests; some silica formation was found which was enhanced for the sample tested in 40 mbar (~9 at% Oxygen for the sample tested under vacuum and ~15 at% Oxygen for the sample tested at air pressure of 40 mbar).

XRD spectra on areas without cracks and characterised by two different colours were very similar: the black area (Figure 7.17-IC) was composed by Silicon Carbide with the presence of a little amount of graphitic Carbon. The grey area (Figure 7.17-IA) had the same composition with trace of Titanium Oxide.

On the other hand the XRD measurement on the different areas selected on Sample #9 (Figure 7.17-II) showed the presence of only Silicon Carbide with some graphite traces, independently on the colour of them.

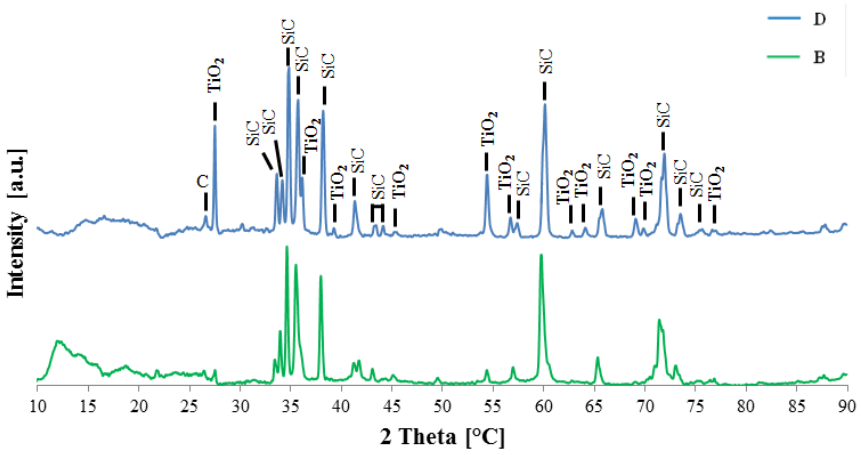

Figure 7.18 XRD pattern for areas B and D.

7.4 Up-scaling of the processing method

Samples in form of bars (with size 60x10x1.8mm) and small plates (up to 50x50x1.8mm) of the different kind of multilayer were formerly prepared for microstructure investigation and in order to study the mechanical and thermal properties. The manufacture process of these ceramic laminates was tape casting because this technology has been adopted at industrial plant level since many years and it is well suitable for processing hybrid laminates with layers showing different microstructure and composition. Anyway in the frame of SMARTEES project the processing method parameters were adjusted in order to perform the up-scaling required for the production of the TPS at the technological sample level. In fact in order to produce at first sub-systems by joining together some of the different components of Thermal Protection System (such as multilayer joining to CMC and ceramic foam) and then to fabricate the full-scale TPS structure, sample up-scaling was required.

Up-scaling process was formerly performed at Politecnico producing plates of suitable size for several research activities such as the joining trials and the production of laminates and sub-systems for thermal shock tests; laminates with all SiC layers and alternating SiC and composite interlayers have been prepared trying to progressively increase the size.

7.4.1 Silicon Carbide based multilayer

The up-scaling of laminate containing all layers with the same composition was possible after optimization of debinding cycle: this treatment, as explained in Chapter 3, had the aim to promote the decomposition and move away organic components from the “green” material. Respect to the small ones, the wide surface of samples with increasing size make more difficult

the removal of organics in form of gaseous specie. It was so necessary decrease the thermal gradient during debinding cycle.

In Figure 7.19 plates with increasing size are shown: the maximum dimensions of multilayer which can be processed at our laboratories was limited by the size of the chamber of both debinding and sintering furnaces. Figure 7.19B showed a plate with dimension 120x120x1.8 mm^3 which represented the biggest laminate produced at Politecnico.

However it was possible to produce sample with size up to 150x150x1.8 mm^3 in collaboration with Tecnalia which provided for the debinding and sintering treatments in its bigger oven.

Moreover, since a technology sample of TPS should have aerial mass as low as possible, a strategy adopted in order to decrease the multilayer system weight was the decreasing of the number of layers. With this aim a laminate made of 6 SiC layers has been produced as shown in Figure 7.19 A.

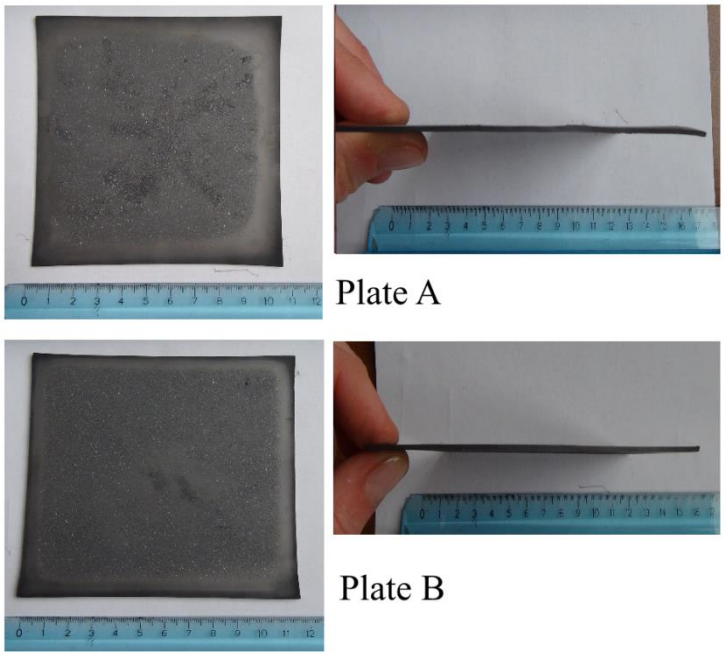

Figure 7.19 Plate A) made of 6 SiC layers with size 107x107x1.1 mm^3 and Plate B) made of 10 SiC layers with size 120x120x1.8 mm^3.

7.4.2 Multilayer integrating SiC and ZrB_2/SiC composite

The up-scale of laminates alternating ZrB_2/SiC layers into SiC ones presented many difficulties: increasing the size of the sample, the extension of interfaces between layers with different composition was strongly increased. The resultant stresses in sintering phase were too much higher and lead to formation of cracks and delamination as it was possible to see from Figure 7.20 A and B.

On the base of the observation made in section 5.3.1, getting homogeneous the two components particle size could improve the sinterability of the material; for this reason it has been done a

milling of ZrB_2 powder. Thanks to this powder pre-treatment it has been possible to obtain intact sintered plates with size 50x50x1.8mm^3 integrating composite layers in between SiC ones (Fig. 7.20 C and Fig.7.20D).

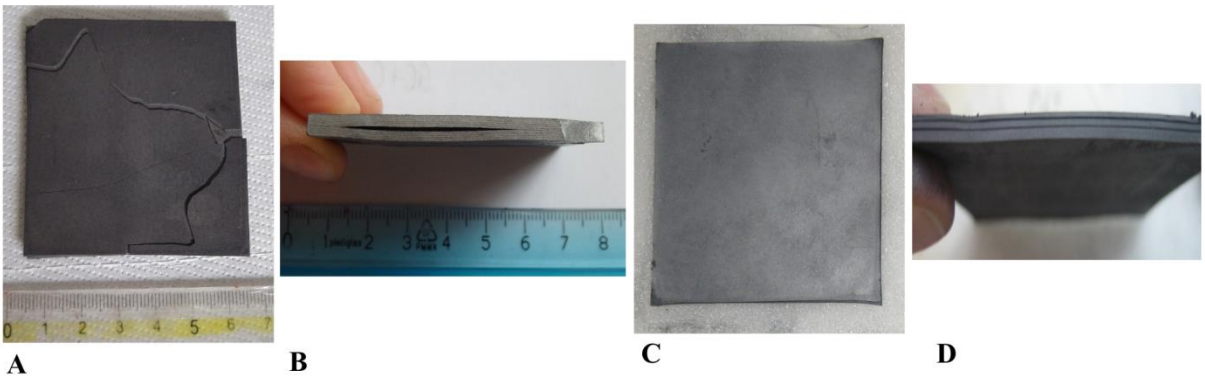

Figure 7.20 Results of different attempt to produce plates integrating composite and SiC layers: A) Failure due interlayer delamination B) Failure due to delamination in correspondence of the core sample C) Photographs of a well sintered plate and D) Cross section of the sintered plate.

The following attempts to sinter samples with further increasing dimensions failed just after debinding (Figure 7.21).

In order to produce large sample integrating composite layers in between SiC ones it is necessary a systematic investigation on the possible factors that have influence on the debinding and sintering processing of them. For example it should be interesting change the thickness of the interlayers respect the Silicon Carbide ones (on the principles exposed in Section 5.3.2) or make a simulation of the stress distribution along the whole laminate.

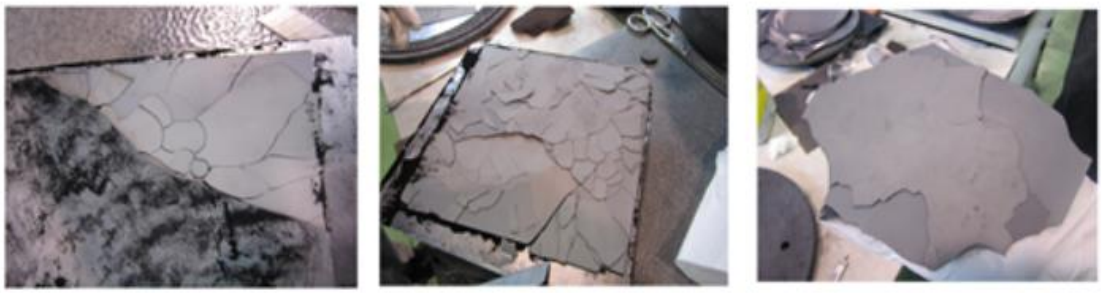

Figure 7.21 Failed debinding of a large plate integrate ZrB_2/SiC composite in between SiC ones.

Chapter 8
Conclusions

This thesis addressed on the production and characterisation of multilayer ceramic materials to be used as hot part of a reusable thermal protection system. This kind of application requires materials which have to show good performances in the hostile thermal and mechanical environment. The TPS has to sustain the high and ultra-high temperature ceramics are promising candidates for this applications thanks to their favourable thermal stability, mechanical properties and oxidation resistance.

This work of thesis focused the attention on ZrB_2/SiC system: laminates made of SiC, ZrB_2 and their composites with SiC/ZrB_2 ratio progressively changing from 100% SiC to 100% ZrB_2 were prepared by tape casting of a slurry, layer stacking, debinding and pressureless sintering at 2200°C.

Boron and Carbon proved to be suitable sintering aids for SiC multilayer as well as for composite laminates with SiC matrix. Several sintering aids have been investigated for the pressureless sintering of Zirconium Diboride (C, TiC and $ZrSi_2$) or for ZrB_2-based composites (SiC, B, C, B_4C, VC, TiC and Si_3N_4) : among them the addition of TiC lets to obtain the best results in term of densification degree and mechanical properties.

In the case of composites with ZrB_2 matrix the Silicon Carbide acted itself as a sintering aid; a systematic investigation on multilayer ceramics with different SiC/ZrB_2 ratio has been done. The composition with 80vol%ZrB_2-20vol%SiC has been identified as the best compromise in term of residual porosity and mechanical features.

The oxidation resistance represents one of the most important factors to be considered for aerospace applications: for this reason a detailed study on the oxidation resistance in air up to 1600°C of laminates with different SiC:ZrB_2 ratio has been done.

SiC has several applications as TPS components thanks to the formation of a silica passive layer on its surface which prevents a further Oxygen penetration up to 1600°C. At higher temperature the damaging of this layer after melting and the mechanism of active oxidation limited the use of this compound.

All composite laminates displayed passive behaviour since the oxidation products formed on the material surface were able to slow down the oxidation process.

For laminates with amount of SiC up to 20vol% it was observed the formation of a rather thin cristobalite passive layer on the surface.
The oxide scales grown on composite laminates with at least 40 % vol. of ZrB_2 were more complex consisting of three sub-layers :

- An external glassy layer mainly consisted of a borosilicate glass with some Carbon inclusions;
- An intermediate layer consisting of crystalline ZrO_2 plus borosilicate glass;
- An inner porous layer characterized by a SiC depletion coming from the mechanism of active oxidation of SiC to Si and CO.

The laminates submitted to an oxidation treatment in air for one day at 1500° C retained appreciable strength and stiffness; the mechanical features of these oxidized material improved with the increase of SiC:ZrB_2 ratio.

Hybrid laminates integrating composite layers in between SiC ones have been also prepared and characterized: the oxidation of external SiC layers involves the formation of a silica passive layer which is able to protect the material from further Oxygen penetration up to 1600°C. For higher temperature the formed silica is not more effective; the underlying layer made of ZrB_2/SiC composite would offer oxidation protection slowing down the action of Oxygen.
From processing point of view alternating layers with different chemical compositions causes the development of residual stresses which leads the formation of cracks propagating in the composite layers. With the aim to reduce these stresses the effects of the starting powders particle size and the thickness of the interlayers have been investigated.

The processing method of laminates was optimized in order to perform the up-scaling.

Conclusively, because of the ZrB_2/SiC system has been studied to be used as external part of a TPS structure, total emissivity and thermal conductivity measurements have been performed.
Both SiC and ZrB_2/SiC composites show high emissivity which lets to reduce the maximum surface temperature reached during the re-entry phase.

The thermal conductivity of SiC multilayer decreases with the increasing of temperature up to 1500°C.

Moreover technological demonstrators sustained several tests under re-entry conditions in vacuum up to 1794°C or at low pressure at temperature up to 1392°C. The cracks or defects

formed on the samples surface are caused to thermal stresses coming from the different CTEs of multilayer, CMC and brazing agent using for the joining of them. These cracks are sealed by the melting of the brazing agent.

Using a brazing component with higher thermal compatibility respect to the multilayer it should be possible reduce or avoid the formation of cracks and defects on the multilayer surface during re-entry tests.

Publications/ Conference proceedings

◆ Journal publications

1. **E. Padovano**, C. Badini, E. Celasco, S. Biamino, M. Pavese and P. Fino, "Oxidation behaviour of ZrB_2/SiC laminates: effect of composition on microstructure and mechanical strength". *In press*, Journal of European Ceramic Society

2. **E. Padovano**, C. Badini, S. Biamino, M. Pavese, W.S. Yang, P. Fino, "Pressureless sintering of ZrB_2/SiC composite laminates, using boron and carbon as sintering aids". Advance in Applied Ceramics 2013, 112: 478-486.

3. W.S Yang, S. Biamino, **E. Padovano**, M. Pavese, S. Marchisio, G. D'Amico, S. Ceresa Mio, X. Chen, P. Fino, C. Badini. "Thermophysical properties of SiC multilayer prepared by tape casting and pressureless sintering". Composite Structures 2013, 96: 469–475.

4. W.S Yang, S. Biamino, **E. Padovano**, M. Pavese, S. Marchisio, X. Chen, P. Fino, C. Badini. "Microstructure and mechanical properties of milled fibre/SiC multilayer composites prepared by tape casting and pressureless sintering". Materials Science and Enginnering: A. 2013, 588: 103-110.

5. W.S Yang, S. Biamino, **E. Padovano**, L. Fuso, M. Pavese, S. Marchisio, D. Vasquez, C. Vega Bolivar, P. Fino, C. Badini. "Microstructures and mechanical properties of short carbon fibre/SiC multilayer composites prepared by tape casting". Composites Science and Technology 2012, 72: 675–680.

◆ Conference proceedings

J, Barcena, M. Lagos, I. Agote, C. Jimenez, C. Badini , **E. Padovano**, S. Gianella, D. Gaia, K. Mergia, S. Messoloras , P. Yialouris, C. Wilhelmi, A. Ortona and C. D'Angelo and V. Liedtke, "SMARTEES FP7 Space Project – Towards A New Tps Reusable Concept For Atmospheric Reentry From Low Earth Orbit", Proceedings of 7th European Workshop on TPS & Hot Structures, ESA/ESTEC, Noordwijk, The Netherlands, 8 to 10 April 2013

C. Badini, **E. Padovano**, J. Barcena M. Lagos I. Agote, C. Jimenez, X. Hernandez(S. Gianella D. Gaia, V. Liedtke K. Mergia, S. Messoloras, P. Yialouris Y. Panayiotatos,, A. Ortona, C. D'Angelo and C. Wilhelmi, "Oxidation Behaviour Of Laminate Ceramics Belonging To SiC-ZrB_2 System", Proceedings of 7th European Workshop on TPS & Hot Structures, ESA/ESTEC, Noordwijk, The Netherlands, 8 to 10 April 2013

K. Mergia, C. Jimenez P. Yialouris, M. Lagos, I. Agote, Y. Panayiotatos, L.Volker, **E. Padovano**, C. Badini C. Wilhelmi, S. Messoloras and J. Barcena, "Joining of ceramic matrix composites to high and ultra high temperature ceramics for thermal protection systems",

Proceedings of 7th European Workshop on TPS & Hot Structures, ESA/ESTEC, Noordwijk, The Netherlands, 8 to 10 April 2013

E. Padovano, W. Yang, A. Antonini, S. Biamino and M. Pavese, **"**Pressureless sintering of ZRB_2 with different amounts of Silicon Carbide." Proceeding of International Conference on Mechanics of Nano, Micro and Macro Composite Structures. Turin, Italy, 2012, June 18-20.

References

1. Motion. *Returning from Space: Re-entry* .

2. *Storia del rientro atmosferico.* R.De Chiara and R.Monti, Napoli: s.n., 2006. Atti del 1° Convegno Nazionale della Storia dell'Ingegneria . p. 789.

3. *Atmospheric Re-Entry* . J. C. Adams. 2003.

4. *Thermal Protection System Technology and Facility Needs for Demanding Future Planetary Missions.* E.Venkatapathy, B.Laub and. Lisbon: s.n., 2003. International Workshop on Planetary Probe Stmospheric Entry and Descent Trajectory Analysis and Science .

5. *Ceramic Matrix Composite (CMC) Thermal Protection System (TPS) and Hot Structures for Hypersonic Vehicles* . Glass, D. E. Dayton, Ohio: s.n., 2008. 15th AIAA Space Planes and Hypersonic System and Technologies Conference.

6. *Advanced CMC TPS Design Concepts for Re-usable Re-entry Vehicles.* H. Lange, A. Steinacher, K. Handrick, S. Weiland, D. Glass, K. Wurster, J. Robinson and F. Greene. Noordwijk : s.n., 2006. 5th European Workshop on Thermal Protection Systems and Hot Structures.

7. *Apollo Thermal-Protection System Development.* R.B. Erb, D:H: Greenshields, L:T: Chauvin and J.E. Pavlosky. 6, 1970, Journal of Spacecraft and Rockets, Vol. 7, pp. 727–34.

8. *Forebody TPS Sizing with Radiation and Ablation for the Stardust Sample Return Capsule.* D. Olynick, Y.K. Chen and M.E. Tauber. 1997, AIAA Paper, pp. 1997-2474.

9. *The Shuttle Tile Story.* P.A. Holloway and P.F.Cooper. 1, 1981, Astronautics and Aeronautics, Vol. 19, pp. 24-34.

10. *Reusable Launch Vehicle Technology Program.* D.C. Freeman, T.A. Talay and R.E. Austin. 11, 1997, Acta Astronautica, Vol. 41, pp. 779-90.

11. *VenturestarTM Single Stage to Orbit ReusableLaunch Vehicle Program Overview.* R.I. Baumgartner, [ed.] College Park American Institute of Physics. 1997. AIP Conference Proceedings. pp. 1033-40.

12. *Development of Advanced Metallic, Thermal-Protection-System Prototype Hardware.* M.L. Blosser, R.R. Chen, I.H. Schmidt, J.T. Dorsey, C.C. Poteet. 2, 2004, Journal of Spacecraft and Rockets , Vol. 41, pp. 183-94.

13. *Preliminary Thermal-Mechanical Sizing of a Metallic Thermal Protection System.* C.C. Poteet, H. Abu-Khajeel andS.-Y. Hsu. 2, 2004, Journal of Spacecraft and Rockets, Vol. 41, pp. 173–82.

14.UHTCs:Ultra High Temperature Ceramic Materials for extreme environment applications. E.Wuchina, E.Opila, M.Opeka, W.Fahrenholtz and I.Talmy. *The Electrochemical Society Interface.* 2007, pp. 30-36.

15. *Material properties of a sintere alpha-SiC.* R.G. Munro. 5, 1997, J. Phys. Chem. Ref. Data, Vol. 26, pp. 1195-1203.

16. *Sintering of silicon carbide I. Effect of carbon.* L.Gubernat and A.Stobierski 2003, Ceram. Int., Vol. 29, pp. 287-92.

17. *Sintering of silicon carbide II. Effect of boron.* L. Gubernat and A Stobierski. 2003, Ceram. Int. , Vol. 29, pp. 355-61.

18. *Sintering of 6H(alpha)-SiC and 3C(beta)-SiC powders with B4C and C additives.* H.N. Yoshimura, A.C. Da Cruz, Y. Zhou and H. Tanaka. 8, 2002, J. Mat. Sci. , Vol. 37, pp. 1541-6.

19. *Refractoriy diborides of zirconium and Hafnium.* W.G. Fahrenholtz, G.E. Hilmas, I.G. Talmy and J.A. Zaykoski. 5, 2007, J. Am. Ceram. Soc., Vol. 90, pp. 1347-64.

20. *On the validity of the Hall-Petch relationship in nanocrystalline materials*. A.H. Chokshi, A. Rosen , J. Karch and H. Gleiter. 1989, Scripta Metallurgica, Vol. 23, pp. 1679-84.

21. *Synthesis of Oxidation Resistant Metal Diboride.* E. Clougherty, P. Pober and L. Kaufman. 1968, Trans. Met. Soc. AIME, Vol. 242, p. 1077.

22. *Thermogravimentric study of the oxidation of ZrB_2 in the temperature range of 800° to 1500°. C.* Graham, WC Tripp and HC. 7, 1971, J. Electrochem. Soc., Vol. 118.

23. *Influence of TiB_2 content on microstructure and hardness of TiB_2-B_4C composite.* T.S. Srivatsan, G. Guruprasad, D. Black, R. Radhakrishnan ans T.S. Sudarshan. 2005, Powder Technology , Vol. 159, pp. 161-7.

24. *Pressureless sintering of Titanium Diboride with nickel, nickel boride and iron additives.* M.A. Einarrud, E. Hagen, G. Pettersen and T. Grande. 12, 1997, J. Am. Ceram. Soc. , Vol. 80, pp. 3013-20.

25. *Synthesis of oxidation resistant metal diboridecomposites.* E.V. Clougherty, R.L. Pober and L. Kaufman. 1968, Trans. Met. Soc. AIME, Vol. 242, pp. 1077-82.

26. *Phase Equilibrium Diagrams – Phase Diagrams for Ceramists1994.* A.E. McHale. National Instituteof Standards and Technology . s.l.: the American Ceramic Society , 1994. pp. 131-45.

27. *Investigation of Boride Compounds for Very High.* E.V. Kaufman and L. Clougherty ManLabs Inc . Cambridge: Air Force Technical Documentary Report, 1963.

28. *Phase Diagrams for Ceramist.* A.E. McHale, [ed.] National Institute of Standards and Technology. *Phase Equilibrium Diagrams.* s.l. : The American Ceramic Society , 1994, Vol. 10, p. 131.

29. *Investigation of Boride Compounds for Very High Temperature Applications.* L.Kaufman and E.V. Clougherty. Cammbridge : ManLabs, Inc. , 1963 . Air Force Technocal Documentary Report .

30. B. Aronsson, T. Lundstrom and S. Rundqvist. Borides . New York : Wiley & Sons, 1965.

31. *Activated sintering of zirconium diboride.* G.A Gorbunow and A.F. Meeson. 1968, Inorg. Mater., Vol. 4, pp. 267-70.

32. *Metallic Borides: preparation of solid bodies, sintering methods and properties of solid bodies.* M. Pastor. Boron and refractiry borides. New York: Springers, 1977, pp. 457-93.

33. *Hot pressing of zirconium diboride-molybdenum dilicide mixture.* M. Kinishita, M. Koss and Y.Hamano. 2, 1970, Yogyo-Kyokai-Shi, Vol. 78.

34. *Effect of thermal exposure on strength of ZrB_2-based composites with nanosize SiC particles.* S.Q. Guo, Y.M. Yang and Y. Kagawa. 14, 2008, Comp. Sci. Technol., Vol. 68, pp. 3033-40.

35. *Microstructure and properties of the refractory compounds TiS_2 and $ZrSi_2$.* R. Prommeyer and G. Rosenkranz. 9, 1992, Metalkd, Vol. 83, pp. 685-9.

36. *On the preparation of bio-nano structural ceramics and composites by spark plasma sintering.* M. Shen and Z. Nigren. 2003, Solid State Sci , Vol. 5, pp. 125-131.

37. *Mechanical and physical behaviour of spark plasma sintered ZrC–ZrB_2–SiC multiphase composites.* S.Q. Guo, Y. Kagawa, T. Nishimura, D. Chung and J.-M. Yang. 2008, J. Eur. Ceram. Soc, Vol. 28, pp. 1279–1285.

38. *Densification of ZrB2-based composites and their mechanical and physicval properties: A review.* S.Q. Guo. 2009, J. Eur. Ceram. Soc., Vol. 29, pp. 995-1011.

39. *Low-temperature densification of zirconium diboride ceramics by reactive hot pressing.* A.L. Chamberlain, W.G. FahrenholtZ and G.E. Hilmas. 12, 2006, J. Am. Ceram. Soc , Vol. 89, pp. 3638-45.

40. *Reactive hot pressing of ZrB_2-SiC composites.* G.J Zhang, Z.Y Deng, N. Kondo, J.F. Yang and T. Ohji. 9, 2000, J. Am. Ceram. Soc., Vol. 83, pp. 2330-2.

41. *A comprehensive treatment.* H. Hallebrand. Chapter 7. Tape casting. Materials Science and technology. s.l.: J.W. & Sons, 1996, Vol. 11, pp. 190-260.

42. *Method of Producing High-Dielectric High-Insulation Ceramic Plates.* G.N. Howatt. *U.S. Patent 2,582,993* 22 January 1952.

43. R.E. Mistler and E.R. Twiname. *Tape Casting. Theory and Practice.* 2000.

44. *Correlation between slurry rheology, green density and sintered density of tape cast yttria stabilised zirconia.* A. Mukherjee. 7, 2001, Ceramics International , Vol. 27, pp. 731-9.

45. *A simple way to make tough ceramics.* W.J. Clegg, K. Kendall, N. Mcn. Alford, T. W. Button, J. D. Birchall. 347, 1990, Nature, pp. 455-7.

46. *Characterization of ceramic powder.* R.N. Katz. Treatise on materials science and technology . 1976, Vol. 9, pp. 35-49.

47. *Characterization of ceramic powders.* S.G. Malghan. [ed.] ASM Internaltional. Engineering Material Handbook . s.l.: S.J. Schneider , 1991, Vol. 4, pp. 63-74.

48. *Modern Aspects of Particle Size Analysis.* T. Davies and R. Allen. Advances in Ceramics . Westerville: G.L. Messing et al., 1987, pp. 721-46.

49. *Mechanical Packing of sherical particles.* R.K. McGeary. 10, 1961, J. Am. Ceram. Soc. , Vol. 44.

50. *Processing of Ceramics.* R. J. Brook, R. W. Cahn, P. Haasen and E.J. Kramer. 1996. Material Science and Technology: a comprehensive treatment.

51. *Organic Additives and Ceramic Processing.* D.J. Shanefield. Boston: IZluwer Academic Publishers , 1995 , pp. 115-26.

52. *Tape Casting and Properties of Mullite and Zirconia- Mullite Ceramics.* P. Chartier and T. Bosh 1991, J. Am. Ceram. Soc., Vol. 74.

53. *Solubility Parameters.* H. Burrel. s.l.: 14, 1955, Interchem. Rev. , Vol. 1, pp. 3-16.

54. *Potential of SiC multilayer ceramics for high temperature applications in oxidising environment.* M. Pavese, P. Fino, A. Ortona and C.Badini. 2008, Ceramics International , Vol. 34, pp. 197-203.

55. G.E.Dieter, *Mechanical metallurgy Chapter 9. Hardness.* 1988, pp. 325-337.

56. *Modern Physical Metallurgy and Materials Engineering. Science, process, applications.* R.E. Bishop and R.J. Smallman. s.l. : Butterworth-Heinemann Press, 1999. p. 237.

57. *Materials for ultrahigh temperature structural applications.* K. Upadhya, J.-M. Yang and W.P. Hoffman. 12, 1997, Am. Ceram. Soc. Bull., Vol. 76, pp. 51-56.

58. *Zirconium diboride* . C. Mroz. 6, 1994, Am. Ceram. Soc. Bull. , Vol. 73, pp. 141-2.

59. *Engineering properties of borides.* R.A. Cutler. [ed.] Materials Park ASM International. *Engineered materials handbook:Ceramics and Glasses.* Columbus: S.J. Schneider, 1991, Vol. 4, p. 787.

60. *Pressureless sintering of zirconium diboride.* A.L. Charberlain, W.G. Fahrenholtz and G.E. Hilmas. 2006, J. Am. Ceram. Soc., Vol. 89, pp. 450-6.

61. *Boride-based hard materials*. R. Telle, L.S. Sigl and K. Takagi. [ed.] Wiley-VCH Verlag GmbH. Handbook of ceramic hard materials. Weinheim : R. Riedel, 2000, pp. 802-945.

62. *Sintering of zirconium boride with activating additions.* B. Cech, P.Oliverius and J. Sejbal. 15, 1965, Powder Metall., Vol. 8, pp. 142-51.

63. *Effect of Fe and Cr addition on the sintering behaviour of ZrB_2 produced by self-propagating high-temperature synthesis.* S. K. Mishra, S. K. Das, A. K. Ray and P. Ramachandrarao. 11, 2002, J.Am. Ceram. Soc., Vol. 85, pp. 2846-48.

64. *Effect of Ni additives on pressureless sintering of SHS ZrB_2.* A. K. Godkhindi and M.M. Khanra. 6, 2005, Advances in applied Ceramics, Vol. 104, pp. 273-6.

65. *Effects of $MoSi_2$ additions on the properties of Hf– and Zr–B_2 composites produced by pressureless sintering.* L. Sciti and D. Silvestroni. 2007, Scripta Materialia , Vol. 57, pp. 165-8.

66. *Properties of a Pressureless-Sintered ZrB_2–$MoSi_2$ Ceramic Composite.* D. Sciti, S. Guicciardi and A. Bellosi. 7, 2006, J. Am. Ceram. Soc., Vol. 89, pp. 2320-2.

67. *Pressureless sintering and physical properties of ZrB_2-based composites with $ZrSi_2$ additive.* S. Guo, Y. Kagawa, T. Nishimurac and H. Tanaka. 2008, Scripta Materialia , Vol. 58, pp. 579-82.

68. *Pressureless densification of zirconium diboride with boron carbide additions.* S.C. Zhang, G.E. Hilmas and W.G. Fahrenholtz. 5, 2006, J. Am. Ceram., Vol. 89, pp. 1544-50.

69. *Pressureless sintering of zirconium diboride: particle size and additive effects.* W.G. Fahrenholtz, G.E.Hilmas , S.C.Zhang and S. Zhu. 5, 2008, J. Am. Ceram. Soc. , Vol. 91, pp. 1398–1404.

70. *Improved Oxidation resistance of zirconium diboride by tugsten carbide additions,.* S.C. Zhang, G.E. Hilmas and W.G. Fahrenholtz. 11, 2008, J. Am. Ceram., Vol. 91, pp. 3530-5.

71. *Pressureless sintering of zirconium diboride using boron carbide and carbon additions.* S. Zhu, W.G. Fahrenholtz, G.E. Hilmas and S.C. Zhang. 11, 2007, J. Am. Ceram. Soc., Vol. 90, pp. 3660-3.

72. *Pressureless sintering of carbon-coated zirconium diboride powders.* S. Zhu, W G. Fahrenholtz, G.E. Hilmas and S.C. Zhang. 2007, Materials Science and Engineering A , Vol. 459, pp. 167-71.

73. *Pressureless densification of ZrB_2–SiC composites with vanadium carbide.* J. Zou, G.-J. Zhang, Y.-M. Kana and P.-L. Wanga. 2008, Scripta Materialia, Vol. 59, pp. 309-12.

74. *Oxidation-based materials selection for 2000°C + hypersonic aerosurfaces: Theoretical considerations and historical experience.* M.M. Opeka, I.G. Talmy and J.A. Zaykoski. 19, 2004, J. Mat. Science, Vol. 39, pp. 5887-5904.

75. *Evaluation of ultra-High Temperature Ceramics.* S.R. Levine, E. Opila, M.C. Halbig, J.D. Kiser, M. Singh and J. A. Salem. 2002, J. Eur. Ceram. Soc., Vol. 22, p. 2757.

76. *Effect of an SiC addition on the oxidation of ZrB_2.* W.C. Tripp, H.H. Davis and H.C. Graham. 1973, Ceram. Bull., Vol. 52, p. 612-6.

77. *Effect of carbon and titanium carbide on sintering behaviour of zirconium diboride.* L.C.Pathak, S.K. Mishra and. 2008, Journal of Alloy and Compounds, Vol. 465, pp. 547-555.

78. *Role of Carbon in the sintering of boron-doped silicon carbide.* W.J. Clegg. 2000, J. Am. Ceram. Soc., Vol. 83, pp. 1039-43.

79. *Multilayer SiC for thermal protection system of space vehicles:manufacturing and testing under simulated re-entry conditions.* S. Biamino, V. Liedtke, C. Badini, G. Euchberger, I.Huertas Olivares, M. Pavese and P. Fino. 2008, J. Eur. Ceram. Soc. , Vol. 28, pp. 2791-2800.

80. *Pressureless sintering mechanism and microstructure of ZrB_2–SiC ceramics doped with boron.* X.-G. Wang, W.-M. Guoa and G.-J. Zhanga. 2009, Scripta Materialia, Vol. 61, pp. 177-180.

81. *Self passivating behaviuor of multilayer SiC under simulated atmospheric re-entry conditions.* C. Badini, V. Liedte, G. Euchberger, E. Celasco, S. Biamino, M. Pavese and P.Fino. 2012, J. Eur. Ceram. SoC., Vol. 32, pp. 4435-45.

82. *High temperature oxidation of multilayered SiC processed by tape casting and sintering.* C. Badini, P. Fino, A. Ortona and C. Amelio. 2002, J. Eur. Ceram. Soc., Vol. 22, pp. 2071-9.

83. *ZrB_2-based laminates produced by tape casting.* V. Medri, P. Pinasco, A. Sanson, E. Roncari, S. Guicciardi and A. Bellosi. 2012, Int. J. Appl. Ceram. Technol., Vol. 9, pp. 349-357.

84. *Elastic properties of polycrystalline TiB_2, ZrB_2 and HfB_2 from room temperature to 1300K.* D.E: Wiley, W:G: Fahrenholtz and G.E.Hilmas. 1969, J. Less-Common Met. , Vol. 18, pp. 149-157.

85. *High-strength Zirconium diboride-based Ceramics.* A.D. Chamberlain, W.G. Fahrenholtz and G.E. Hilmas. 6, 2004, J. Eur. Ceram. Soc., Vol. 87, pp. 1170-2.

86. *Laminated ZrB_2-SiC ceramic with improved strength and toughness.* P. Zhou, P. Hu, X. Zhang and W. Han. Scripta Materialia: s.n., 2011, Vol. 64, pp. 276-9.

87. *Pressureless sintering of ZrB_2-SiC Ceramics.* S.C. Fahrenholtz, G.E. Zhang and W.C. Hilmas. 1, 2008, J. Am. Ceram. Soc., Vol. 91, pp. 26-32.

88. *Ultra High Temperature Ceramics: Densification, Properties and thermal stability*. J.F. Jankowiak and A. Justin. The Onera Journal of Aerospace Lab . 3, 2011.

89. *Pressureless sintering of ZrB_2-SiC ceramics: the effect of B_4C.* H. Zhang, Y. Yan, Z. Huang, X. Liu and D. Jiang. 2009, Scripta Materialia , Vol. 60, pp. 559-62.

90. *Properties of ZrB_2-SiC ceramics by pressureless sintering.* H. Zhang, Y. Yan, Z. Huang, X. Liu and D. Jiang. 7, 2009, J. Am. Ceram. Soc. , Vol. 92, pp. 1599-1602.

91. *Proprietà elastiche di compositi contenenti particelle*. C.Badini. Materiali compositi per l'ingegneria. Torino: Celid, 2003, pp. 117-8.

92. *Estimation of Elastic Moduli of particulate composites by new models and comparison with moduli measured by tension, dynamic and ultrasonic tests.* G. Bourkas, I. Prassianakis, V.Kytopoulos, E. Sideridis and C.Younis. *Advanced in Materials Science and Engineering* . 2010, pp. 1-13.

93. *Processing and properties of ZrB_2-SiC composites obtained by aqueous tape casting and hot pressing.* Z. Lu, D. Jiang, J. Zhang and Q. Lin. 2011, Ceramics International , Vol. 37, pp. 293-301.

94. *Engineering Properties of Carbides.* [ed.] S.J. Schneider. Engineered Materials Handbook: Ceramics and Glasses. Columbus : ASM International , Vol. 4, p. 808.

95. *Ultra High Ceramic composites* . [ed.] N.P. Bansal. Handbook of Ceramic Composites . Boston : Kluwer Academic Publishers, 2005, p. 211.

96. *Design of ceramic laminates for strctural applications.* W.J. Clegg, June 1998, Materials Science and Technologies, Vol. 14, pp. 483-495.

97. *The fabrication and failure of laminar ceramic composites.* W.J. Clegg, 1992, Acta Metall. Mater., Vol. 40, pp. 3085-93.

98. *Thermal Properties of Materials* . [ed.] J. F. Shackelford and W. Alexander. Materials Science and Engineering Handbook . Third. 2001, p. 475.

99. *Interfacial Effects in Particulate, Fibrous and Layered Composite Materials.* S.J. Howard, R.A. Stewart and W.J. Clegg. Key Engineering Materials. T.W. Clyne, 1996, Vol. 116, pp. 331-50.

100. *Stability charactyerization of Diboride Composites under high velocity atmospheric flight conditions.* D.Rasky and J.Bull. 1992. 24th International SAMPE Conference.

101. *Ceramic laminates with tailored residual stresses.* C.Baudin and A.J. Sanchez-Herencia. 6, 2009, Boletin de la societad espanola de ceramica y vidrio , Vol. 48, pp. 311-320.

102. *Material properties of sintered SiC.* R.G.Munro. 5, 1997, J. Physic. Chem. , Vol. 26, pp. 1195-1203.

103. *A theoretical and experimental approach to the active-to-passive transition in the oxidation of Silicon Carbide.* B. Schneider, A. Guette, R. Naslain, M. Cataldi, A. Costecalde. 33, 1998, Journal of Materials Science, pp. 535-47.

104. *$SiO_{(g)}$ formation from SiC in mixed oxidizing-reducing gases.* EJ Jacobson and NS Opila. 6, 1995, Oxidation of metals, Vol. 5, pp. 527-44.

105. *The high-temperature oxidation, reduction, and volatilization reactions of silicon and silicon carbide.* E.A. Jansson and S.A.Gulbrasen and 1972, Oxid. Met., Vol. 4, pp. 181-201.

106. *Active oxidation of SiC.* N.S. Myers and D.L. Jacobs. 75, 2011, Oxid. Met., pp. 1-25.

107. *The High-Temperature Oxidation, Reduction, and volatilization reactions of silicon and silicon carbide.* E.A. Jansson and S.A. Gulbransen. 3, 1972, Oxidation of Metals , Vol. 4, pp. 181-201.

108. *Oxidation transitions for SiC Part II. Passive-to-Active Transition.* B. Harder, N. Jacobson and D. Myers. 2, 2013, J. Am. Ceram. Soc., Vol. 96, pp. 606-12.

109. *The Oxidation Kinetics of Zirconium Diboride and Zirconium Carbide at High Temperatures.* AK. Margrave and JL. Kuriakose. 7, 1964, Vol. 111, pp. 827-31.

110. *Oxidation characteristics of Hafnium and Zirconium Diboride.* L Kaufman, EV Clougherty and JB Berkowitz-Mattuck. 4, 1967, Trans. Metall. Soc. AIME, Vol. 239, pp. 458-66.

111. *Resistivity, oxidation kinetics and diffusion barrier properties of thin film ZrB_2.* JR Shappirio, JJ Finnegan, RA Lux and DC Fox. 119, Thin Solid Films: s.n., 1984, Vol. 1, pp. 23-30.

112. *The oxidation of titanium diboride and zirconium diboride at high temperature.* RJ Worsley and IG. Irving. 16, 1968, J. Less-Common Metals, pp. 103-12.

113. *Thermodynamic Analysis of ZrB_2-SiC oxidation: Formation of a SiC-depletion region.* WG. Fahrenholtz. 1, 2007, J. Am. Ceram. Soc., Vol. 90, pp. 143-8.

114. *Oxidation behaviour of Zirconium diboride-silicon carbide at 1800°C.* J. Han, P. Hu, X. Zhang and S. Meng. 2007, Scripta Materialia, Vol. 57, pp. 825-8.

115. *Thermochemical and mechanical stabilities of the oxide scale of ZrB_2+SiC and oxygen transport mechanism.* J. Lenoski and T.J. Li. 5, 2008, J. Am. Ceram. Soc., Vol. 91, pp. 1475-80.

116. *Convection patterns in liquid oxide films on ZrB_2-SiC composites oxidized at a high temperature.* J.W.Halloran and S.N. Karlsdottir. 9, 2007, J. Am. Ceram. Soc., Vol. 90, pp. 2863-7.

117. *Formation of oxide scales on zirconium diboride-silicon carbide composites during oxidation: relation of subscale recession to liquid oxide flow.* S.N. Halloran and W. Karlsdottir. 11, 2008, J. Am. Ceram. Soc., Vol. 91, pp. 3652-8.

118. *Oxidation of ZrB_2-SiC: Influence of SiC content on solid and liquid oxide phase formation* . J.W.Halloran and S.N. Karldottir. 2, 2009, J. Am. Ceram. Soc. , Vol. 92, pp. 481-6.

119. *High-temperature oxidation at 1900°C of ZrB_2-xSiC Ultrahigh-temperature ceramic compistes.* W.B. Han, P. Hu, X.H. Zhang, J.C. Han and S.H. Meng. 10, 2008, J. Am. SoC., Vol. 91, pp. 3328-34.

120. *Oxidation mechanism and resistance of ZrB_2-SiC composites.* P. Hu, W. Guolin and Z. Wang. 51, 2009, Corrosion Science , pp. 2724-32.

121. *Initial stages of ZrB_2-30vol% SiC oxidation at 1500°C.* K. Shugart, W. Jennings and E. Opila. 2014, J. Am. ceram. Soc., pp. 1-7.

122. *Modeling oxidation kinetics of SiC-Containing refractory diborides.* T.A. Parthasarathy, R.A. Rapp, M. Opeka and M.K. Cinibulk. 1, 2012, J. Am. Ceram. Soc, Vol. 95, pp. 338-49.

123. *Kinetic analysis of ZrB_2-SiC composites.* I.B. Zhabrev and V.A Ban'kovskaya. Glass physics and chemistry . 2004, Vol. 31, 4, pp. 482-8.

124. *Oxidation-resistant ZrB_2-SiC composites at 2200°C.* J. Han, P. Hu, X. Zhang, S. Meng and W. Han. 2008, Composites Science and Technology, Vol. 68, pp. 799–806.

125. SMARTEES PROJECT . *http://www.smartees-project.eu/english/homepage.* [Online]

126. *Recombination coefficients and spectral emissivity of Silicon Carbide-based thermal protection materials.* S.Pidan, M: Auweter-Kurtzm G. Hendrich and M.Fertig. 4, 2005, Journal of Thermophysics and Heat Transfer , Vol. 19, pp. 566-571.

127. *Characterization of candidate materials for the catalytic re-entry experiment phlux on expert.* M. Schubler, M. Auweter-Kurtz, G. Herdrich and S. Pidan. NASA Astrophysic Data System . 2006.

128. *A Combined Transient and Brief Steady-State Technique for Measuring Hemispherical Total Emissivity of Electrical Conductors at High Temperatures: Application to Tantalum* . T. Cezairliyan and A. Matsumoto. 6, 1997, International Journal of Thermophysics , Vol. 18.

129. *Characterization of candidate materials for the catalytic re-entry experiment philux on expert.* M. Schubler, M. Auweter-Kurtz, G.Herdrich and S.Pidan. s.l.: NASA Astrophysics Data System, 2006. 5th European Workshop on TPS Hot Structures.

130. *Surface characterization of metallic and ceramic TPS-materials for reusable space vehicles.* M. Schubler, M. Auweter-Kurtz, G. Herdrich and S.Lein. 2009, Acta Astronautica, Vol. 65, pp. 676-686.

131. *Thermisches Verhalten von C/C-SiC.* R. Brandt, G. Jaroma-Weiland, G. Neuer, P. Pohlmann and E. Schreiber. [ed.] G. Neuer. Teilprojekt B3.

132. *Radiative properties characterization of ZrB_2–SiC-based ultrahigh temperature ceramic at high temperature.* S. Meng, H. Chen, J. Hu and Z. Wang. 1, 2011, Materials & Design, Vol. 32, pp. 377-381.

133. *Ultra High Temperature Ceramics: Densification, Properties and Thermal Stability.* J.F Jankowiak and A. Justin. Onera Journal of Aerospace Lab . 1, 2011, pp. 1-11.

134. *Verification Specification for SMARTEES TPS Development.* V. Liedtke. 2012. pp. 1-31.

135. *Thermophysical properties of SiC multilayer prepared by tape casting and pressureless sintering.* W.S. Yang, S. Biamino, E. Padovano, M. Pavese, S. Marchisio, G. D'Amico, S. Ceresa Mio and X. Chen,. 2013, Composite Structures, Vol. 96, pp. 479-85.

136. *Influence of MgO/CaO ratio on the properties of MgO–CaO–Al_2O_3–SiO_2 glass – ceramicsfor LED packages.* S. Kang and S.Jang. 2012, Ceramics International, Vol. 38, pp. 543-6.

137. *Report on the harsh environment ground testing & validation of TPS thermal performance.* V. Liedtke. 2013.

138. *Standard test method for flexural strength of advanced ceramics.* C1161-94, ASTM standard. 1994.

139. *Multilayer SiC for thermal protection system of space vehicles: manufactoring and testing under simulated re-entry conditions.* S. Biamino, V. Liedke, C. Badini, G. Euchberg, I. Huertas Olivares, M. Pavese and P. Fino. 2008, J. Eur. Ceram. Soc, Vol. 22, pp. 2791-2800.

140. *Influence of microstructure on the thermophysical properties of sintered SiC ceramics.* Y.Sakka and B.K. Jang. 1999, J. Am. Ceram. Soc. , Vol. 82, pp. 3105-12.

Acknowledgements

In these last three years many things happened, many things changed and if now I am who I am is thanks to these changes.

The activities of my PhD have been performed within the framework of the European Project "SMARTEES" (G.A. n. 262749) with the financial support By the European Community. The Thesis only reflects the view of the authors and the European Community is not liable for any use of the information contained therein.

I would like to express my sincere gratitude to Prof. Badini for the opportunity he gave me to work with him putting his trust in me four years ago by now.
Thank you to all Smartees' partners for giving me the possibility to join the group and learn many things gaining from their knowledge and experiences.

A deserved thanks to all HTMAT group: thank you to Prof. Pavese, Prof. Fino and Prof.ssa Biamino for their suggestions, encouragements and knowledge.
Thank you to the "old" friends I started this adventure with such as Veronica M., Silvia M., Lorenzo M., Simone B. Emiliano d.R. and Mathieu T. and to the patient friends who sustained and got behind me during all these years at Politecnico such as Eleonora D., Andrea Colo and Claudio D.A.: with them I shared a lot of beautiful and funny moments and, don't forget, I have learnt to play Briscola. Some of them were good friends more than only colleagues. Thank you to the numerous colleagues I knew more recently such as Alberta A., Giulio M., Giorgio B., Luca L., Karolina T., Giovanna C., Federico C., Hamed S., Oxana O. and Andrea C. which have gladdened my break time with good coffees and desserts.
Thank you to Laura F. and Cristina P. for their helps from Dronero.

Thank you to my friends going back a long way such as Tati, Tizzy, Claudia, Ely, Moni and their respective partners, Fabio&Marghe and everyone I "left" in the neighbourhood of Gassino. Moreover thank you to Carmen and Roberto who have welcomed me in Turin.

Thank you to my family (natural, furry and almost in-law members) who has always supported me in all my decisions and changes (even if sometimes they were very strange and unexpected) in spite of everything. I love them because they are my strength.

Finally thank you very much to Andrea, he is the most beautiful surprise of my life. Thank you for his support, his words of encouragement, his love, all his surprises as well as all his efforts in order to obtain a thesis with as few mistakes and defects as possible. I love you.